# NANOPARTICLE INDUCED SUPPRESSION OF MICROBIAL BIOFILM

**THESIS**

**SUBMITTED FOR THE AWARD OF THE DEGREE OF**

Doctor of Philosophy

IN

**BIOTECHNOLOGY**

BY

**SHATAVARI KULSHRESTHA**

**UNDER THE SUPERVISION OF**

**Dr. ASAD ULLAH KHAN**

**INTERDISCIPLINARY BIOTECHNOLOGY UNIT**
**ALIGARH MUSLIM UNIVERSITY**
**ALIGARH (INDIA)**

**2015**

# *Certificate*

*This is to certify that the thesis entitled* ***"Nanoparticle induced suppression of microbial biofilm"*** *herewith submitted by* ***Shatavari Kulshrestha****, in fulfilment of the requirements for the degree of* ***Doctor of philosophy in Biotechnology*** *of the Aligarh Muslim University, is an authentic record of the research work carried out by her under my supervision and guidance and that no part, thereof, has been presented before for any other degree.*

***Prof. Asad Ullah Khan***
*(Supervisor)*

# *Declaration*

*I, hereby, declare that the thesis entitled "**Nanoparticle induced suppression of microbial biofilm**" is free from any sort of plagiarism.*

(*Shatavari Kulshrestha*)

# *Declaration*

*I, hereby, declare that the thesis entitled "**Nanoparticle induced suppression of microbial biofilm**" embodies the work carried out by me.*

(*Shatavari Kulshrestha*)

**COURSE WORK/COMPREHENSIVE EXAMINATION/**
**PRE- SUBMISSION SEMINAR COMPLETION CERTIFICATE**

This is to certify that **Ms. Shatavari Kulshrestha**, Interdisciplinary Biotechnology Unit, has satisfactorily completed the Course work/Comprehensive examination/Pre-submission seminar requirement which is a part of her Ph.D. programme.

**Date: ……**

**(Signature of the Chairman)**

# ACKNOWLEDGEMENT

***All praises to the God, the almighty for providing me this opportunity and granting me the capability to proceed successfully …..***

*I take this opportunity to express my deep and sincere gratitude to my supervisor* ***Dr. Asad U Khan****, Professor, Interdisciplinary biotechnology unit AMU, for giving me the opportunity to do research and providing invaluable guidance throughout this study. His dynamism, vision, sincerity and motivation have deeply inspired me. Despite being extremely busy, he gave me the privilege and liberty to encroach on his valuable time. I could not have imagined having a better advisor and mentor for my Ph.D. I am indebted to him much more than I can express.*

*I would also like to thanks* ***Prof. M. Saleemuddin, Prof. Rizwan Hasan Khan, Prof M. Owais, Dr. Hina Younus*** *and* ***Dr. Shahper Nazir*** *of Interdisciplinary Biotechnology Unit for their valuable support and encouragement.*

*I deeply appreciate and acknowledge my seniors* ***Dr. Shakir Khan, Dr. Sadaf Hasan, Dr. Mohammad Faheem, Dr. Mohd. Adil and Dr. Tabish Rehman*** *for their help and cooperation. They were always being ready to lend their helping hand along with their scientific advices. Their support and friendly nature helped me to keep my focus and to overcome my endless doubts.*

*I would also like to specially thank my colleagues* ***Lama Misba, Shariq Qayyum*** *and* ***Shadab Parvez*** *for always being there. For encouraging and helping me in every possible way. They were there for me in the time of happiness and trouble. I am really thankful to all three of them for supporting me in both professional and personal fronts.*

*I am highly grateful to my other seniors* ***Dr. Saeedut Zafar, Dr. Rozina Khan and Dr. Arbab Khan*** *for being very helpful and supportive. I am cordially grateful to my lab mates* ***Azna, Lubna, Hira, Abid, Megha, and Amit****. I am really short of words to thank* ***Mohd. Danishuddin*** *for being ever ready to help. It was a pleasure to work with them.*

*I also thank* ***Mr. Lal Mohd. Khan, Mr. Syed Faisal Maqbool, Mr. Iqtedar Husain, Dr. Parveen Salahuddin, Mr. Amir Ali, Mr. Ramesh Chandra, Mr. Isham Khan, Mr. Mohd. Nasir, Mr. Ashraf, Mr. Chandra Pal, Mr. Mashkoor, Mr. Rajendra, Mr. Rajesh, Mr. Naresh*** *and* ***Mr. Zakir*** *for their help and cooperation whenever needed.*

*I would like to gratefully acknowledge* ***Basic scientific research (UGC)*** *for providing financial assistance during my research. I would also like to acknowledge the Advanced Instrumentation Research Facility, JNU, University Sophisticated Instruments Facility (USIF), A.M.U and Centre of Excellence in Material Sciences (Nanomaterials), A MU, for providing instrumental support.*

*I owe my deepest gratitude to my parents for their support love, sacrifice and care. I especially like to thanks my mother* ***Dr. Kalpana Kulshrestha*** *for being an inspiration for me. For playing multiple roles in my life by being my teacher, my best friend, greatest support and biggest motivation. I am short of words to thanks my elder brother* ***Shashank Kulshrestha*** *for his guidance and advices which helped me to move ahead. I am also thankful to my Bhabhi* ***Arpita Prabhat*** *for being there for me and encouraging me. Without the support and love of my family it would have been very difficult for me to complete this study.*

*Last but certainly not the least I would like to express heartfelt and loving gratitude to my husband* ***Gaurav Kulshrestha*** *and his family for being extremely supportive. I thank my husband for understanding me and helping me in every possible way. His support has encouraged me to think positively and efficiently. I am thankful to him for his patience and affection.*

*Finally, I would to thank every person who were important in the successful completion of this thesis and I also like to express my apology to those whose names are not mentioned here but they were there to help whenever I needed.*

***(Shatavari Kulshrestha)***

# *LIST OF ORIGINAL CONTRIBUTIONS*

This thesis is based on the following original contributions

1. **Shatavari Kulshrestha**, Shakir Khan, Ramovatar Meena, Braj R. Singh and Asad U Khan. A graphene / zinc oxide nanocomposite film protects implant surfaces against cariogenic *Streptococcus mutans.* (Published in **Biofouling: The Journal of Bio adhesion and Biofilm Research,** 2014; 30(10): 1281-1292).

2. **Shatavari Kulshrestha**, Shakir Khan, Sadaf Hasan, Ehtisham Khan, Lama Misba and Asad U. Khan. Calcium fluoride nanoparticles induced suppression of *Streptococcus mutans* biofilm: An *in vitro* and *in vivo* approach (Under revision in **Applied Microbiology and Biotechnology**).

3. **Shatavari Kulshrestha**, Shariq Qayyum and Asad U. Khan. Facile green synthesis of graphene oxide-silver nanocomposite using *Lagerstroemia speciosa* floral extract: A study of its antibiofilm mechanism on *Streptococcus mutans* and *Enterobacter cloacae* (Communicated).

# *LIST OF ABBREVIATIONS*

| | |
|---|---|
| ATCC | American Type Culture Collection |
| $CaF_2$-NPs | Calcium fluoride nanoparticles |
| CFU | Colony forming unit |
| CLSI | Clinical and Laboratory Standard Institute |
| CLSM | Confocal Laser Scanning Microscopy |
| CR | Congo red |
| CV | Crystal violet |
| EDX | Energy-dispersive X-ray spectroscopy |
| EPS | Extracellular polymeric substances |
| FTIR | Fourier transform infrared spectroscopy |
| GO | Graphene oxide |
| GO-Ag | Graphene oxide silver nanocomposite |
| GTFs | Glucosyl transferase enzymes |
| GZNC | Graphene/zinc oxide nanocomposite |
| HEK-293 | Human Embryonic Kidney-293 cells |
| MBC | Minimum bactericidal concentration |
| MIC | Minimum inhibitory concentration |
| MTCC | Microbial Type Culture Collection |
| NCCS | National Centre for Cell Science |
| OD | Optical density |
| PI | Propidium iodide |
| RNA | Ribonucleic acid |
| qRT-PCR | Quantitative reverse transcriptase polymerase chain reaction |
| SEM | Scanning electron microscopy |

| | |
|---|---|
| TEM | Transmission electron microscopy |
| XRD | X-ray diffraction |
| QS | Quorum sensing |
| ROS | Reactive oxygen species |
| Ag-NPs | Silver nanoparticles |
| QACs | Quaternary ammonium compounds |
| COM | Chronic otitis media |
| Ftf | Fructosyl transferase enzyme |
| UV | Ultra violet |

# *LIST OF FIGURES*

# *LIST OF TABLES*

Microbial biofilms are surface attached colonies of microbes surrounded by self-produced extracellular matrix. These biofilm cause chronic infections which results in increased cost of treatment and prolonged hospitalization time. Biofilm architecture provides bacteria with enhanced antibiotic resistance, thus raising the need to search for alternative therapies that can inhibit the bacterial colonization. Nanotechnology based approaches are being employed for development of nanoparticles and nanocomposites which may be used to circumvent biofilm associated infections. The aim of our study was to synthesize and characterize different nanomaterials and to investigate their applicability in reduction of bacterial biofilms.

We initiated this study with the formation of graphene/zinc oxide nanocomposite (GZNC). The synthesized GZNC was characterized by UV-visible absorption spectroscopy, X- ray diffraction analysis (XRD), Fourier transform infrared spectroscopy (FTIR), Thermo gravimetric analysis (TGA) and Transmission electron microscopy (TEM). The results revealed the formation of well dispersed zinc oxide nanoparticle onto the surface of graphene oxide nanosheets. Further, the prospective of GZNC against the cariogenic properties of *Streptococcus mutans* like adherence, exopolysaccharide formation, acid production, acid tolerance and obstinate biofilm formation was explored. The anti-biofilm behaviour of artificial acrylic tooth surfaces coated with GZNC was also examined. Acrylic teeth are good choice for implants as they are of low cost, have low density and can resist fracture. Microscopic studies and anti-biofilm assays illustrated a significant reduction in biofilm in the presence GZNC. It was also found to be nontoxic against HEK-293 (human embryonic kidney cell line). The results indicate the potential of GZNC as an effective coating agent for dental implants by efficiently inhibiting *S. mutans* biofilm.

In second study, sub inhibitory concentrations of calcium fluoride nanoparticles ($CaF_2$-NPs) were assessed for their effect on biofilm forming ability of *S. mutans in vivo* and *in vitro* models. $CaF_2$-NPs were characterized using various techniques (TEM, XRD, FTIR and UV-visible spectroscopy). The *in vitro* studies revealed 89% and 90% reduction in biofilm formation and EPS production respectively. Moreover, acid production and acid tolerance abilities of *S. mutans* were also reduced considerably in the presence of $CaF_2$-NPs. Confocal laser microscopy and transmission electron microscopy images were in

accordance with other results indicating inhibition of biofilm without affecting bacterial viability. The qRT-PCR gene expression analysis showed significant down regulation of various virulence genes (*vicR, gtfC, ftf, spaP, comDE*) associated with biofilm formation. Furthermore, $CaF_2$-NPs were found to substantially decrease the caries in treated rat groups as compared to untreated in *in vivo* studies. Scanning electron micrographs of rat's teeth further validated our results. These findings suggest that $CaF_2$-NPs can be used as an antibiofilm agent against *S. mutans* and may be applied as a topical agent to reduce dental caries.

In our third study, we have reported a non-toxic and eco-friendly route for synthesis of graphene oxide-silver nanocomposite (GO-Ag) using a floral extract of *Lagerstroemia speciosa* (L.) Pers. plant. Nanocomposite was characterized using TEM, UV-visible spectroscopy, XRD and EDX (Energy-dispersive X-ray spectroscopy). Sub inhibitory concentrations of green synthesized GO-Ag reduced the biofilm formation in both gram-negative (*Enterobacter cloacae*) and gram-positive (*Streptococcus mutans*) bacterial models. Growth curve assay, membrane integrity assay, scanning electron microscopy (SEM) and confocal scanning laser microscopy (CSLM) revealed different mechanisms of biofilm inhibition in *E. cloacae* and *S. mutans*. Biofilm inhibition in *E. cloacae* was due loss of viability of planktonic cells while in *S. mutans* there was no loss of viability. Moreover, quantitative RT-PCR (qRT-PCR) showed significant down regulation of *vicR*, *spaP* and *comDE* genes which play crucial role in *S. mutans* biofilm formation, suggesting GO-Ag is acting on its biofilm formation cascade. Antibiofilm concentrations GO-Ag was also found to be non-toxic against HEK-293. The whole study highlights the therapeutic potential of GO-Ag to restrain the onset of biofilm formation of both gram-negative and gram-positive bacteria although its mode of action is species specific.

## 1.1 Biofilms

Conventionally bacteria were regarded as unicellular organisms growing in homogeneous planktonic free floating populations. But in their natural environment, bacteria can live in sessile surface adhered communities called biofilm [Costerton *et al.* 1999; Vlamakis *et al.* 2013]. Biofilm is a structured association of bacteria embedded in the pool of self-produced polymeric matrix consisting of protein, polysaccharide and DNA [Høiby *et al.* 2010]. Biofilms are formed to capitalize on energy, spatial arrangement, communication and to maintain the community of microorganisms. Bacteria living within the biofilms are protected and hence this architecture prove to be superior over planktonic bacteria. Biofilms are enclosed in a slimy extracellular matrix which guard them from the surrounding environment as well as from attack of antibiotics and other chemotherapeutic agents (Figure 1.1).

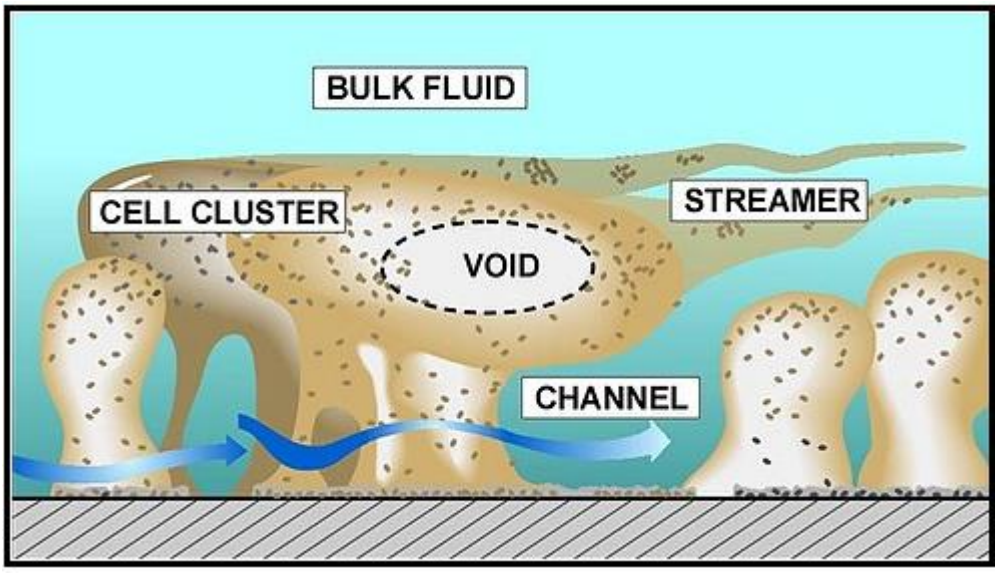


**Figure 1.1** General architecture of mature biofilm.
(Source:https://www.biofilm.montana.edu/files/CBE/images/BiofilmWbWithLabels.preview.jpg)

Biofilms are omnipresent; they develop on almost all surfaces immersed in natural aqueous environments. A chief benefit of living in biofilm community is the shield that biofilm offers to the colonizing species from competing microbes, environmental factors and toxic substances like fatal chemicals or antibiotics. Furthermore, the void and water channels formed in biofilm help in the uptake and processing of nutrients, elimination of

metabolic by-products, resembling primitive circulatory system [Lang *et al.* 2008]. A noteworthy attribute of bacteria living in biofilm community is cell density mediated gene expression or quorum sensing [Rutherford & Bassler 2012]. The quorum sensing is triggering of intracellular response due to accumulation of signalling compounds which regulate the expression of specific genes, thus providing biofilms distinct properties for their unhindered survival [Solano *et al.* 2014].

## 1.2 Stages of biofilm formation

The formation of biofilms involves a coordinated and sequential series of events. There are three main steps of biofim development. First initial contact to substratum is established followed by irreversible attachment. After attachment phase biofilm start to mature and finally disperse its cell in the environment which again initiate the biofilm of new surface (Figure 1.2).

### 1.2.1 *Initial contact and irreversible attachment*

The first step in biofilm formation is the introduction of bacteria to the surface; this process is driven by a balance of attractive and repulsive forces between the bacteria and the surface. These interactions are influenced by surrounding hydrodynamic forces [Beloin *et al.* 2008; Habimana *et al.* 2014]. These forces vary according to the changes in nutrient levels, pH, ionic force of medium and temperature [Pavlovsky *et al.* 2015]. Motile bacteria make use of flagella for initial attachment as flagella movement helps them to overcome hydrodynamic and repulsive forces. *Pseudomonas aeruginosa* and *Vibrio cholera* are some of the pathogens in which function of flagellar motility in primary attachment has been well documented [Toutain *et al.* 2007]. Initial attachment is reversible and dynamic during which bacteria can again rejoin the planktonic population depending on the hydrodynamic forces and nutrient availability [Characklis *et al.* 2012]. Irreversible attachment is influenced by the presence of surface adhesions like capsular polysaccharide/adhesion (PS/A) [Veerachamy *et al.* 2014] and fimbrial adhesins [Beloin *et al.* 2008]. Also, other surface and extracellular proteins are involved in this process [Foster *et al.* 2014].

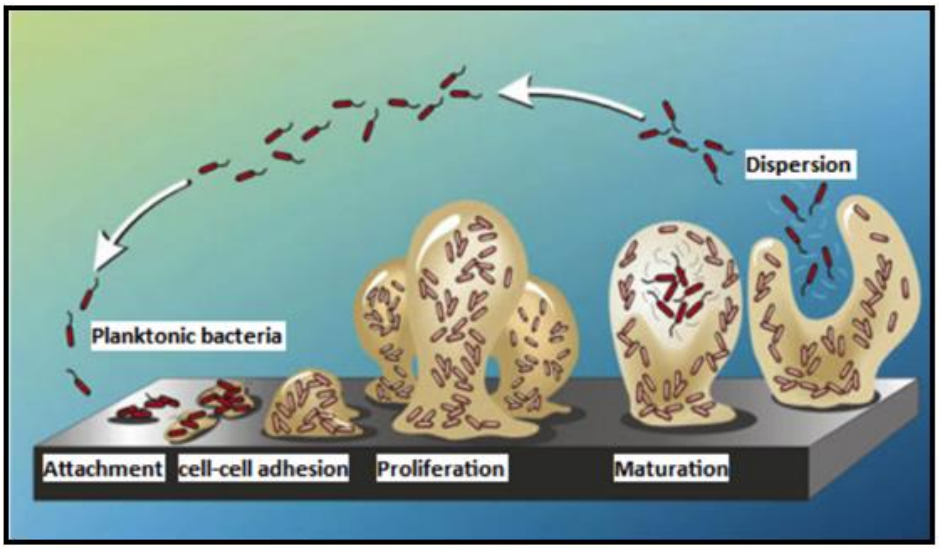


**Figure 1.2** Stages of biofilm formation. (Source: http://entkent.com/images/biofilm1.jpg)

### 1.2.2 *Maturation*

In maturation phase, attached bacteria undergo a series of changes that are due to the change in gene expression and are marked by the formation of three dimensional biofilm structures. During this stage bacterium continues to multiply and start producing extracellular polysaccharides [Kostakioti *et al.* 2013]. The bacterial adhesion and biofilm architecture in this phase is influenced by bacterium–bacterium interactions (quorum sensing) and extracellular matrix components. In addition to EPS, several studies have revealed that DNA is critical for stabilization of biofilms [Whitchurch *et al.* 2002].

### 1.2.3 *Extracellular polymeric substances (EPS)*

The bacterial biofilm is held together and secure by a matrix of secreted polymeric compounds called extracellular polymeric substances or exopolysaccharide [Lembre *et al.* 2012]. Most of the exopolysaccharides present in biofilm matrix are of very long chains (MW. 500-2000 kDa). They may be composed of the same units (homo-polymers) or different units (heteropolymeric). Homo-polymeric EPS includes dextran, cellulose, curdlan and examples of hetero-polymeric EPS are alginate, xanthan [Wingender *et al.* 2012]. Exopolysaccharide can be of branched chain or linear. The main constituents of these chains are monosaccharides but there may be substituents other than carbohydrates such as pyruvate, acetate, phosphate, and succinate [Andersson 2009]. A large amount of the EPS is more or less intensely hydrated. The

microcolonies in biofilms are separated by interstitial voids and channels containing mainly water. This liquid phase form the viscous part of the biofilm [Flemming & Wingender 2010]. Hence, the EPS provides the biofilm with mechanical stability and also influence the structure of the biofilm.

### 1.2.4 *Quorum sensing*

There are frequent changes in cell population density in different stages of biofilm formation and these changes leads to variations in gene expressions [Rutherford 2012]. These changes in gene expression are coordinated by bacterial communication by utilizing quorum sensing (QS) systems [Solano *et al.* 2014]. Quorum sensing (QS) is a bacterial cell–cell communication process that involves the production, detection, and response to extracellular signaling molecules called autoinducers (AIs) [Novick & Geisinger 2008]. The increase in bacterial population density to threshold level leads to the accumulation of AIs in the environment and these signals are monitored by bacteria to collectively alter gene expression. Gram-negative bacteria generally use acylhomoserine lactones (AHLs) for communication, which are small autoinducer molecules [Wei *et al.* 2011]. While gram-positive bacteria use autoinducing peptides (AIPs) as signalling molecules. Swarming mortality, rhamnolipids, and siderophores are some quorum sensing regulated processes in *P. aeruginosa* which contribute in its biofilm formation [Rahman *et al.* 2010]. Biofilm formation in *V. cholera* is also controlled by the quorum sensing system along with other factors [Zhao *et al.* 2013].

### 1.2.5 *Dispersal*

Dispersal of biofilm is optional and depends on requirement according to environmental changes. Although, passive dispersal can occur due to shear stresses. Bacteria have developed ways to judge the environmental changes and decide whether it is still beneficial to reside within the biofilm or it is time to resume a planktonic lifestyle. Environmental changes which can induce dispersal of biofilm include oxygen fluctuation, alterations in nutrient availability, increase of toxic products, or other stress-inducing conditions [Hong *et al.* 2010; Rowe *et al.* 2010]. Studies in *P. aeruginosa* have shown that EPS-degrading enzymes like alginate lyase contribute to detachment of bacteria from the matrix and the dispersal of biofilm [Yang *et al.* 2012]. Cell death may also serve as an additional factor for dispersal mechanism as it creates voids in biofilm and free some

bacteria which have the capacity to initiate the biofilm formation in presence of suitable environment.

### 1.3 Biofilm associated infectious disease

Bacterial biofilms are the cause of chronic infections as the cells in biofilms becomes 10-100 times more resistant to the effect of antimicrobial agents [Mah 2012]. The tolerance of biofilms to antibiotic is of major clinical relevance and studies are rapidly shedding light on bio-molecular pathways leading to sessile growth as well as on the mechanisms of biofilm resistance to antibiotics [Høiby *et al.* 2011; Nguyen *et al.* 2011]. Biofilms can grow on many medical implants such as sutures, contact lenses, catheters and cause infections, which can only be treated by removal of the implant. Thus, not only increasing the cost of treatment, but also becomes traumatic for patients having implants [Costerton *et al.* 2005]. Some of the major biofilm associated infections are listed in Table 1.1.

**Table 1.1** Biofilm associsted infection and diseases and their adherent surfaces

| **Bacterial species** | **Surface** | **Infection/Diseases** | **References** |
|---|---|---|---|
| ***Streptococcus* sp.** | Tooth surface<br>Vascular grafts | Dental caries<br>Endocarditis<br>Necrotizing fasciitis | Eshed *et al.* 2012;<br>Selwitz *et al*. 2007 |
| ***Pseudomonas aeruginosa*** | Contact lenses<br>Lungs<br>Middle Ear<br>Central venous catheters<br>Prostheses | Cystic fibrosis<br>Otitis media<br>Nosocomial infection | Huse *et al.* 2013;<br>Wiley *et al.* 2012 |
| ***Staphylococcus* sp.** | Middle ear<br>Sutures<br>Central venous catheters<br>Bones<br>Prosthetic heart valves<br>Prostheses<br>Surfaces/deep skin<br>Arteriovenous shunts | Otitis media<br>Mucoloskeletal infections<br>Nosocomial infections<br>Chronic wounds<br>Endocarditis | Arciola *et al.* 2012 |
| ***Enterococcus faecalis*** | Heart valves<br>Urinary catheter | Endocarditis | Minardi *et al.* 2012 |

| *Table 1.1 cont….* | | | |
|---|---|---|---|
| ***Mycobacterium tuberclosis*** | Lungs | Cystic fibrosis | Qvist *et al.* 2014 |
| ***Burkholderia cepacia*** | Lungs | Cystic Fibrosis | Zlosnik *et al.* 2012 |
| ***Escherichia coli*** | Urinary catheter<br>Urinary tract<br>Middle ear<br>Prostheses | Bacterial prostatitis<br>Urinary tract infection<br>Otitis media | Plotkin *et al.* 2014;<br>Jackson *et al.* 2002 |
| ***Enterococcus faecalis*** | Heart valves<br>Urinary catheter | Endocarditis | Minardi *et al.* 2012 |
| ***Haemophilus influnzae*** | Middle ear | Otitis media | Takei *et al.* 2013 |

(Adapted from de la Fuente-Núñez *et al.* 2013)

### 1.4 Gram-positive bacterial biofilms and clinical relevance

Many chronic infections are related to biofilms of gram-positive bacteria. Gram-positive biofilm forming bacteria include microbe like *Staphylococcus aureus, Streptococcus mutans, Enterococcus faecalis*. The infections caused by these microbial biofilm are very difficult to treat by current antibiotic therapies.

#### 1.4.1 *Streptococcus mutans*

*Streptococcus mutans* is a gram-positive anaerobic bacterium that inhabits mouth and can survive in temperature range of 18-40˚C. It is long chained coccobacillus with oval shape. *Streptococcus mutans* is one of the most persistently perceived microorganisms on the tooth surface and is a crucial etiological agent of human dental caries [Hasan *et al.* 2012]. It has various unique virulence factors which helps in the development of caries. It adheres to the dental surface by virtue of exopolysaccharide production (EPS). Furthermore, it can produce acid and can survive in acidic condition which makes *S. mutans* dominant bacterium in low pH conditions. In the presence of sucrose it forms a biofilm which is very difficult to eradicate and cause dental caries.

### 1.4.1.1 Virulence factors of *S. mutans*

**(A) *Adherence***

The attachment of *S. mutans* to the tooth surface occur via two modes sucrose dependent and sucrose independent. The initiation of adherence to the enamel pellicle is sucrose independent while establishment and the colonization of *S. mutans* biofilm on dental enamel is mediated by sucrose dependent means.

**a) Sucrose-independent adherence**

Sucrose independent adherence of *S. mutans* is mainly influenced by surface protein *Spa P*, which is a protein of Antigen I/II family with molecular weight of 185 kDa. It has been assigned with various names like P1, Sr, Pac and antigen B [Hasan *et al.* 2014]. Its interaction with salivary components is known to eventualize by its alanine-rich and proline-rich domains [Sullan *et al.* 2015]. Heim *et al.* demonstrated that mutant lacking N and C termini of *S. mutans* P1 (antigen I/II) have lower binding abilities as compared to wild type [Heim *et al*. 2013]. Thus, *SpaP* plays an important role in sucrose independent adherence. Process of initial adherence of *S. mutans* to pellicle surface is summarized in Figure 1.3.

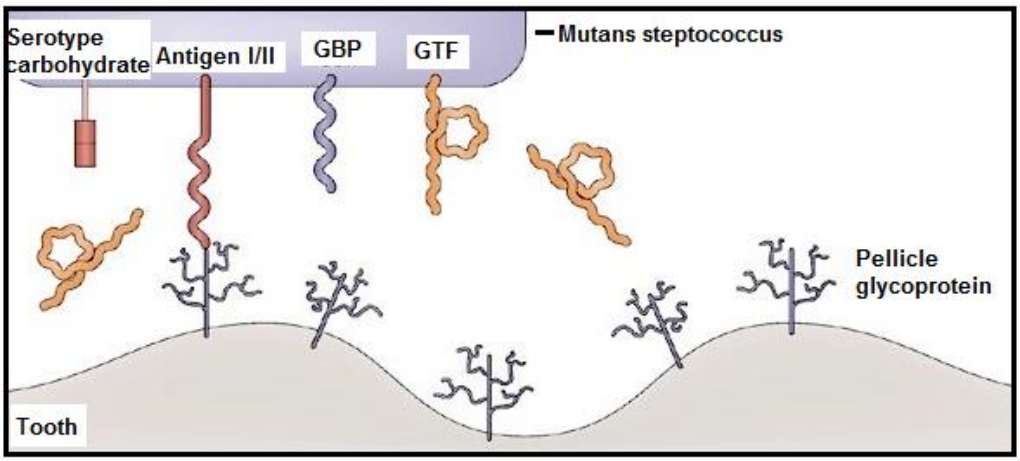


**Figure 1.3** Process of initial adherence of *S. mutans* to the tooth pellicle surface: *SpaP* or Antigen I/II interact with the pellicle glycoprotein.
(Source:http://www.nature.com/nri/journal/v6/n7/images/nri1857-f1.jpg, modified)

**(b) Sucrose-dependent adherence**

Glucan synthesis by action of glucosyltransferases (GTFs) is the main mechanism behind sucrose-dependent adherence. Enzymatic activity of GTFs can cleave the sucrose into glucose and fructose [Bowen *et al*. 2011]. The glucose is then utilized to form glucans (Figure 1.4). Three types of GTFs are identified in *S. mutans* encoded as GTF B, GTF C and GTF D. They collectively synthesize water soluble and water insoluble glucans. α-1,3-linked glucan are synthesized by GTF B while GTF D produces α -1,6-linked glucan and GTF C synthesizes both the types of glucans. Hydrogen bonding of glucan to salivary pellicle and bacteria facilitate the process of adherence [Sharma *et al.* 2014]. Along with GTFs other non-enzymatic glucan binding proteins (GBPs) are also reported to be playing role in sucose-dependent adherence.

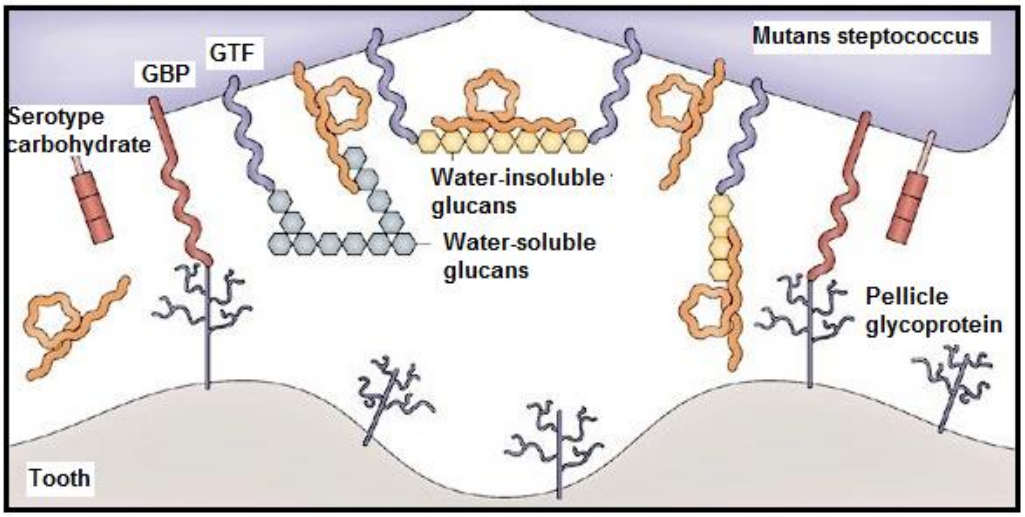


**Figure 1.4** Sucrose-dependent adherence of *S. mutans*: Formation of water soluble and water insoluble glucans.

(Source:http://www.nature.com/nri/journal/v6/n7/images/nri1857-f1.jpg, modified)

**(B) *Carbohydrate metabolism***

The metabolism of carbohydrates is considered as major virulance facter of *S. mutans*. Along with GTFs other facters which help in metabolism of sucrose and glucans include fructosyltransferase (Ftf), an extracellular dextranase (DexA), a fructanase (FruA), and proteins responsible for intracellular polysaccharide accumulation (Dlt1-4). Fructosyltransferase or Ftf catalyzes the synthesis of fructans and acts as an energy reservoir. Fructanase or FruA may break down fructans for energy use [Smith *et al.*

2012]. Extracellular dextranase or DexA possibly help in the glucan synthesis or may be in the breakdown of glucans [Kim *et al.* 2011] and Dlt1-4 helps in accumulation of intracellular polysaccharide and aids in energy reserve [Mazda *et al.* 2012].

**(C) *Acidogenecity and Acid tolerance***

*S. mutans* is an anaerobic bacteria and can produce acid by fermentation of glucose . The major product of its glycolytic pathway is lactic acid. The rate of acid production by *S. mutans* is mostly higher than other *Streptococci* [de Soet *et al*. 2000]. Figure 1.5 reperesents the process of acid production and formation of dental cavities by *S. mutans*.

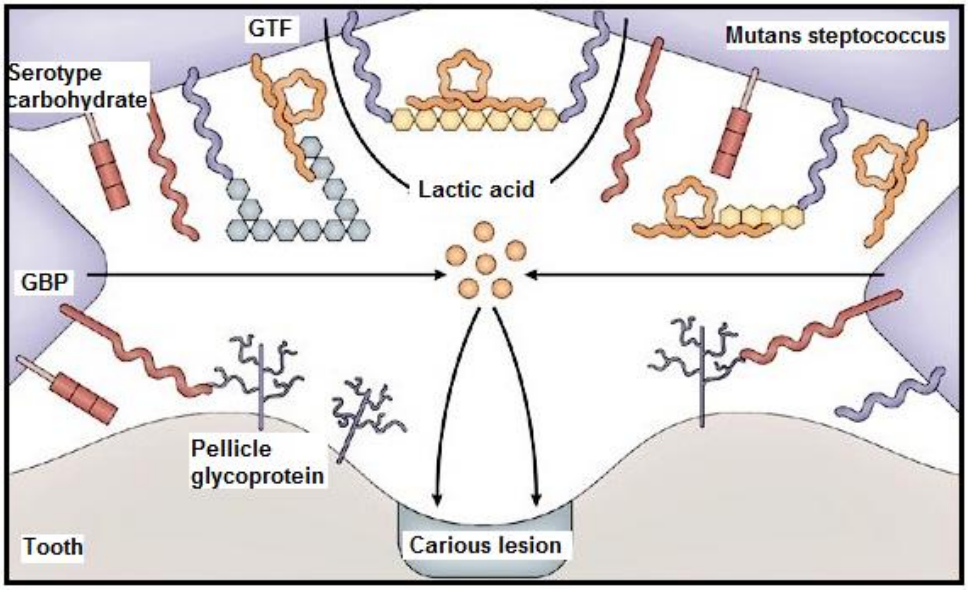


Figure 1.5 Process of acid production by *S. mutans* leading to development of carious lesion on the tooth surface.
(Source:http://www.nature.com/nri/journal/v6/n7/images/nri1857-f1.jpg, modified)

By virtue of this property, *S. mutans* creates a change in ecology in the plaque flora which further increase the proportion of other acidogenic species and eventually considerably decrease the pH of the region, which results in demineralization of tooth and formation of dental cavities. Sustained pH value below 5 favors demineralization of tooth. Along with the property of acid production another factor unique to *S. mutans* is acid tolerance. It sustains its glycolytic strength at even very low pH levels (close to pH 4.4), that distinguishes *S. mutans* from other *Streptococci* [ Li *et al.* 2014]. There are evidences that acid-tolerance is enhanced by the synthesis of water-insoluble glucans and biofilm

formation. *S. mutans* cells within a biofilm have better capability to survive an acid challenge than their planktonic counterpart [McNeill *et al.* 2003].

**(D) *Quorum sensing (QS)***

The quorum sensing is initiation of intercellular response due to accumulation of signalling compounds which regulate the expression of specific genes, thus providing biofilms distinct properties for their unhindered survival [Solano *et al*. 2005]. The QS system contributes in the regulation of many physiological activities related to biofilm differentiation and stress management in *S. mutans*. There are two main QS system in *S. mutans* that coordinate to deal with the stresses and biofilm formation. The first one is competence regulon, that require signalling molecule (low molecular weight peptide) which is sensed by two component regulatory systems. Li *et al.* reported that inactivation of *comD* and *comE* imparted acid sensitive phenotype to *S. mutans* and resulted in the reduced biofilm formation [Li *et al.* 2001; Li *et al.* 2002]. Another QS is widely distributed *luxS* system, which produces AI-2, a furanosyl borate diester [Goldstone *et al.* 2012] that regulates a large panel of genes in a variety of microorganisms.

### 1.4.1.2 Biofilm of *S. mutans* and dental caries.

These virulance factors and stress responses aids in biofilm development and stress tolerance in *S. mutans*. These factors also facilitate *S. mutans* in cariogenesis resulting in dental caries. Figure 1.6 shows the process of caries initiation and demineralization of tooth surface. Dental caries is also termed as tooth decay, is an infection of bacterial origin. The caries develope due to demineralization of dental enamel by acids produced by fermentation of sugars and other starchy material accumulated on tooth suface by microbes [Marsh 2010]. Process of tooth decay begins by formation of thin layer of bacterial biofilm on tooth surface called plaque which further produce acid by fermentation of sugars. These acids demineralise the upper layer of enamel, the progression of cavity occur by spread of the infection through the enamel and subsequent formation of caves in the tooth surface. If left untreated it may decay further and enter dentin followed by dentinal tubule until they reach pulp. After reaching pulp it can spread and form an apical abscess which can be extremely painful [Hasan *et al.* 2012; Filoche *et al.* 2010].

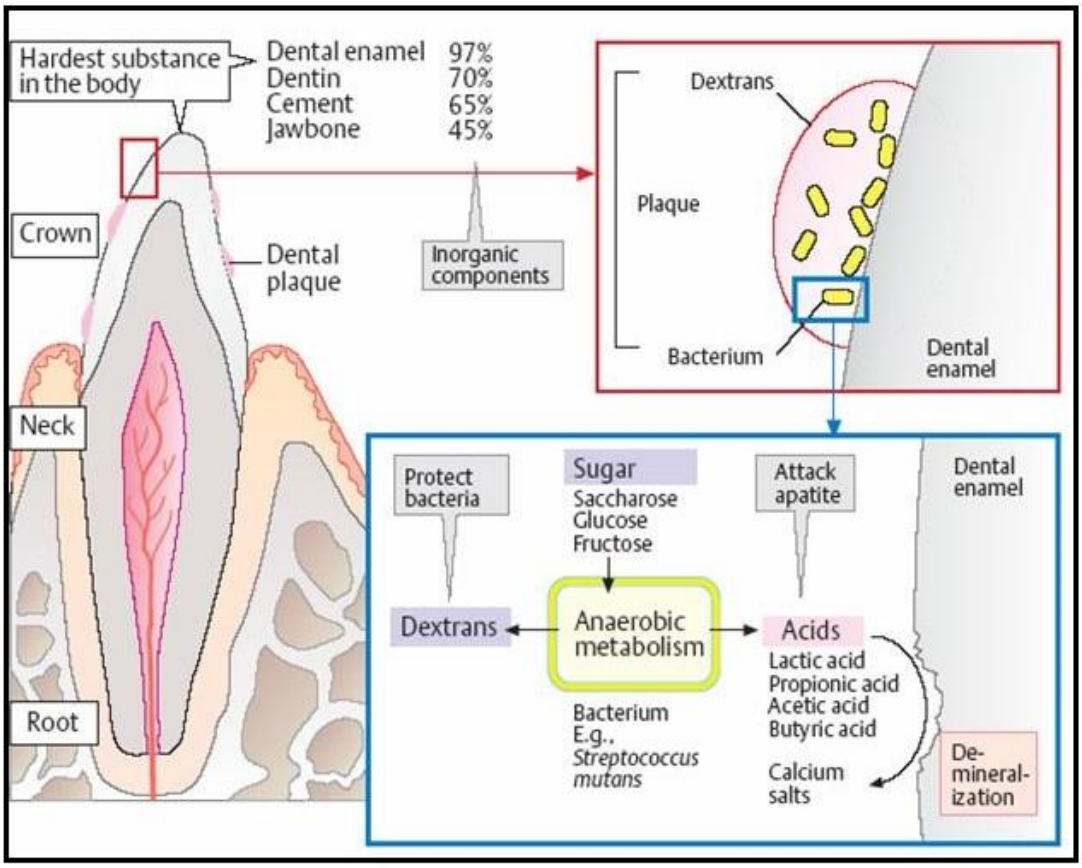


**Figure 1.6** Demineralization and initiation of carious lesions by bacterial biofilm. (Source:http://intranet.tdmu.edu.ua/data/kafedra/internal/chemistry/classes_stud/en/stomat/ptn/2/13.%20Biochemistry%20of%20connective%20tissue.files/image034.jpg)

### 1.4.1.3 *S. mutans* and infective endocarditis: risk of mortality

Infectious endocarditis is an infection of the cardiac tissue that initiate when several species of microorganisms attach to cardiac tissue. Endocarditis may cause morbidity and mortality [Hasan *et al*. 2012]. Certain oral *streptococci* have been proven to stimulate platelet aggregation, a trait that is thought to be important in the pathogenesis of streptococcal mediated infective endocarditis [Jung *et al.* 2012]. Development of the infective vegetation causes local myocardial abscess that inhibits the valvular function, and ultimately results in congestive heart failure [Biswas *et al.* 2010].

### 1.4.2 *Staphylococcus aureus*

*Staphylococcus aureus* is a gram-positive bacterial species which lives in human anterior nares as commensal [Ellis *et al.* 2014]. Due to its presence in nasal region there are increased risk of its dissemination to other areas and formation of biofilms which are major cause of nosocomial and other chronic infections [Wunderink *et al.* 2012]. *S. aureus* have abilities to produce multilayered biofilms enclosed within slimy glycocalyx with heterogeneous protein expression throughout. It has been reported that main components of its glycocalyx are techoic acid, staphylococcal and host proteins and polysaccharide intercellular antigen (PIA). Infections caused by *S. aureus* biofilm accounts for 25% of all mortalities in US [Archer *et al.* 2011]. Its biofilms are unmanageable by antimicrobial treatment and the host response, as a result are the etiological agent of many persistent infections. Diseases associated with *S. aureus* biofilm includes

**(A) Osteomyelitis**

*S. aureus* has been found to be one of the culprit behind osteomyelitis along with other bacteria. When bacteria invade the host it starts producing adhesins (e.g., fibrinogen, fibronectin, osteopontin, elastin, collagen etc.) in its planktonic mode and on adherence to localized area of trauma in bone it start dividing to form early biofilm. Further, with the help of quorum sensing it forms mature biofilm [Hwang *et al.* 2015]. Figure 1.7 summerizes the process of biofilm formation by *S. aureus* and its maturation and dispersal.

**(B) Implant based infections**

Orthopedic implants are prone to *S. aureus* biofilm infection. These include wires, screws, prosthetic joints, plates, external fixaters and mini large fragment implants. Apart from this other medical device on which its biofilm grows are ventilators, catheters, mechanical heart valve, pacemaker, penile implants and many more [Costerton *et al.* 2005]. Its biofilm grows on the implant, producing an enormous amount of exopolysaccharide and can only be treated by removal of the implant.

**(C) Chronic wound infection**

*S. aureus* is most commonly isolated bacteria from the chronic wound infection like, venous stasis ulcers, diabetic foot ulcers and pressure sores. Studies involving diabetic foot wound patients found that, the presence of *S. aureus* biofilm increase the healing time 2 fold [Bowling *et al.* 2009]. Likewise, it has been reported that re-epithelialization is delayed in presence of *S. aureus* biofilm and thus increasing the healing time [Schierle *et al.* 2009].

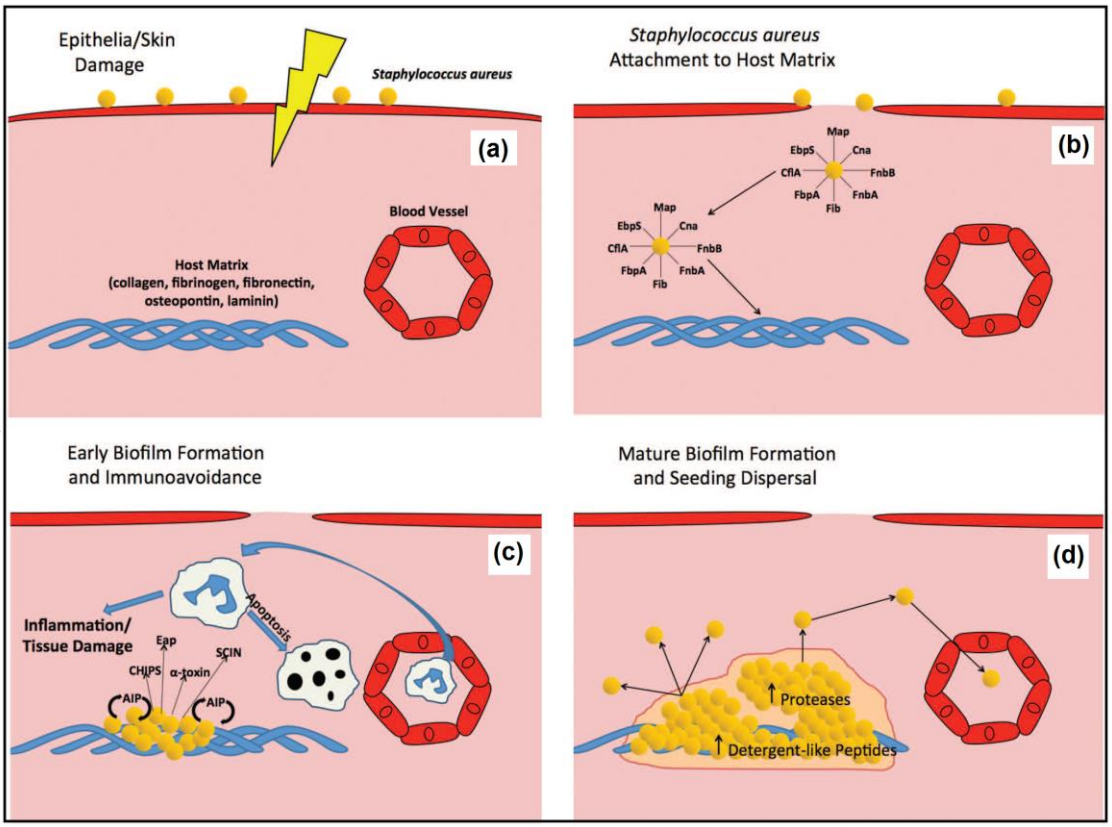


**Figure 1.7** (a) *S. aureus* invades the epithelial layer by damaged region (b) Binds to host matrix (c) Initial attachment produces an early *S. aureus* biofilm and avoids immunological destruction (d) The large biofilm aggregates detach releasing planktonic bacterial cells which migrate into the circulatory system and adhere to to distal tissues forming biofilm again. (Source: Archer *et al.* 2011; modified image)

**(D) Ocular infection**

Keratitis, conjunctivitis and endopthalmitis are some of the ocular infections associated with *S. aureus* biofilm [Murugan *et al.* 2010]. Methicillin resistant *S. aureus* cultures have

been commonly isolated from patients suffering from severe ocular infections. Moreover, *S. aureus* bacterial biofilm is the second most frequent reasons of post-operative endopthalmitis [Leid *et al.* 2002].

### 1.4.3 *Enterococci spp.*

*Enterococci* are documented as opportunistic pathogens with their natural niche being normal intestinal flora, oral cavity and female genital tract. *Enterococcus faecalis* and *Enterococcus faecium* are most frequently detected enterococcal species. They are associated with prevalent hospital-acquired diseases that infect bloodstream, urinary tract, pelvic region and surgical sites [Paganelli *et al.* 2012]. *Enterococcus faecalis* accounts for 80-90% of human enterococcal infection [Jones *et al.* 2004]. Both these bacteria have been found to form biofilm on response to environmental and genetic factors. Its biofilm can adhere to various medical devices (silicone gastrostomy devices, biliary stents, intravenous catheters) and are cause of infection and implant removal. *E. faecalis* have been reported to form biofilm on ocular lense materials like silicon, acrylic and polymetmethacrylate [Miller *et al.* 2011].

## 1.5 Gram-negative bacterial biofilms and clinical relevance

The most common gram-negative biofilm forming bacteria are *Pseudomonas aeruginosa*, *Escherichia coli* and *Enterobacter cloaceae.* They are generally found associated with device related infections like catheters and urinary tract infections. The fundamental steps of biofilm formations are similar to gram-positive bacteria *i.e.* adhesion, exopolysaccharide formation, maturation and dispersal.

### 1.5.1 *Pseudomonas aeruginosa*

*Pseudomonas aeruginosa* is opportunistic gram-negative bacterium and is common casue of nosocomial infections. It is most studied single-species biofilm forming microbe [O'Toole *et al.* 2000]. It predominantly lives in biofilm form and is responsible for many acute and chronic infections [Høiby *et al.* 2010]. The bioflm lifestyle is triggerred by presence of adhering surface and environmental stresses. The hardness of biofilm and antibiotic resistance make the clearance of these biofilm difficult, thus, becoming a prevalent problem in hospital settings [Peleg & Hooper 2010]. Infections caused by *Pseudomonas aeruginosa* include :

**(A) Cystic Fibrosis**

Cystic fibrosis (CF) is autosomal recessive disorder and is caused by mutation in cystic fibrosis trans-membrane conductance regulator (CFTR). CF patients are prone to *P. aeruginosa* biofilm related respiratory tract infection [Rudkjøbing *et al.* 2012]. Figure 1.8 gives a overview of *P. aeruginosa* biofilm development in cystic fibroses patients.

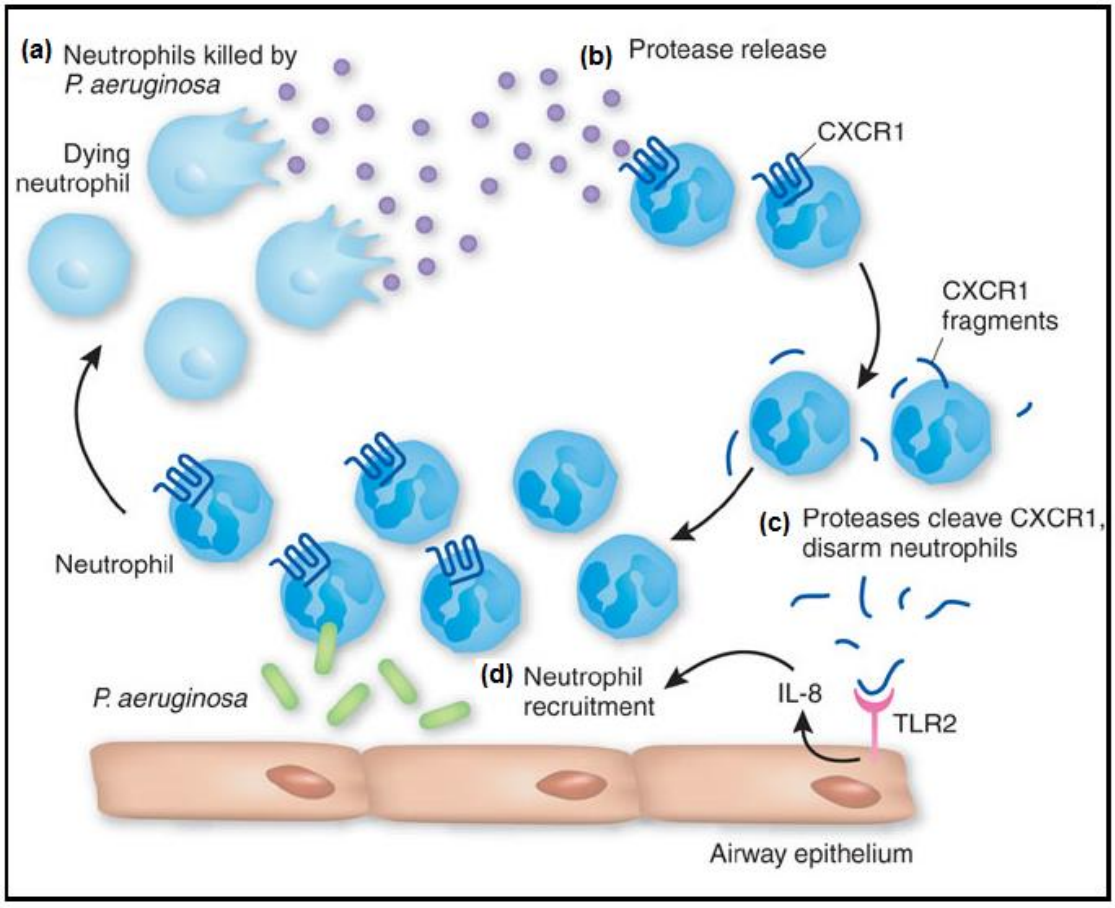


**Figure 1.8** (a) *P. aeruginosa* products cause neutrophil death (b) Proteases are released that may cause inflammation and tissue damage (c) They also cleave CXCR1 from the surface of any viable neutrophils (d) This cleavage reduces neutrophil induced killing and final dysregulation of chronic inflammatory response in which the bacterium is able to persist (Source:http://www.nature.com/nm/journal/v13/n12/images/nm1207-1417-F1.jpg)

*P. aeruginosa* initially colonize in paranasal sinuses and substequently infect the lower respiratory tract [Burns *et al.* 2001]. The presence of *P. aeruginosa* in lungs of CF patients initiate inflammatory response mainly polymorphonuclear leukocytes (PMNs). The released PMNs produce huge quantities of enzymes and free radicals, which results

in degradation of the matrix and elastic tissues of bronchi and bronchioles [Jensen *et al.* 2007]. *P. aeruginosa* produce compounds which can lyse PMNs thus this property make bacteria resistant to attack of PMNs. During its activity in bronchiole PMNs release DNA in airway, which is used by bacteria as a component of biofilm matrix. This process increases the biofilm along with that, the reduction of the mucociliary clearance, elevate the microbial densities (~ $10^{11}$/ml of sputum) [Høiby *et al.* 2001]. This further leads to chronic bronchitis, mucopurulent plugging of bronchiole, fibrosis and eventually respiratory failure [Hassett *et al.* 2010].

**(B) Chronic otitis media (COM)**

Otitis media is infection of the middle ear and is most prevalent childhood infection worldwide. In some cases this infection results in conductive hearing loss [Rovers *et al.* 2004]. Acute otitis media is caused by several microbial species like *Moraxella catrrhallis, Heamophilus influenza* but chronic otitis media (COM) is predominantly caused by *P. aeruginosa* biofilm [Verhoeff *et al.* 2006].

### 1.5.2 *Escherichia coli*

*Escherichia coli* is a gram-negative, facultative anaerobe, it is ubiquitous microbe generally found in the lower intestine of warm blooded animal. *E. coli* has been used as a model organism for in-vitro investigation of biofilm on abiotic surfaces [Van Houdt *et al.* 2005]. K-12 strain of *E. coli* possesses many cell surface components that assist in biofilm formation and adherence. These cell surface components include flagella, colanic acid, outer membrane proteins, poly (β-1,6-GlcNAc) and type I fimbriae [Reisner *et al.* 2003]. *E. coli* is associated with diarrheal diseases and various extraintestinal infections, which comes under many categories of biofilm-associated infections [O'Toole *et al.* 2000]. It is a frequent cause of recurrent urinary tract infections (RUTIs) [Ejrnæs 2011]. Figure 1.9 represents the process of invasion and spread of *E. coli* biofilm in urinary bladder cells, leading to recurrent urinary tract infection. Along with UTI its biofilm has been found associated with acute otitis media and surgical device related infections [Fux *et al.* 2005]. Antibiotic resistance in *E. coli* along with biofilm formation makes treatment of associated infection very difficult.

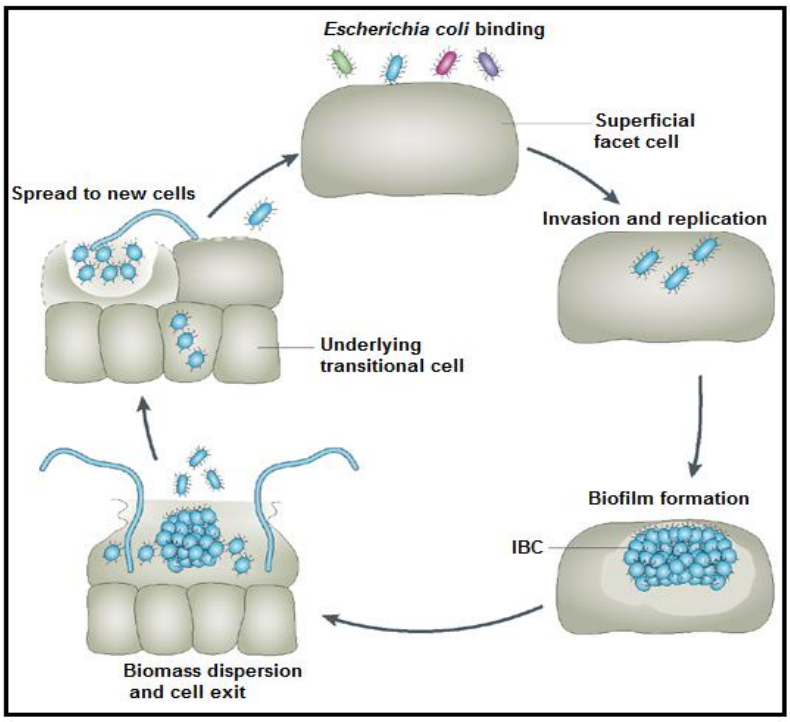


**Figure 1.9** *E. coli* invade the that line the bladder lumen, where they multiply to form a biofilm-like intracellular bacterial community (IBC), they thrive there for months and form complex biofilm, they spread in nearby tissues by dispersal of biofilm. (Source:http://www.nature.com/nrmicro/journal/v6/n1/images/nrmicro1818-f1.jpg)

### 1.5.3 *Enterobacter spp.*

*Enterobacter* is a genus of family Enterobacteriaceae. They are gram-negative, facultative anaerobic bacteria. Sewage, soil and human gastrointestinal tract are their natural ecological niche. The group Enterobacter cloacae complex (ECC) has six species, namely, *E. cloacae*, *E. asburiae* , *E. kobei*, *E. hormaechei*, *E. ludwiggii* and *E. nimipressuralis* [Ahmed & Ceroni 2013] . They are associated with nosocomial infections and are chief cause of pneumonia, post surgical peritonitis and urinary tract infections. All these bacteria have the ability to produce biofilm and have antibiotic resistance [Kim *et al.* 2012]. Among the ECC group bacteria, *E. cloacae* is most commonly found from neonatal units of hospitals. *E. cloacae* is associated with contamination of various medical devices and its nosocomial outbreaks have been connected to its biofilm formation on surgical devices [Dalben *et al.* 2008]. One of the prominent reservoir of *Enterobacter cloacae* is a heparin solution used to irrigate certain intravascular devices

continually. This fluid had been indicted as a reservoir for device-associated infections [Musil *et al.* 2010].

### 1.6 Antibiotic resistance in biofilm

The complexity and heterogeneous nature of biofilm suggest that there are likely to be numerous mechanisms of antibiotic resistance at work within a single community (Figure 1.10). These mechanisms differ according to the bacteria forming the biofilm and the type of antibiotic. These mechanisms include diffusion barrier, slow growth rate, activation of stress response, heterogeneity, presence of 'persisters' and origin of biofilm specific phenotype.

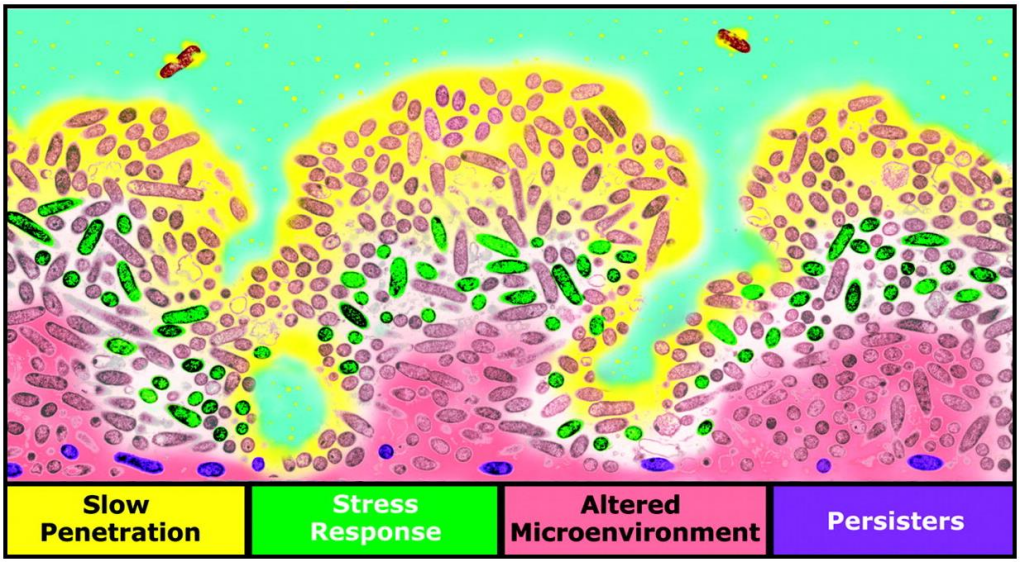


**Figure 1.10** Mechanisms of antibiotic resistance in biofilm.
(**Source**:http://aem.asm.org/content/72/3/2005/F1.large.jpg)

#### 1.6.1 *Inefficacy of antibiotics to penetrate biofim*

Impenetrability of microbial biofilm during antimicrobial treatment is suggested the prime cause to sustenance of microbial infection. This retardation or imperviousness assumed to be caused by biofilm matrix. The matrix of biofilm is composed of exopolysaccharides called glycocalyx and it is reckoned to be preventing the approach of antibiotics to the bacterial cells embedded in biofilm [de la Fuente-Núñez *et al.* 2013]. This limited penetration may be either due to the reaction of antimicrobial agent to biofilm matrix component or adsorption of these compound to the matrix. In their study

Tseng *et al.* reported that rate of transport of tobramycin reduced in biofilm colonized surface as compared to sterile surface and they suggested that this hinderance is due to binding of tobramycin to the biofilm components [Tseng *et al.* 2013].

### 1.6.2 *Slow growth and stress reponse*

The cells in deep layers of mature biofilm experience nutrients limitation and this nutrient starvation leads to slow growth rates. This starvation induced stationary phase is generally connected with the resistance to antibiotics [Nguyen *et al.* 2011]. Studies have reported that growth rates of bacterial cells directly affect the sensitivity of antibiotics, with an increase in growth rates, sensitivity of antibiotics also increases [Lebeaux *et al.* 2014; Olsen *et al.* 2015]. Slow growth rate transforms planktonic bacteria to less susceptible phenotype which account for biofilm resistance to antibiotics. Furthermore, metabolic inactivity force bacteria to actively adapt to stress. In presence of environmental stresses bacteria can turn on stress-response genes. Bacteria under stress condition encode various sigma factors like RpoS. These genes protect bacteria from killing by environmrntal toxins, antibiotics and other adverse conditions. RpoS mRNA has been reported to be present in sputum of cystic fibrosis patient having chronic biofilm of *P. aeruginosa* [Wei & Ma 2013].

### 1.6.3 *Heterogeneity*

The bacterial cells within the biofilm experience a nutrient gradient due to which cells in each layer of biofilm have different physiology. The generation of secondary metabolites, waste products and signalling factors forms a chemical gradient which results in stratification in biofilm. Chemical gradients may interact and overlap forming numerous microenvironments inside the biofilms. Due to this heterogeneity cells respond and adapt to their local environmental condition. Furthermore, mutations, recombination and other genetic alterations that produce sub populations which are different in phenotype and genotype [Xiao *et al.* 2012; Williamson *et al.* 2012]. Thus, the antibiotic susceptibility greatly differ, depending on the microenvironment of cell in biofilm. Gu *et al.* reported that biofilm cells show structural heterogeneity and the shape vary according to the location of cells in biofilm [Gu *et al.* 2013]. Figure 1.11 shows the different hypothesis proposed for antibiotic resistance in biofilm including heterogeneity.

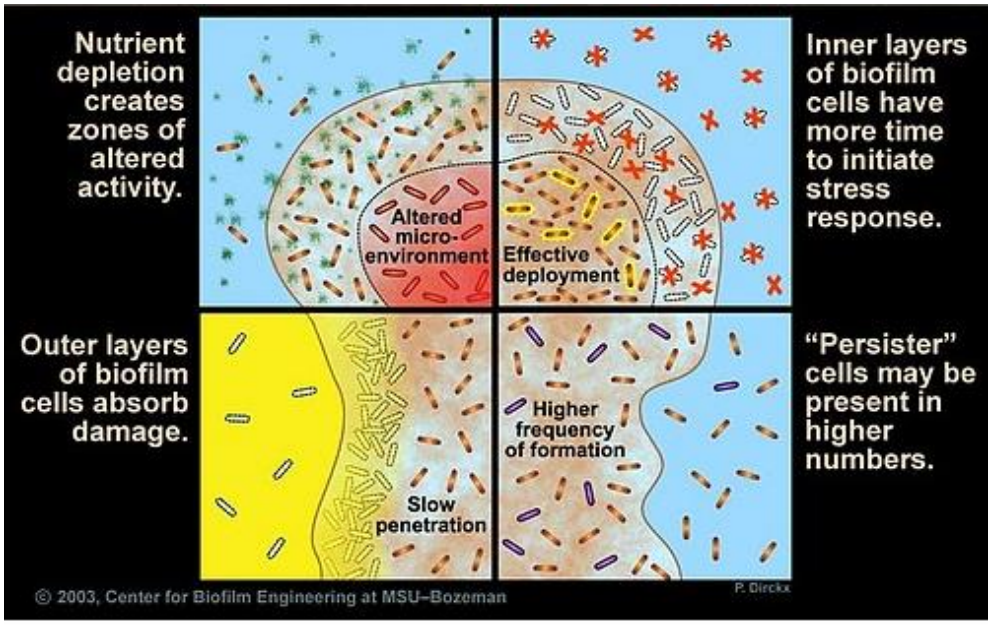


**Figure 1.11** Hypothesis for antibiotic resistance in biofilm.

(Source:https://www.biofilm.montana.edu/files/CBE/images/CBE03_MultiDefens.preview.jpg)

### 1.6.4 *Persisters cells*

Bacterial cell microcolony which become tolerant to antibiotics behave like highly resistant cells in free floating cultures and these bacterial cells were termed as "persisters" [Lewis 2010]. Persisters population occupies <0.1% of total infectious bacterial population. The concept of persisters is based on the hypothesis that antibiotics cause damage that initiate programmed cell death in bacteria, but some subpopulation of bacteria come in non growing state and inhibit the programmed cell death thus, surviving in the presence of antibiotics. These cells display dormancy like situation and remain dormant at adverse environment conditions. Consequently, these cells maintain the contingency plans during adverse condition, and maintain the cells survival and their morphological stability. Hence, persisters increased the anti-biofilm compound tolerance level. It was reported that *E. coli*, *S. aureus* and *P. aeruginosa* in stationary phase have more persisters as compared with log phase bacterial cells [Percival *et al.* 2011]. Several studies have addressed the presence of persisters among bacterial population [Amato & Brynildsen 2014; La Fleur *et al.* 2006]. On the molecular level, it was suggested that the over expression of dormancy genes results the survival of persisters [Wu *et al.* 2012].

## 1.7 Nanoparticle based therapies

Nanotechnology has emerged as a new frontier for development of novel therapeutic approaches. It is a multidisciplinary field which uses the principals of chemistry, biology and physics to intend and form nanoscale devices [Farokhzad & Langer 2009]. In its rigid definition nanotechnology entails the synthesis and manipulation of structures in the size range of 1-100 nm in at least one dimension [McNeil 2011; Ochekpe 2009]. The particles in this size range have a unique capabilities based on their physicochemical properties, which are very different from particles of macroscopic, microscopic or atomic size. These physicochemical properties of nanoparticle influence their interaction when they come into contact with biological system. Furthermore, many biological phenomena such as immune recognition and passage across biological barrier are governed by size consideration [Parboosing *et al.* 2012; Armstead & Li 2011]. Conventionally used therapeutic treatments have limited cellular penetration and poor retention. At present there is need for the advanced treatment method. Drugs designed on nanoscale may confer all these pharmacological advantages as compared to conventional agent. The amalgamation of knowledge of nanoparticle with resent understanding of molecular and cellular function may let to the development of novel and superior 'nanodrugs'.

### 1.7.1 *Nanoparticles to combat antimicrobial resistance*

Nanoparticles based therapeutics have potentials to replace antibiotics. They have properties to combat multidrug resistance and biofilm based resistance where, antibiotic treatments are unsuccessful [Pelgrift & Friedman 2013; Huang *et al.* 2010]. In present scenario, several nanoparticles are being used as antimicrobials like organic nanoparticles, metal nanoparticles, metal oxide nanoparticle and their various combinations. The antibacterial mode of action of these nanoparticle varies greatly (Figure 1.11) [Baek & An 2011]. Factors which determine the mode of action of nanoparticles include diverse intrinsic and chemical properties, physicochemical properties of nanoparticles (shape, size, chemical modification), genetics, cell wall structure, metabolic pathways of target bacteria, physiological state of bacteria (planktonic cells, biofilm cells, stationary or starved cells), the ratio between bacteria and nanoparticle is critical for its toxicity and environmental factors like aeration, pH and temperature.

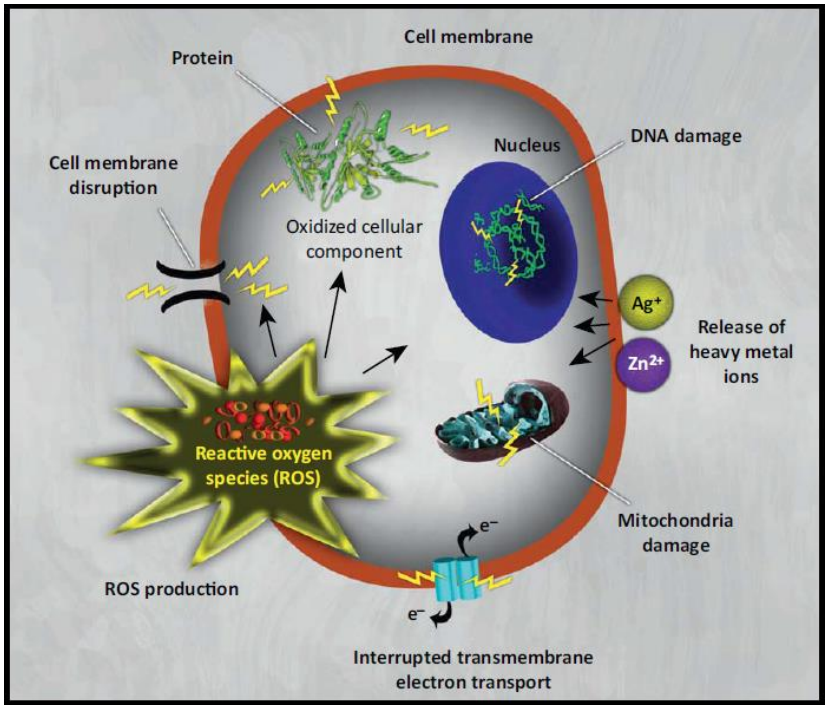


**Figure 1.12** Antibacterial mechanism of nanoparticles. (Source: Hajipour *et al.* 2012, modified image)

The factors affecting the antibacterial mode of activity of nanoparticles are complex, thus there are many contradictory reports about the suggested mode of action of nanoparticles [Hajipour *et al.* 2012]. Broadly, there are two major antibacterial pathways suggested for antibacterial activity of nanoparticles, which include

### 1.7.1.1 Disruption of membrane integrity

Nanoparticle can damage the bacterial membrane by binding with it electrostatically**,** this may lead to changes in membrane potential, depolarization of membrane and overall loss of membrane integrity. This may further result in impaired respiration, unbalanced translocation of materials, loss of energy transduction and finally cell death [Beyth *et al.* 2015].

### 1.7.1.2 Reactive oxygen species formation (ROS)

Various reports revealed that certain nanomaterials have property to exhibit spontaneous ROS production while other nanoparticles generate ROS only in the presence of selected cell systems. This is based on material composition and surface features of nanoparticles [Xia *et al.* 2006]. Reactive oxygen species (ROS) production is one of the primary

mechanisms by virtue of which nanoparticle affects the bacterial cell functioning [Premanathan *et al.* 2011]. When the ROS production by nanoparticles exceeds the capacity of the cellular antioxidant defense system, it can cause oxidative stress which can further initiate lipid peroxidation, thus damaging the cell membranes and eventually leading to cell death [Lovrić *et al.* 2005].

### 1.7.2 *Broad categories of antimicrobial nanoparticles*

Based on their composition there are mainly two types of nanoparticles used in antibacterial therapies organic and inorganic nanoparticles.

#### *1.7.2.1 Organic nanoparticles*

These nanoparticles are generally polymeric and lipid based (Figure 1.21) and show their antibacterial effect by release of entrapped or attached antibiotic, antibacterial peptides and other agents which can affect the bacterial viability [Beyth *et al.* 2015].

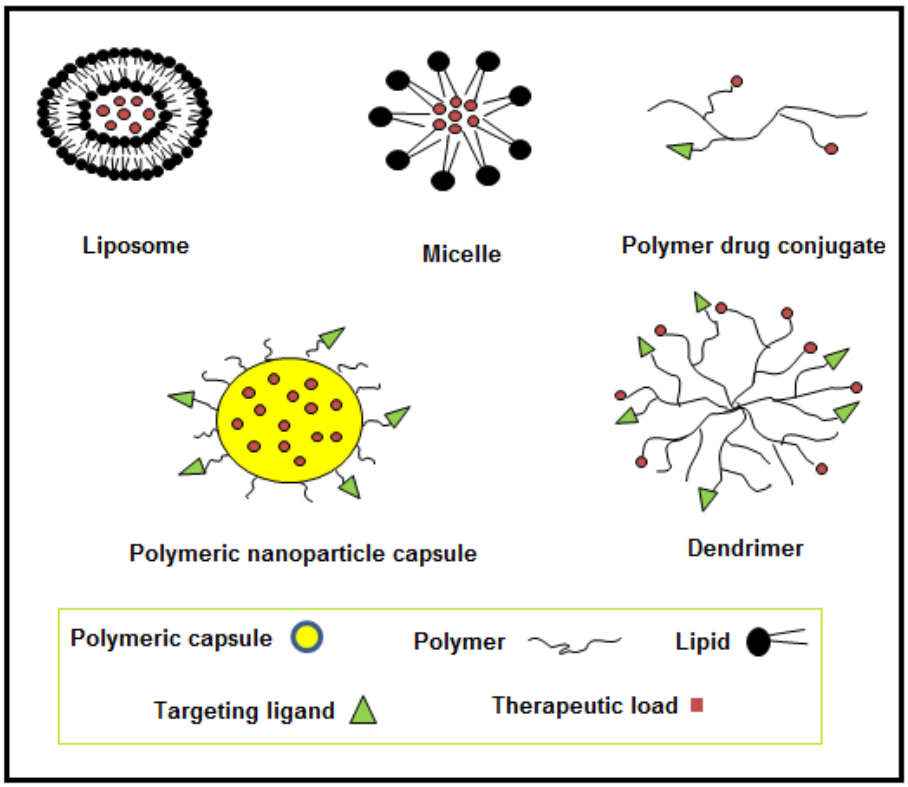


**Figure1.13** Types of organic nanoparticles

Another way is by contact killing of bacteria due to cationic surfaces of nanoparticle like chitosan, quaternary ammonium compounds and many more. Various mechanisms have been proposed for antibacterial action of cationic groups present on nanoparticle surface. Which primarily include bursting and penetration of bacterial membrane by hydrophobic chains *via* ion exchange between bacterial membrane and charged surface [Licher & Rubner 2009].

**(A) *Chitosan nanoparticles***

Chitosan is derivative of chitin, which is a long polymeric chain of N-acetyl-glucosamine residues. Deacetylation of chitin at random monomer residue results in formation of chitosan. The protonation of deacetylated amino groups of chitosan at pH lower than 6.5, provides it a positive charge [Friedman 2013]. Persuing this positive charge chitosan has property to associate with negative charge surface of bacteria causing osmotic damage by increased permeability of bacterial membrane [Huang *et al.* 2011]. Chitosan can also bind to DNA and inhibit transcription and translation, it can chelate the metal ions and reduce the activity of metalloproteins [Huh & Kwon 2011]. The formulation of chitosan into nanoparticles increases its antibacterial activity. As compared to chitosan its nanoparticles have been reported to be having a good solubility *in vivo*, furthermore, high surface to volume ratio of nanoparticles increases the density of positive charge on its surface, hence elevating the frequency of microbial attachment to its surface [Blecher *et al.* 2011]. Chitosan nanoparticles have been reported to possess greater efficacy against *S. aureus* and *E. coli* compared to chitosan alone [Freidman 2013]. Nanoparticles having high molecular weight chitosan have greater antibacterial activity against gram-positive bacteria while low molecular weight chitosan nanoparticles have higher antibacterial efficacy against gram-negative bacteria [Huh & Kwon 2011]. It has been suggested that chitosan nanoparticle might be more effective against gram-negative bacteria as it can displace calcium and magnesium ions which can destabilize the lipopolysaccharide membrane of gram-negative bacteria, thus increasing its permeability [Pelgrift & Friedman 2013] .

**(B) *Quaternary ammonium compounds (QACs)***

The disinfectant properties of QACs are well known [Buffet-Bataillon *et al.* 2012]. The antibacterial properties of these compounds are due to the presence of n-acetyl side chain. The length of its side chain determine the antibacterial activity, chain length having 12-14 alkyls is sufficient to kill gram-positive bacteria while for gram-negative bacteria optimum length required is 14-16 carbon [Thorsteinsson *et al.* 2003]. They denature structural enzymes and protein by interacting with the bacterial membrane and integrating its hydrophobic tail in the bacterial hydrophobic membrane core. Beyth *et al.* have reported the antibacterial activity of dental composite containing quaternary ammonium polyethylenimine nanoparticles against dental pathogen *S. mutans*. The mechanical properties of these composite were comparible to the original composite and they showed remarkable and sustained antibacterial activity [Beyth *et al.* 2006].

**(C) *Liposomes***

Liposomes are molecule of ampiphilic lipids that assemble to form bilayered spherical vesicles. The common building blocks of liposome are phosphatidyl ethanolamine and phosphatidylcholine. Liposomal membrane may frequently incorporate cholesterol, which improves their stability and rigidity [Couvreur & Vauthier 2006]. The liposomal formulation is able to change surface charge properties by changes in pH of the solution. The charge switch at acidic pH results in its fusion with the cell membrane during endocytosis uptake, allowing the escape of the nanocarriers into the cytoplasm to deliver the therapeutic load. Because of their distinctive structure, liposomes can be used to load hydrophilic drugs in their aqueous core and hydrophobic drugs in their lipid bilayered membrane simultaneously [Castor 2005]. By virtue of this property liposome may be used as a platform for combination drug delivery. Ampicillin loaded liposome have been acquainted to be more effective as compared to the free antibiotic in combating infection of *Salmonella typhimurium* and *Listeria monocytogenes* [Blecher *et al.* 2011]. Liposomal formulations having encapsulated penicillin were found to inhibit the growth of various bacteria resistance strains (*Bacillus licheniformis, Escherichia coli, Staphylococcus aureus*) [Pinto-Alphandary *et al.* 2000]. Furthermore, piperacillin loaded liposomes have been shown to inhibit the antibiotic from hydrolysis by β-lactamases [Alipour & Suntres 2014].

**(D) *Polymeric nanoparticle***

Polymeric nanoparticles can be used to entrap drugs for antimicrobial treatments [Beyth *et al.* 2015]. These nanoparticles are composed of biocompatible and biodegradable materials like poly (lactic-co-glycolic acid) (PLGA) and polycaprolactone (PCL) and several natural polymers [Kumari *et al.* 2010]. These nanoparticle possess all the properties which are necessary for an ideal drug delivery system like a sustained drug release, enhance stability, better stability, higher loading capacity, manageable physicochemical properties. These nanoparticles are also made of amphiphilic diblock copolymers that self assemble into nanoparticles in aqueous solutions [Kenawy *et al.* 2007]. Mohammadi *et al.* prepared azithromycin encapsulated PLGA nanoparticle by nanoprecipitation technique and the formulation was more effective aginst *S. typhi* as compared to free azithromycin [Mohammadi *et al.* 2010]. Cinnamaldehyde and eugenol loaded PLGA nanoparticles have been reported to show better antimicrobial activity against both gram-positive and gram-negative bacteria [Gomes *et al.* 2011]. There are various literature on increased efficiency of nanoparticle entrapped drugs as compared to free formulation [Soppimath *et al.* 2001].

Temperature instability is the major problem of organic nanomaterial. This instability leads to several difficulties in preparation of these nanoparticle furthermore, there ability to withstand harsh conditions is also less. Inorganic nanoparticle is comparatively more stable at higher temperature. Consequently, inorganic nanoparticles are more frequently used as antimicrobials.

### 1.7.2.2 Inorganic nano-materials

There are several literatures on use of metal and metal oxides as antibacterial material [Li *et al.* 2008; Hajipour *et al.* 2010; Beyth *et al.* 2015] . There are various metal nanoparticle containing several metal elements like silver (Ag), copper (Cu), Zinc (Zn), Titanium (Ti), Magnesium (Mg) and Gold (Au). The mechanisms behind their antimicrobial activity highly depend on the type of metal ion present. They mainly kill or inhibit the growth of microbes by production of reactive oxygen species (ROS) and by membrane disruption [Pelgrift & Freidman 2013]. Some of the metal and metal oxide nanoparticles possessing antibacterial activity are discussed below

**(A)** ***Silver nanoparticles (Ag-NPs)***

Silver and its formulations have been identified to be having medical relevance from ancient times. They are being used in disinfectants, water purifiers and wound healing ointments from several decades [Silvestry-Rodriguez *et al.* 2007]. Nowadays its nanoparticles (Ag-NPs) are gaining much attention as they have broad spectrum antimicrobial activity and they do not promote drug resistance [Lara *et al.* 2010]. Several studies have suggested the antibacterial effect of Ag-NPs is due to release of silver ions ($Ag^{+}$) from its surface [Hajipour *et al.* 2010; Beyth *et al.* 2015]. These $Ag^{+}$ ions may interact with thiol groups of cell wall of bacteria and create holes in the membrane facilitating flow of cytoplasmic material out of the cell. This may cause cell death.

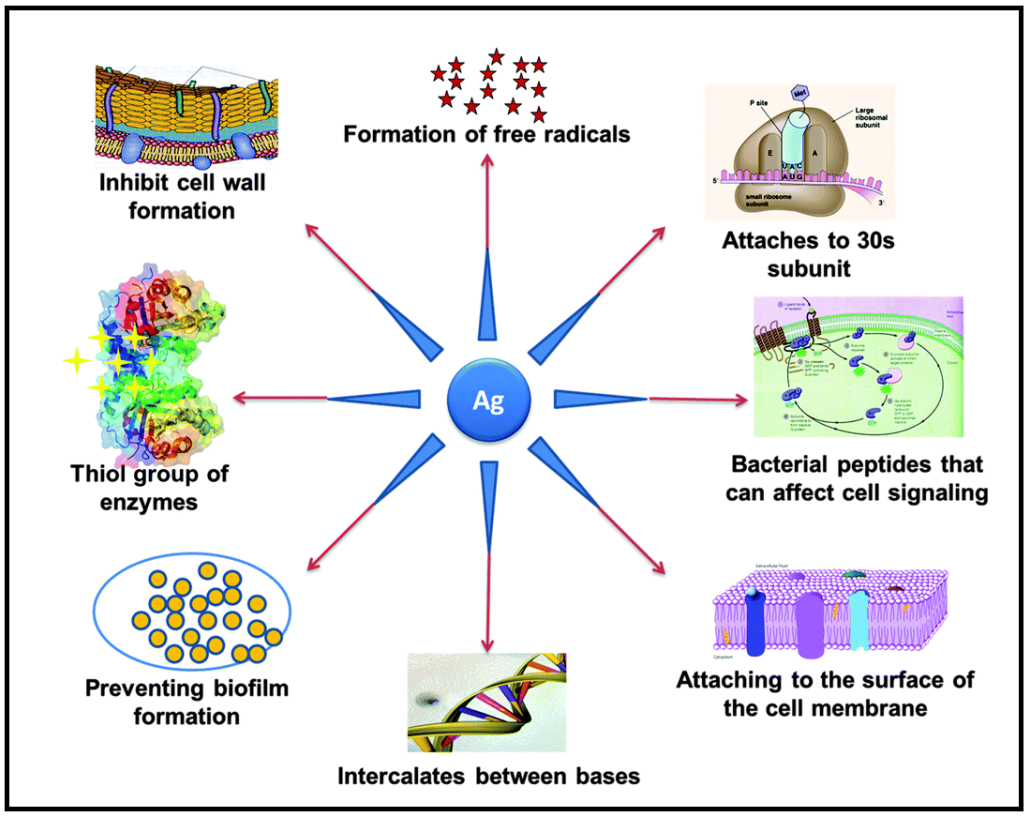


**Figure 1.14** Proposed antibacterial mechanisms of silver nanoparticles. (Source:http://pubs.rsc.org/services/images/RSCpubs.ePlatform.Service.FreeContent.ImageService.svc/ImageService/Articleimage/2014/CC/c4cc03001j/c4cc03001j-f1_hi-res.gif)

Moreover, these Ag+ ions may interact with DNA, inhibiting DNA replication and cell division [Knetsch & Koole 2011]. The antibacterial activity of silver nanoparticle is

dependent on its shape and size. It has been reported that silver nanoparticles having size < 10 nm show greater bactericidal activity as compared to bigger nanoparticles [Pal *et al.* 2007]. Furthermore, the shapes of nanoparticle which may increase their surface area provide them with more antibacterial potency. Greater surface area results in higher release of metal ion and thus higher antibacterial activity. Ag-NPs have been shown to kill gram-negative bacteria by pit formation in there cell wall suggesting membrane disruption while the same is not true in gram-positive bacteria [Sondi & Salopek-Sondi 2004]. ROS production has been proposed as another mechanism which impart antibacterial property to Ag-NPs [Carlson *et al.* 2008]. Although, Ag-NPs show remarkable antibacterial properties against wide range of microbes but the exact mechanism is not fully understood. There are lots of controversies and debate on the mode of action of these nanoparticles but they are perhaps the most promising antibacterial metal nanoparticles. Different mechanisms of antibacterial action of silver nanoparticles are summarized in Figure 1.14.

**(B) *Zinc oxide nanoparticles***

Zinc oxide is used as food additive and has been approved by Food and Drug Administration as GRAS (Generally recognized as safe) [Espitia *et al.* 2012]. Zinc oxide in its nanoparticle form is believed to be antibacterial and relatively non toxic, safe and biocompatible as compared to other metal nanoparticles [Raghupati *et al.* 2011]. Zinc oxide nanoparticles are being widely used as drug carriers, preservatives, in cosmetics and filling in medical materials [Applerot *et al.* 2012]. Zinc oxide nanoparticles have been reported to inhibit the growth of methicilline resistant strains of *S. aureus* (MRSA) and *S. epidermidis* (MRSE) [Ansari *et al.* 2012]. There are numerous literature on antibacterial activity of these nanoparticle which include there effect on broad range of bacteria such as *Escherichia coli*, *Streptococus mutans*, *Listeria monocytogenes*, *Staphylococcus aureus*, *Klebsiella pneumonia* [Jin *et al.* 2009, Kasraei *et al.* 2014, Liu *et al.* 2009]. It has been proposed that in its aqueous suspension ZnO-NPs generate extensive amount of reactive oxygen species (ROS) which contribute to its antibacterial potential. Among all the ROS hydrogen peroxide ($H_2O_2$) interaction with bacterial membrane have been suggested as a dominant antibacterial mechanism of ZnO-NPs (Figure 1.15). Like other nanoparticle they also release a $Zn^{2+}$ metal ion which helps in its antibacterial mode of action [ Shi *et al.* 2014].

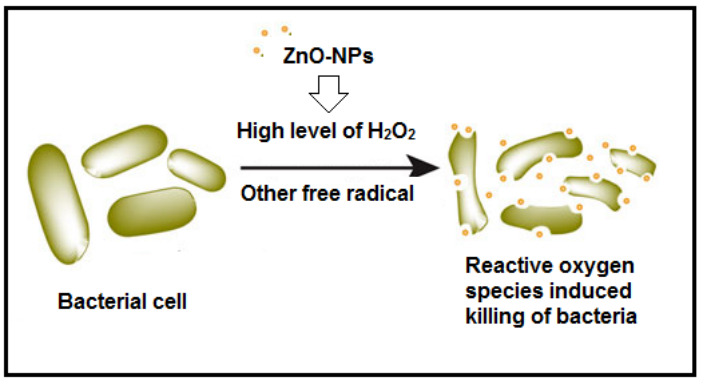


**Figure 1.15** ROS mediated antibacterial activity of Zinc oxide nanoparticles. (Source:http://www.nanowerk.com/spotlight/id36012.jpg)

**(C) *Copper oxide nanoparticles***

Copper oxide nanoparticles (CuO-NPs) show antibacterial activity against different microbes, but their antibacterial potency is much lower than silver and zinc oxide nanoparticles [Ren *et al.* 2009]. Thus, they are antibacterial at higher concentrations. Cu ions interact with the amine and carboxylic groups of bacterial membrane and disrupt it. Hence, bacteria which posses higher density of these groups on their surface (*B. subtilis*) are more prone to CuO-NPs attack [Ruparelia *et al.* 2008]. Therefore, in some bacteria, use of CuO-NPs is much beneficial than other nanoparticles.

**(D) *Magnesium containing nanoparticles***

Magnesium has been utilized in formation of different nanoformulations which show antibacterial activity. Magnesium oxide nanoparticles are easy to synthesize and show antibacterial activity against both gram-negative and gram-positive bacteria, spores and viruses [Blecher *et al.* 2011]. Its mechanism is also dependent on ROS production like other nanoparticles. Magnesium fluoride nanoparticle have been reported to inhibit the biofilm formation in *E. coli* , *S. aureus* and *S. mutans* [Lellouche *et al.* 2009; Eshed *et al.* 2013].

**(E) *Titanium dioxide-containing nanoparticles***

Titanium dioxide ($TiO_2$) have been long reported as antibacterial material. In its nanoform it show antibacterial activity which enhances in the presence of visible and UV light. When exposed to light they show photocatalytic activity thus facilitating the

formation of enormous amount of ROS which damage the bacterial membrane and DNA of bacterial cell. Visible and UV light assisted photocatalytic activity of $TiO_2$ nanoparticles have been reported to kill various gram-negative and gram-positive bacteria [Liou & Chang 2012].

**(F) *Gold containing nanoparticles***

Gold containing nanoparticles lack antibacterial activity but they can be used as carriers of antibacterial drugs and peptides. Brown *et al.* have reported that gold nanoparticle functionalized ampicilline have potential of destroying many drug resistance bacterial strains such as *Pseudomonas aeruginosa*, *Enterobacter aerogegenes* and MRSA [Brown *et al.* 2012]. Gold nanoparticles have been suggested to enhance the photodynamic therapy based killing of microbes by ROS production [Khan *et al.* 2012].

**(G) *Graphene oxide (GO)***

Graphene oxide (GO) is one atom thick $sp^2$ hybridized carbon atom layer bearing numerous oxygen containing groups on its surface and edges. Its edges have carboxylic groups while there are epoxy and phenol hydroxide groups on its basal plane [Paredes *et al.* 2008]. GO is getting much attention as a nanomaterial and as a precursor of many graphene related materials [Novoselov & Geim 2007]. A number of reports have shown the antibacterial activity of graphene oxide, but its antibacterial potential is much less than other nanomaterial [Akhavan & Ghaderi 2010; Hu *et al.* 2010]. The lateral dimensions of graphene oxide has been found to affect its antibacterial ability [Liu *et al.* 2012]. In other report Liu *et al*. have suggested a three step antibacterial mechanism of Graphene oxide, which mainly relates to close contact of bacteria with GO surface, membrane puncture and oxidative stress [Liu *et al.* 2011]. These nanosheets possess many reducible groups which can be functionalized with any antimicrobial material [Ocsoy *et al.* 2013]. GO is being extensively used as supporting material for other nanoparticles as it provide a better platform for interaction of bacteria with the attached nanoparticles [Ma *et al.* 2011; de Fariaa *et al.* 2014; Tang *et al.* 2013; Xu *et al.* 2011]. It has been reported to have good biocompatibility to human noral cell at very high concentrations [Chang *et al.* 2011] thus making it a suitable material for fabrication of effiecient antibacterial composite.

### 1.7.3 *Nanoparticle in prevention of biofilm formation*

Biofilms creates an environment that enhances microbial resistance. In addition to their direct bactericidal activity nanoparticle are known to inhibit the biofilms formation. Nanoparticle can be exploited to eliminate preformed biofilms [Iannitelli *et al.* 2011] or it can be exploited to restrict biofilm formation [Beyth *et al.* 2015].

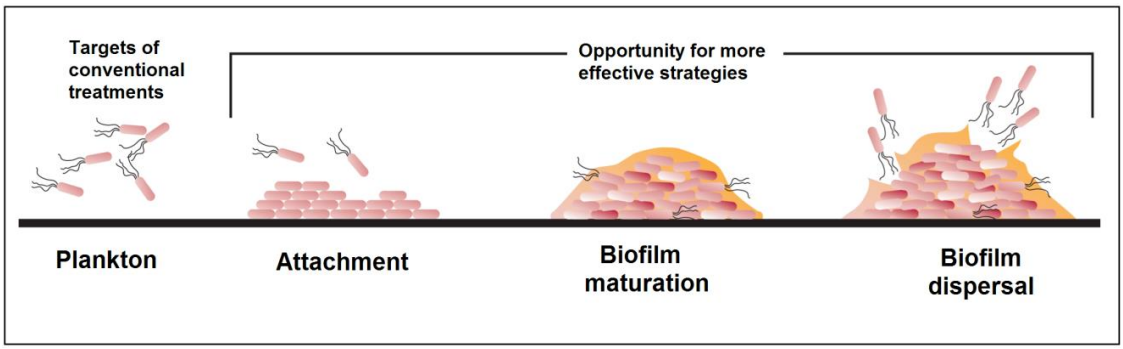


**Figure 1.16** Biofilm cascade inhibition provide opportunitie for preparing more effective therapeutics. (Source:http://www.4inno.com/wp-content/uploads/2014/01/diagram.png)

Figure 1.16 represent the possible targets in biofilm casade for designing more effective therapeutic stratagies. There are several independent studies going on the use of nanoparticle to eliminate the preformend biofilms. Zerovalent bismuth nanoparticles has been shown to completely inhibit the biofilm of *S. mutans* [Hernandez-Delgadillo *et al.* 2012]. The novel class of ultrathin (~1-2 nm) silver ring coated super paramagnetic iron oxide nanoparticles (SPIONs) with ligand gap exhibit antimicrobial characteristics against bacteria by maintaining remarkable compatibility with the cells moreover SPIONS with double ligand gaps have been developed with that could be potentially used as multimodal antibacterial agents. Due to their magnetic core both nanoparticle are able to penetrate in bacterial biofilms when external magnetic field applied, SPIONs have shown high therapeutic index against *Staphylococcus aureus* and *Staphylococcus epidermidis* infections [Mahmoudi & Serpooshan 2012]. Nanoparticles may also be used to enhance the photodynamic therapy which is a novel therapeutic approach to inhibit biofilms. Gold nanoparticle have been used to enhance the methylene blue induced photodynamic therapy to inhibit *Candida albicans* biofilm and it has been confirmed that gold nanoparticle-methylene blue conjugate work by Type I photo toxicity which hydroxyl free radical [Khan *et al.* 2012]. Another study revealed that there is significantly

higher inhibition of microbial biofilms by chitosan nanoparticle loaded erythrosine induced photodynamic treatment than erythrosine in free form [Chen *et al.* 2012].

The more efficient way to deal with biofilm related infection is the prevention of biofilm formation at an early step of its development. Nanoparticles may be utilized to for functionalizing the surfaces of medical appliances by coating and impregnation. In an investigation the magnesium fluoride nanoparticle coated catheters effectively restricted biofilms formation in both growth media and biologically relevant fluids [Lellouche *et al.* 2012; Eshed *et al.* 2013]. ZnO nanoparticle-coated surfaces have been found to inhibit bacterial biofilm formation and increase antibiotic susceptibility [Applerot *et al.* 2012] Although there are several studies on the inhibition of bacterial biofilm with the help of nanoparticle but the exact mechanism and mode of inhibition of biofilm has not yet been identified. There is need for new nanoparticles based approaches which may be designed to inhibit the adherence and biofilm formation cascade of bacterial species.

### 1.8 Aims and Objectives of the study

In the consideration of present background, we initiated our study with the following objectives

- To synthesize graphene /zinc oxide nanocomposite (GZNC) and to evaluate its effect on *Streptococcus mutans* biofilm and its cariogenic potentials. Also, to investigate its use as a coating material for dental implant surface to inhibit biofilm growth.
- To synthesize Calcium fluoride nanoparticle ($CaF_2$-NPs) and to accesses its *in vitro* and *in vivo* effect on *Streptococcus mutans* biofilm and its virulance factors associated with caries development.
- To develop graphene oxide-silver nanocomposite by an eco-friendly and less toxic route of green to reduce the agglomeration of silver nanoparticle. Also, to analyse the effectiveness of this nanocomposite in prevention of biofilm of both gram-positive and gram-negative bacteria.

## 2.1 Materials

| Source | Chemical/Reagents/Solvents |
|---|---|
| Hi-Media Laboratories Pvt. Ltd, Mumbai, India | Bacteriological Agar |
| | Brain Heart Infusion broth |
| | Dibasic sodium phosphate |
| | Ethidium bromide |
| | Glutaraldehyde-SEM grade |
| | Mitis Salivarius Agar |
| | Monobasic sodium phosphate |
| | Nutrient Broth |
| | Paraformaldehyde |
| | Phosphate buffer Saline |
| | Potassium chloride |
| | Sodium chloride |
| | Sodium hydroxide (NaOH) |
| | TE Buffer |
| | Tris-HCl buffer |
| Sigma- Aldrich St. Louis, USA | Bovine Serum albumin |
| | Bradford reagent |
| | Congo red dye |
| | DCFH-DA (2, 7-Dichlorofluorescin diacetate) |
| | Menadione |
| | MTT (3-(4,5-Dimethylthiazol-2-yl)-2,5-diphenyltetrazolium bromide) |
| | PI (Propidium iodide) |
| | XTT(2,3-Bis(2-methoxy-4-nitro-5-sulfophenyl)-5-([phenylamino]carbonyl)-2H-tetrazolium hydroxide) |
| Qualigens Fine Chemicals Mumbai, India | Ammonium fluoride |
| | Calcium chloride |

| | |
|---|---|
| | Crystal violet |
| | EDTA |
| | Formaldehyde |
| | Hydrogen per oxide ($H_2O_2$) |
| | Potassium per magnet ($KMnO_4$) |
| | Silver nitrate |
| | Sodium carbonate |
| | Sulphuric acid |
| | Zinc acetate |
| SRL Chemicals, Mumbai, India | Agarose |
| | Chloroform |
| | Glycerol |
| | Hydrochloric acid (HCl) |
| | Isopropanol |
| | Magnesium chloride |
| | Sodium acetate |
| | Sucrose |
| Merck (India) Ltd. Mumbai, India | Ethanol |
| Loba Chemie, Mumbai, India | Graphite powder |
| Axiva, Delhi, India | 96-well microtiter plate |
| | 12-well microtiter plate |
| Genetix Biotech Asia Pvt. Ltd, New Delhi, India | Sterile coverslips |
| | Adhesion type cover glass bottom disc |
| Invitrogen, India | Syto®-9 |

| | |
|---|---|
| Millipore, Billerica MA, USA | 0.45 μm filter |
| | 0.20 μm filter |
| Applied Biosystems, California, USA | SYBR Green PCR master mix |

## 2.2 Methods

### 2.2.1 *Ethical consideration*

This research was conducted in agreement with institutional ethical standards. The study on animals was approved by "Interdisciplinary Biotechnology Unit, Institutional Ethical Committee."

### 2.2.2 *Bacterial strains and culture conditions*

*S. mutans* (MTCC SM 497), an ATCC analogue of UA159 strain was purchased from IMTECH, Chandigarh, India. The clinical isolates of *S. mutans* (SM 497, SM 34 and SM 06) [Islam *et al.* 2008] and biofilm forming *Enterobacter cloacae* [Khan & Nordmann 2012] used in this study were isolated and characterized earlier in our laboratory. CLSI guidelines were followed for the isolation and characterization of all strains. Strains were routinely grown in Brain Heart Infusion broth (BHI) at 37˚C. The cultures were stored at -80ºC in BHI containing 25% glycerol. A final concentration of 5% (w/v) of sucrose was added to the liquid medium before sterilization for biofilm based experiments. Up to 2% agar was added to BHI prior to sterilization to obtain solid media for plating.

### 2.2.3 *Synthesis of nanoparticles and nanocomposites (Nanomaterials)*

#### 2.2.3.1 Graphene oxide

Graphene oxide (GO) was prepared according to the method described by Hummers and Offman (1958) with slight modification. $H_2SO_4$ (100 ml) was added to 2 g of graphite powder while stirring on an ice-water bath. $KMnO_4$ (25 g) was slowly added to the solution. The mixture was kept on a stirrer at room temperature until it became pasty brown. It was then diluted with the slow addition of 200 ml of water. Finally, 10 ml of a 30% aqueous solution of $H_2O_2$ was added. The impurities were removed from the graphene oxide (GO) using 3% HCl with repeated washing [Hummers & Offman 1958].

#### 2.2.3.2 Graphene/zinc oxide nanocomposite

For the synthesis of the GZNC, 100 mg of zinc acetate and 200 mg of GO were dispersed into 200 ml of absolute ethanol followed by sonication overnight. After that formed GZNC was harvested by centrifugation at 5,000 rpm for 5 min. It was then washed with 80% ethanol. The pellet was vacuum dried and 100 mg of this dried sample was mixed

with 100 ml of ethylene glycol using sonication for 10 min. The resulting mixture was heated to 140°C with vigorous stirring on a magnetic stirrer (REMI, Mumbai, India; Model: 1MLH) for 3 h. The synthesized GZNC suspension was centrifuged, washed with 80% ethanol and dried in a vacuum oven at 60°C.

#### 2.2.3.3 Calcium fluoride nanoparticles

Calcium fluoride nanoparticles ($CaF_2$-NPs) were synthesized by simple co-precipitation method as described earlier with slight modification [Pandurangappa & Lakshminarasappa 2011]. In a typical procedure, Calcium chloride ($CaCl_2$) and Ammonium fluoride ($NH_4F$) were dissolved in 100 ml distilled water in a molar ratio of 1:2 and the mixture was continuously stirred for 2 hours using a magnetic stirrer. The calcium fluoride nanoparticle formation was indicated by the gradual change of mixture from transparent to opaque white suspension. A few drops of ammonia were added into the mixture for precipitation. The stirred solution was centrifuged for 15 minutes at 8000 rpm and a white residue was obtained. The residue was washed thoroughly with ethanol and water. The obtained product was put in a ceramic petridish and dried slowly in the vacuum oven overnight at 60ºC and sintered at 300ºC for 3 hrs.

#### 2.2.3.4 Green synthesized graphene oxide-silver nanocomposite

**(a)** ***Flower extract preparation of Lagerstroemia speciosa (L.) Pers***

Flowers of *Lagerstroemia speciosa* were collected from the young and healthy tree and washed several times with double distilled water to remove the dust particles and surface contaminants. They were then oven-dried (80°C) to remove the residual moisture. The dried (2g) inflorescence was powdered using mortar and pistil and boiled in presence of 20 ml of sterile double distilled water for 5 min. The aqueous extract was separated by filtration with Whatman No. 1 filter paper (Maidstone, UK) and then centrifuged at 5,000 rpm for 5 min to remove heavy biomaterials. The extract was stored at 4°C.

**(b)** ***Synthesis reduced graphene oxide (RGO)***

For synthesis of reduced graphene, the GO solution was first sonicated and then plant extract was added in solution (10:1 ratio) and kept for 8 hours at room temperature for its reduction. Than reduced GO was centrifuged and washed with distilled water.

**(c) *Synthesis of Graphene oxide silver nanocomposite (GO-Ag)***

In a typical reaction procedure, 200 µL of the extract was assorted with 800 µL of $1\times10^{-3}$ M aqueous $AgNO_3$ solution. This solution was immediately added into the reduce graphene oxide solution and kept on magnetic stirrer (REMI, Mumbai, India; Model: 1MLH) at room temperature for 24 h. Further, the produced nanocomposite was centrifuged at 8000 rpm and supernatant was removed having excess silver ion, the nanocomposite was washed several times with deionised water using repeated centrifugation and supernatant removal. It was then lyophilized and stored in screw-capped vials at room temperature.

### 2.2.4 *Characterization of nanoparticles and nanocomposites*

Characterization of nanoparticle and nanocomposites was performed using various techniques which include:

#### 2.2.4.1 UV-visible spectroscopy

The synthesis of nanomaterial in solution was monitored by measuring absorbance using a UV-visible spectrophotometer (Perkin Elmer Life and Analytical Sciences, CT, USA) in the wavelength range of 200 nm to 800 nm.

#### 2.2.4.2 Transmission electron microscopy (TEM)

TEM analysis of nanomaterial was performed using a JEM-2100F TEM (Jeol, Tokyo, Japan) operating at 120 kV and nanoparticle size was calculated by examining a TEM image by Image J software (Image J 1.46r; Java 1.6.0_20).

#### 2.2.4.3 Scanning electron microscopy (SEM)

Scanning electron microscopy (SEM) was employed to study the surface topography of nanomaterial. The samples were coated with gold and observed by SEM (EVO 40; Zeiss, Jena, Germany) at 20 kV.

#### 2.2.4.4 Fourier transform infrared spectroscopy (FTIR)

The nanomaterials were mixed with spectroscopic grade potassium bromide (KBr) in the ratio of 1:100 and spectra were recorded in the range 400 - 4000 wave number ($cm^{-1}$) on

a Perkin Elmer FTIR Spectrum BX (PerkinElmer Life and Analytical Sciences) in the diffuse reflectance mode at a resolution of 4 $cm^{-1}$ in KBr pellets.

#### 2.2.4.5 X-ray diffraction (XRD)

The X-ray diffraction (XRD) patterns of the powdered samples of nanoparticles and nanocomposites were recorded on a MiniFlex™ II bench top XRD system (Rigaku Corporation, Tokyo, Japan) operating at 40 kV.

#### 2.2.4.6 Energy dispersive X-ray spectroscopy (EDX)

Energy-dispersive X-ray spectroscopy (EDX) was employed to investigate the elemental composition of type of nanocomposite.

#### 2.2.4.7 Thermogravimetric analysis (TGA)

The thermal stability of nanocomposite was investigated by thermogravimetric analysis (TGA) at a heating rate of 10°C $min^{-1}$ under a nitrogen atmosphere.

### 2.2.5 *Determination of bacteriostatic (MIC) and bactericidal (MBC) concentrations*

Minimum inhibitory concentration (MIC) of nanomaterials against bacterial strains were determined by the micro dilution method. Overnight growth culture were diluted ($10^5$-$10^6$ CFU $ml^{-1}$) into fresh BHI (final concentration ~ $5\times10^5$ CFU $ml^{-1}$ in each well) containing various concentrations of serially diluted nanoparticles and nanocomposites. The MIC was determined as the lowest concentration that totally inhibits visible bacterial growth. Minimum bactericidal concentration (MBC), on the other hand was determined by sub culturing the test dilutions on a BHI agar plates and incubating for 24 h at 37˚C. The concentration showing no growth on agar plates was taken as MBC.

### 2.2.6 *Effect on adherence*

The glass surface adherence assay was performed to evaluate the effect of sub inhibitory concentrations of nanoparticles and nanocomposites on adherence of *S. mutans* [Hamada *et al.* 1980]. The bacteria (~ $5\times10^5$ CFU $ml^{-1}$) were grown for 6 h at 37ºC at an angle of 30º in a glass tube containing BHI with 5% sucrose and various sub inhibitory concentrations of nanoparticles and nanocomposites. The solvent controls included BHI (with 5% sucrose) and equivalent amount of nanoparticles and nanocomposites. After

incubation, planktonic cells were decanted, and the attached cells were removed by 0.5 M of sodium hydroxide. Planktonic and adhered cells were quantified using UV-spectrometer by taking O.D. at 600 nm. Percent adherence was calculated using formula:

% Adherence = (O.D.600 of adhered cells / O.D.600 of total cells) ×100

### 2.2.7 *Effect on biofilm formation (Crystal violet assay)*

Biofilm formation was assessed by using crystal violet assay. The overnight growth culture of bacteria were diluted into fresh BHI with 5% sucrose (final concentration $5\times10^5$ CFU $ml^{-1}$ of cells in each well) containing sub inhibitory concentrations of nanomaterials with respective controls. After incubation for 24 h at 37˚C, the media having unattached cells was decanted from the microtiter plates and the wells were gently rinsed with sterile water. The adhered biofilms were stained with 200 µL of 0.1% crystal violet for 15 min at room temperature. The dye was removed and biofilms were washed with two rinses of distilled water. The bound dye was released from the cells with 100 µl of 95% alcohol. Plates were then set on a shaker for 5 min. Biofilm formation was quantified by measuring optical density at 630 nm by BIORAD iMark TM Microplate reader, India.

### 2.2.8 *Effect on exopolysaccharide production*

#### 2.2.8.1 Congo red binding assay

The Congo red (CR) binding assay which detects glucose containing polymers was used to evaluate exopolysaccharide (EPS) production, as previously reported [Friedman *et al.* 2001; López-Moreno *et al.* 2014]. The experiment was performed in 96 well microtiter plate. The overnight growth culture of bacteria were diluted into fresh BHI with 5% sucrose (final concentration $5\times10^4$ CFU $ml^{-1}$ of cells in each well) containing sub inhibitory concentrations of nanoparticles and nanocomposites. The wells devoid of nanoparticle treatment (media + diluted culture) were taken as controls. After incubation for 24 h at 37°C, the medium was removed and biofilms were washed with PBS and then fresh media (100 µl) was added to each well including the respective controls. Now, 50 µl of CR (0.5 mM) was added to each well. Media (100 µl) along with 50 µl CR were added to another well for blank measurements (Blank CR). Plates were incubated for 60 min at 37˚C. The media in each well was transferred to 200 µl micro centrifuge tubes and

centrifuged at 10,000 × g for 5 min at 37˚C. The supernatant was transferred to empty wells of microtiter plates and absorbance was measured at 490 nm. The absorbance value of the supernatant was subtracted from the absorbance value of the 'blank CR'. The resultant value represents the amount of bound CR or EPS produced. The experiment was conducted in triplicate.

#### 2.2.8.2 CR agar method

Solid agar medium was prepared using BHI (37 g $l^{-1}$), sucrose (5%), agar No. 1 (2%), and CR stain (0.8 g $l^{-1}$). CR was prepared in the form of a concentrated aqueous solution and was autoclaved at 121°C for 15 min, separately. After autoclaving, CR was added to the agar which was cooled to 55°C. For treated samples, sub inhibitory concentrations nanocomposite was added to the medium. Plates were inoculated and incubated aerobically for 24 h at 37°C. EPS production was indicated by black colonies with a dry crystalline consistency.

### 2.2.9 *Effect on preformed biofilm*

Approximately $10^7$ CFU $ml^{-1}$ of *S. mutans* cells were added to each well of a sterile 96-well microtiter plates. Plates were then incubated at 37°C for 24 h to form biofilm. Then, the supernatant containing planktonic cells were removed and washed three times using 100 µL 0.9% (w/v) NaCl. The preformed biofilms were incubated at 37°C in the media (BHI+ 5% sucrose) containing different concentrations of nanoparticles for 24h. Biofilm mass was evaluated by crystal violet assay.

### 2.2.10 *Assessment of cellular viability*

XTT assay was performed as described previously with slight modifications [Islam *et al.* 2008]. XTT (2,3-Bis(2-methoxy-4-nitro-5-sulfophenyl)-5-([phenylamino]carbonyl)-2H-tetrazolium hydroxide) was dissolved in phosphate buffer saline (PBS) at a final concentration of 250 mg $l^{-1}$. The solution was filter sterilized using a 0.22-mm pore-size filter and stored at -80°C until required. Menadione (Sigma-Aldrich) solution (0.4 mM) was also prepared and filtered immediately before each assay. Adherent cells were washed with 200 µl of PBS, then 158 µl of PBS, and 40 µl of XTT, and 2 µl of menadione were added to each well. After incubation in the dark for 4 h at 37°C, 100 µl of the solution were transferred to a new well and a colorimetric change in the solution

was measured using a microtiter plate reader (BIORAD iMark TM Microplate reader) at 490 nm.

### 2.2.11 *Bacterial growth curve*

Overnight growth cultures of bacteria were diluted to get ~$10^6$ CFU $ml^{-1}$ of cells and inoculated in BHI tubes containing 5% sucrose and sub inhibitory concentration of nanomaterials. All cultures were incubated at 37ºC for 24 h. Growth was monitored every hour by taking the absorbance at 600 nm using UV mini 1240, UV-visible spectrophotometer (Shimadzu, New Delhi, India). Untreated samples were used as controls.

### 2.2.12 *Inhibition of water insoluble and water soluble glucan synthesis*

The crude glucosyltransferase (GTF) was prepared from cell-free supernatant of *S. mutans* culture and assayed to evaluate the effect of nanoparticles on glucan synthesis. Cell-free enzymes were precipitated from culture supernatant of *S. mutans* by adding solid ammonium sulphate to 70% saturation (an ammonium cut). The mixture was stirred at 4°C for 1 h and allowed to stand for another 1 h under cold conditions. The precipitate was collected by centrifugation at 12,000 g at 4°C for 20 min, dissolved in a minimum volume of 20 mM phosphate buffer (pH 6.8) and then dialysed against 2 mM phosphate buffer (pH 6.8) at 4°C for 24 h. The crude enzyme was stored at ‑80°C for further experiments. A reaction mixture consisting of 0.25 ml of crude enzyme, varying concentrations of nanoparticles and nanocomposites in 20 mM phosphate buffer (pH 6.8) and 0.25 ml of sodium acetate buffer (pH 5.7, having 0.4 M sucrose) was incubated at 37°C for 2 h. The mixture was then centrifuged at 10,000 g for 5 min at 4˚C to separate water soluble and water insoluble glucans. Total amounts of water-soluble and insoluble glucan were measured by the phenol-sulfuric acid method [Dubois *et al.* 1956]. Three replicates were made for each concentration of the test compounds.

### 2.2.13 *Effect on acid production*

The effect of nanocomposite on the acidogenicity of *S. mutans* and its clinical isolates was assessed using a previously published protocol [Khan *et al.* 2010]. 5 ml of BHI broth containing 5% (w/v) of sucrose and sub inhibitory concentrations of nanomaterials were inoculated with *S. mutans* and incubated at 37°C for 24 h. The pH of the treated samples

and the controls was assessed at 0 h and after incubation for 24 h. All determinations were performed in triplicate.

### 2.2.14 *Glycolytic pH-drop assay and acid production*

Glycolytic pH drop of *S. mutans* was estimated as described elsewhere [Phan *et al.* 2004]. Cells were harvested from suspension culture by centrifugation and washed with salt solution (50 mM KCl + 1 mM $MgCl_2$). The cells were then resuspended in fresh salt solution containing various concentrations of nanoparticles. The pH was adjusted between 7.2–7.4 with 0.2 M KOH solution followed by the addition of glucose (1% w/v). The decrease in pH was assessed every 10 min over a period of 60 min using pH meter. The initial rate of the pH drop, which can give the best measure of the acid production capacity of the cells, was calculated using the pH values in the linear portion (0-10 min).

### 2.2.15 *Protein leakage assay*

To determine the membrane integrity of bacteria the proteins leakage assay was performed. The bacterial cells were inoculated in 10 ml media (BHI supplemented with 5% Sucrose) having sub inhibitory concentrations of nanocomposites. The cultures were incubated at 37±2°C with shaking at 150 rpm for 1h and 4h. After treatment the sample was centrifuged at 12,000 rpm at 4˚C for 5 min, the supernatants were kept at −20°C immediately. The concentrations of proteins in the supernatant were determined using Bradford reagent [Li *et al.* 2010]. Control experiments were conducted without GO-Ag.

### 2.2.16 *Estimation of reactive oxygen species*

Generation of reactive oxygen species (ROS) in the presence of nanoparticles and nanocomposites was assayed using 2′, 7′- dichloro fluorescein diacetate (DCFDA). *S. mutans* and *E. cloacae* cells ($5\times10^4$ cfu $ml^{-1}$) were incubated with 10µM DCFH-DA for 1 h at 37ºC. After 1h, sub inhibitory concentrations of nanoparticles and nanocomposites were added in the media and further incubated at 37ºC for 1h and 12h. Untreated samples were used as control. The ROS production at 1h and 12h of incubation was detected at a fluorescence excitation wavelength of 485 nm and an emission wavelength of 528 nm.

### 2.2.17 *Microscopic analysis of structural integrity of biofilm architecture*

#### 2.2.17.1 Scanning electron microscopy (SEM)

The effects of the nanoparticles and nanocomposites on biofilms were observed by scanning electron microscopy (SEM). The cells were grown in 12 well culture plates having sterile coverslips in each well. The media having sub inhibitory concentrations of nanoparticles were dispensed in each well. The coverslips dipped in media without nanoparticles were used as controls. Further, each well was inoculated with bacterial cells (~$10^6$cfu $ml^{-1}$) and incubated at 37ºC for 24 h. After 24h of treatment coverslips were removed and washed two-three times with sterile PBS. The samples were then fixed with 2% formaldehyde and 2.5% glutaraldehyde in PBS (pH 7.4) overnight at room temperature. After fixing samples were dehydrated in absolute ethanol (ethanolic dehydration) and eventually dried in desiccators. Then samples were coated with gold and observed by SEM (EVO 40; Zeiss, Jena, Germany) at 20 kV.

#### 2.2.17.2 Confocal laser scanning microscopy (CLSM)

Bacterial biofilms were grown in the presence of nanomaterials at 37ºC in covered glass bottom confocal dishes (dish size of 35 mm, 22 mm cover glass, 9.4 $cm^2$ growth area and a working volume of 3 ml). The dishes were washed with PBS and treated with fluorescent dye as molecular probe, Syto-9 (5µM; excitation and emission wavelength; 488 nm, 498 nm) and PI (0.75 µM; excitation and emission wavelength; 536 nm, 617 nm). The stained bacterial biofilm were observed with a FluoView FV1000 (Olympus, Tokyo, Japan) confocal laser scanning microscope equipped with argon and HeNe lasers.

#### 2.2.17.3 Transmission Electron Microscopy (TEM)

Transmission Electron microscopy was used to investigate the intracellular changes in *S. mutans*. Control and nanoparticle treated cultures were suspended using a centrifuge and washed with PBS (pH 7.4). Secondary fixation was done with 2.5% glutaraldehyde (HiMedia) and 1% osmium tetroxide ($OsO_4$) for 2–3 hours at 4°C. Samples were dehydrated by ethanol and embedded in araldite CY 212 (Taab, Aldermaston, UK) resin for making the cell-pellet blocks. Ultrathin sections of cells were stained with uranyl acetate and lead citrate and observed under the TEM (Jeol, Tokyo, Japan) microscope at 120 kV.

### 2.2.18 *RNA extraction, Reverse transcription and Quantitative RT-PCR*

#### 2.2.18.1 Primer designing

Primers were designed using the algorithms provided by Primer Express (Applied Bio systems) for uniformity in size (≤ 95 bp) and melting temperature. Primers pairs are listed in Table 2.1. RT- PCR products of each were run on an electrophoresis gel to ensure that only single product of correct size were amplified.

**Table 2.1** Nucleotide sequence of primer used in this study

| **Genes** | **Description** | **Primer Sequence (5'- 3')** |
|---|---|---|
| **16S rRNA** | Normalizing internal standard | **Fwd:**CCTACGGGAGGCAGCAGTAG<br>**Rev:**CAACAGAGCTTTACGATCCGAAA |
| ***Vic R*** | Two - component regulatory system | **Fwd:**TGACACGATTACAGCCTTTGATG<br>**Rev:**CGTCTAGTTCTGGTAACATTAAGTCCAATA |
| ***gtf C*** | Glucosyl transferase C (GTF C) | **Fwd:**GGTTTAACGTCAAAATTAGCTGTATTAGC<br>**Rev:**CTCAACCAACCGCCACTGTT |
| ***ftf*** | Fructosyl transferase (FTF) | **Fwd:**AAATATGAAGGCGGCTACAACG<br>**Rev:**CTTCACCAGTCTTAGCATCCTGAA |
| ***spa P*** | Cell surface antigen, SpaP (or Ag I/II) | **Fwd:**GACTTTGGTAATGGTTATGCATCAA<br>**Rev:**CTTCACCAGTCTTAGCATCCTGAA |
| ***com DE*** | Competence-stimulating peptide | **Fwd:**ACAATTCCTTGAGTTCCATCCAAG<br>**Rev:**TGGTCTGCTGCCTGTTGC |

#### 2.2.18.2 RNA extraction

To analyze the effect of nanomaterials treatment on the expression of virulence gene of *S. mutans*, qRT-PCR was performed. The organism was cultured in BHI media supplemented with sub inhibitory concentrations of nanomaterial. Bacterial culture

($O.D._{600}$ = 1) was diluted (1:10) and inoculated into fresh BHI media, followed by overnight growth at 37ºC. RNA was isolated using TRIzol reagent (Invitrogen, Life Technologies). Purified RNA was dissolved in diethylpyrocarbonate-treated water and was stored at -80ºC until required for cDNA preparation.

**2.2.18.3 cDNA synthesis**

cDNA was prepared using High Capacity cDNA Reverse Transcription Kit (Applied Bio systems, Foster City, USA). The reverse transcription reaction mixture (20µl) contained 2 µl 10X RT buffer, 0.8 µl 25X dNTP Mix (100 m M), 2 µl 10X RT Random Primers, 1 µl MultiScribeTM Reverse Transcriptase, 1µg of RNA and Nuclease-free $H_2O$ to make up the volume. It was incubated at 25ºC for 10 min, followed by incubation at 37ºC for 120 min. Finally, the reaction was terminated by incubating the mixture at 85ºC for 5 min according to the manufacturer's instructions. cDNA samples were stored at - 20ºC for further use.

**2.2.18.4 Quantitative real time PCR**

For qPCR primers were designed as described in section 2.2.18.2 to amplify the genes of interest (*vicR, gtfC, spaP, comDE,* ftf and 16S rRNA). qRT- PCR was done using the ABI-Prism 7000 sequence detection system (Applied Biosystems, Foster City, CA, USA) with an SYBR Green PCR master mix (Applied Biosystems) and carried out in Micro-Amp® Fast Optical 96 well plates (Applied Biosystems, USA). The reaction mixture (20 µl) contained 1X SYBR Green PCR master mix (Applied Biosystems), 1 µl of the cDNA samples and 0.5 µM of the appropriate forward and reverse primers. PCR conditions included an initial denaturation at 95°C for 10 min, followed by a 40 cycle amplification consisting of denaturation at 95°C for 15 sec and annealing and extension at 60°C for 1 minute.

Fluorescence was detected during the annealing and extension step of each cycle. The critical threshold cycle (Ct) was defined as the cycle in which fluorescence becomes detectable above the background fluorescence and is inversely proportional to the logarithm of the initial number of template molecules. After the last amplification cycle, a dissociation protocol was performed as follows: One cycle of 95°C for 15 sec, followed by 60°C for 1 min. This dissociation was done to ensure that only single products of the

correct size were being generated by the different primer pairs and that no products were produced in any template control samples. A standard curve was plotted for each primer set with Ct values obtained from the amplification of known quantities of *S. mutans* cDNA.

The expression levels of all the tested genes were normalized using the 16S rRNA gene of *S. mutans* was used as an internal standard. No significant difference was observed in the expression of the 16S rRNA gene in the various test conditions. Each assay was performed with at least two independent RNA samples in duplicate, and the x-fold change of the transcription level was calculated by the following equations (ABI Prism 7000 SDS Software version 1.1 with RQ study 1.0, Applied Biosystems):

i. Each cDNA: $\Delta Ct = Ct$ (target gene) – Ct (16S rRNA)

ii. $\Delta\Delta Ct = \Delta Ct$ (reference cDNA) – $\Delta Ct$ (test cDNA)

iii. Ratio = $2^{-\Delta\Delta Ct}$

### 2.2.19 *Coating of acrylic tooth with nanocomposite and estimation of biofilm production*

Nanocomposite coating on the tooth surface was done using sonochemistry as previously described [Eshed *et al.* 2012]. The nanocomposite coating on artificial acryl tooth (obtained from Dr Ziauddin Dental College at the Aligarh Muslim University) was performed by placing the tooth in a nanoparticle suspension in a sonicator. The tooth was kept at a constant distance from the sonicator tip throughout the process. The nanoparticle surface coating was characterized by SEM (EVO 40; Zeiss, Jena, Germany). Artificial coated and uncoated teeth were assayed for estimating the amount of *S. mutans* biofilm formation on their surface. Teeth were placed in a 24-well plate. Each well contained 2 ml of a suspension of *S. mutans* at a final concentration of ~ $1.5 \times 10^8$ CFU $ml^{-1}$ in BHI medium. After incubation for 24 h at 37°C, biofilm formation was assayed using the CV assay as described in section 2.2.7. To examine biofilm morphology, teeth samples were further exposed after incubation in fixative (glutaraldehyde + paraformaldehyde) for 4 h. Finally, samples were dehydrated using increasing concentrations of ethanol. Samples were then air dried and imaged by SEM.

### 2.2.20 *In vivo studies*

#### 2.2.20.1 *In vivo* toxicity studies

Acute oral toxicity of the nanoparticles was evaluated in accordance with the Organization for Economic and Cooperation Development (OECD) guidelines (1998) for testing chemicals. A limit test (2000 mg $kg^{-1}$ body weight of the animal) was carried out using five male Wistar rats in each group (treated and control) ranging from 150-200g in weight. These animals were housed in standard hard bottom, polypropylene cages. They were fed with standard pelletized diet and sterile tap water ad libitum. All animals were observed for change in their weight, behaviour and mortality till 14th day post administration of dose. Efforts were made to minimize animal suffering and the number of animals for experimentation purpose.

#### 2.2.20.2 Caries induction in rats

To determine the effects of nanoparticles on oral establishment and cariogenic potential of *S. mutans*, a total of 20 rats were purchased. These animals were divided into two groups; a control and a test group (n = 10 per group). All the animals were fed with erythromycin water (100 µg $ml^{-1}$) and a regular diet for 3 days in order to reduce the microbial load. To confirm the absence of *S. mutans* colonization in the oral cavity, oral swabs was plated on MSB agar plates. The animals were offered 5% sucrose diet ad libitum throughout the experiment in order to enhance the infection by *S. mutans*. On 4th day, their molar tooth surfaces were inoculated with streptomycin resistant strain of *S. mutans*-MT8148R ($1.4 \times 10^{10}$ CFU). The inoculation was repeated once every day for five consecutive days. After that nanoparticles were topically applied twice a day on the teeth of animals by means of camel's hair brush for 2 weeks. Swab samples were then taken from the surfaces of animal molars on the first day of first, third, sixth, eighth and tenth week's post-inoculation. The samples from control and treated group were pooled in 2 ml of 10 mM potassium phosphate buffer, serially diluted and plated on MSB agar plates containing streptomycin for total cell counts. The plates were incubated at 37°C for 2 days before enumeration of colonies of *S. mutans*. The percentages of the *S. mutans* cells were calculated to determine its oral colonization in the animals. At the end of the experimental period, all the animals were sacrificed. The jaws were then aseptically dissected and sonicated in 5 ml of 154 mM sterile NaCl in order to dislodge the dental

plaque. These samples of plaque were serially diluted and were streaked on mitis salivarius agar plates to estimate the *S. mutans* population. These plates were incubated at 37 °C for 2 days before enumeration of colonies. All of the jaws were de-fleshed, and suspended in 3.7% formaldehyde until caries scoring. All molars of the animals were examined under a dissecting microscope and carious lesions were scored by a Larson's modification of the Keyes system [Larson. 1981]. The results obtained were analyzed by Student's t test, with $p < 0.05$ considered as statistically significant.

#### 2.2.20.3 Scanning electron microscopy of animal tooth's surface

The effect of the nanoparticles on structural integrity of the biofilm and subsequent reduction in caries formation was also observed by scanning electron microscopy (SEM). The aseptically removed jaws of the animals (Wistar rats) were stored in normal saline and were directly visualized under SEM. The experiment was run in triplicates. Samples were analysed by SEM (Hitachi S-3000 N; High Technology Operation, Japan) at several magnifications.

### 2.2.21 *Cytotoxicity assay*

A human embryonic kidney cell line (HEK-293) obtained from National Centre for Cell Science (NCCS) Pune, was cultured in Dulbecco's Modified Eagle's Medium (DMEM) (Biological Industries, Beit HaEmek, Israel), supplemented with 10% heat inactivated foetal calf serum and IX Penstrep antibiotic solution, incubated at 37°C and 5% CO2. HEK-293 cell viability was measured using an MTT (3-(4,5-dimethythiazol-2-yl)-2,5-diphenyl tetrazolium bromide) assay as described earlier [Denizot & Lang 1986]. Exponentially growing cells (~ $10^5$cells well$^{-1}$) were seeded into 96-well culture plates and incubated with various concentrations of nanomaterials for 24h and 48h. Four hours before termination, the supernatants were removed and 90 µl of fresh medium and 10 µl of MTT (1 mg ml$^{-1}$) solution were added to each well. After further incubation for 4 h the formazan crystals formed by the cellular reduction of MTT were dissolved in 150 µl of DMSO and plates were read on an ELISA-reader using a 570 nm filter. All measurements were done in triplicate. The relative cell viability (%) related to control wells containing cells without nanomaterial was calculated as:

$$[A]\ \text{test} / [A]\ \text{control} \times 100$$

Where, [A]test is absorbance of the test sample and [A]control is the absorbance of the control sample.

### 2.2.22 *Intracellular uptake of nanocomposite in HEK- 293 and bio imagining*

HEK-293 cells were cultured in DMEM supplemented with 10% heat inactivated foetal calf serum (Biological Industries) and IX Penstrep antibiotic solution (Biological Industries) and then incubated in a fully humidified 5% $CO_2$ incubator at 37°C. All cells were seeded in culture flasks and were divided into treatment group and control group. When ~ 70% of growth occurred, the cells were washed with 0.1 M PBS (phosphate buffer saline) and old medium was replaced with fresh medium. Culture plates were treated with various concentrations of nanocomposite and incubated at 37°C and 5% CO2 for 24 h. All plates were washed with 0.1 M PBS and cells were collected by trypsinization (0.05% trypsinase). The cell pellets were dissolved in 1 ml of 0.1 M PBS and were imaged under bright field, UV-excitation and blue excitation with an Olympus Fluo ViewTM FV1000 laser scanning confocal microscope.

### 2.2.23 *Statistical analysis*

All experiments were performed in triplicates. For each outcome, data were summarized as mean ± standard deviation. The values obtained for different parameters (adherence, biofilm formation, synthesis of soluble and insoluble glucans, EPS production) were grouped into different classes on the basis of concentration of the compound added to the samples. Class I, was taken as control, where no compound was added. Values obtained for the control group were considered as maximal (100% for all variables). The values for the remaining classes were calculated relative to the control group. SD (standard deviation) was also calculated for all the observations. Differences between two mean values were calculated by Student's t-test using Microsoft excel and $p \leq 0.05$ considered as statistically significant. The one-way analysis of variance (ANOVA) was followed by a post hoc multiple comparisons (Tukey's test) to compare the multiple means using R software (ver 3.2.0). Data with p-values < 0.05 were considered statistically significant.

For qRT-PCR, the data were generated from at least three independent sets of experiments. A one-way analysis of variance (ANOVA) was performed using $2^{-\Delta\Delta Ct}$ values to compare all time points and treatment types P values were generated using the

Tukey's multiple comparison test in order to establish whether pairs of $2^{-\Delta\Delta Ct}$ values were statistically different or not. The ΔΔCt method was used to establish relative expression levels of the transcripts of interest. Based on the mathematics of real time PCR, the ΔΔCt method has been applied to calculate relative quantity of particular gene transcripts. A simple mathematical equation normalizes ΔCt values to reference gene ΔCt values, thereby accounting for variation in cDNA concentrations. Normalizing to an endogenous reference provides a method for correcting results for differing amounts of input RNA. The $2^{-\Delta\Delta ct}$ method uses data generated as part of the real time PCR experiment to perform this normalization function. The formula then compares these normalized samples to an appropriate control to generate a fold change ratio. Baseline values for each amplification curve and the threshold value for each sets were set manually. The Ct values for each sample were exported to a Microsoft Excel spreadsheet. If the PCR efficiency of the sample is not 100% this may invalidate the results, as the ΔΔCt method assumes a PCR efficiency of 100%. To adjust for this, the individual amplification efficiencies of one particular primer pair for each set of primers on a plate were averaged to give a reliable amplification efficiency adjustment.

The mean PCR efficiency was subsequently incorporated into the ΔΔCt equation for data analysis. The results were normalized between samples using the 16s rRNA expression level in order to generate ΔCt values. The ΔCt value describes the difference between the Ct value of the target gene and the Ct value of the corresponding endogenous reference housekeeping gene. 16S rRNA was chosen as the normalizing gene. The ΔΔCt method allows the comparison of the expression of each target transcript between the different treatment groups, and allows the calculation of the average fold change in the control group being 1 (i.e. no change) and the expression levels of the different treatment/outcome groups given as a fold change relative to the average of the control group.

Statistical analysis of these results was performed by R software (ver 3.2.0) and using the ΔCt or ΔΔCt values rather than the fold-change values, due to the fact that fold-change values do not follow a normal distribution. ΔCt and ΔΔCt values are effectively log transformed values and did not deviate significantly from a normal distribution. The results from each experimental set for each treatment type and time point were analyzed using the one-way ANOVA with Tukey's multiple comparison test as a post test.

Significance is expressed as $p \leq 0.05$. For the caries studies, the results were analysed by Student's t- test using Microsoft excel, with $p \leq 0.05$ considered as statistically significant.

## 3.1 Introduction

Oral biofilm are complex three dimensional structures with adherent multispecies bacterial communities contributing to dental caries and numerous periodontal diseases [Selwitz *et al.* 2007; Nance *et al.* 2013]. These are among the common infectious diseases which may lead to a major public health concerns [Falsetta *et al.* 2014]. Biofilms have greater tendency to resist antibiotics and create an environment that enhances microbial resistance with respect to their planktonic counterparts. *Streptococcus mutans* is one of the most frequently detected microorganism on the tooth surface and major etiological agent of human dental caries [Hasan *et al.* 2014]. This bacterium has also been recognized as a causative agent of endocarditis [Abranches *et al.* 2011]. By means of several unique mechanisms *S. mutans* manages its copious growth in oral cavity [Dmitriev *et al.* 2011]. Acidogenicity and aciduricity play a major role in the increase of severity of infection along with the ability to produce extracellular polysaccharide [Krol *et al.* 2014; Koo *et al.* 2003].

In present scenario implant systems are abundantly being utilized to replace missing teeth. Oral biofilm consisting mainly of *Streptococcus* spp. accumulates on implants [Nakazato *et al.* 1989]. The formation of biofilm in these implants is one of the major causes of implant failure [Costerton *et al.* 2005]. The inflammatory changes in the soft tissues surrounding the implant induced by the infection give rise to progressive destruction of the supporting bone [Zitzmann & Berglundh 2008]. Nanoparticle-based implant coatings may well offer useful antimicrobial and antibiofilm functionalities to prevent dental implant failure.

Nanoparticle based approaches are expected to open new horizon for preventing biofilm based infections by their unique mode of action [Ruparelia *et al.* 2008; Raghupati *et al.* 2011]. Zinc oxide nanoparticles (ZnO NP) have already been found as antibacterial against wide range of microorganisms [Huang *et al.* 2008; Xie *et al.* 2011], but its aggregation is one of the drawbacks which make them toxic against mammalian cells [Yuan *et al.* 2010]. Graphene oxide (GO) has unique physical and chemical properties [Wu *et al.* 2013]. GO contains a single layer of $sp^2$ carbon atom with hydroxyl and epoxy functional groups on surface and carboxyl groups at the edges [Dai *et al.* 2014]. These functional groups offer active sites for hybridization with metal and metal oxide, thus acts as a supporting surface for growing these nanoparticles [Ocsoy *et al.* 2013]. Graphene in

its functionalized state has been used for biosensing, photothermal therapy as well as drug delivery [Wang *et al.* 2011]. Recently, graphene and graphene based nanocomposites have gained a substantial interest in the field of nanomedicine as an antimicrobial agent [Ma *et al.* 2011; Xu *et al.* 2011; Tang *et al.* 2013; Fariaa *et al.* 2014]. Moreover, graphene oxide has been reported to show good biocompatibility [Chang *et al.* 2011]. To the best of our knowledge no study has yet been carried out on antibiofilm action of graphene/zinc oxide nanocomposite and GZNC coated teeth surface on *S. mutans*.

The objective of present study was to evaluate the antimicrobial, antibiofilm and anti-adherence activity of GZNC against *S. mutans* which is major cause of caries infection and to access its applicability as coating for dental implants.

### 3.2 Experimental overview

The graphene/zinc oxide nanocomposite (GZNC) was synthesized using method given in section 2.2.3.1 and 2.2.3.2. The characterization was performed using TEM (2.2.4.2), UV-visible spectroscopy (2.2.4.1), FTIR (2.2.4.4), XRD (2.2.4.5) and TGA (2.2.4.7). The sub inhibitory concentrations of GZNC against *S. mutans* (SM 497) and its clinical isolates (SM 34 and SM 06) were evaluated using methodology described in section 2.2.5. The method to investigate the effect of sub inhibitory concentrations of GZNC on virulence traits of *S. mutans* viz., adherence, biofilm formation, exopolysaccharide production, acidogenicity and glucan production is outlined in section 2.2.6, 2.2.7, 2.2.8, 2.2.13 and 2.2.12 respectively. The effect on bacterial viability and growth pattern was studied using methodology given in section 2.2.10 and 2.2.11 respectively. Moreover, SEM and CLSM was utilized to analyse its effect on the biofilm architecture (2.2.17). Amount of ROS produced in the presence of sub inhibitory concentrations of GZNC was evaluated using method outlined in section (2.2.16). Procedure adapted for synthesis and characterization of GZNC coated teeth is described in method section 2.2.19 and its antibiofilm potentials were investigated (2.2.19). Furthermore, cytotoxicity assay on HEK-293 cell line and internalization of GZNC in HEK-293 was performed using method outlined in section 2.2.21 and 2.2.22 respectively.

## 3.3 Results

### 3.3.1 *Characterization of GZNC*

TEM images (Figure 3.1a) of GZNC showed ZnO nanocrystals dispersed on the surface of graphene sheets. The average size of ZnO nanoparticle in composite was found to be in range of 20 to 40 nm (Figure 3.1b). The UV visible spectra of graphene, ZnO and GZNC are shown in Figure 3.1c. FTIR analysis of GZNC is represented in Figure 1d. Figure 3.2a represent the powder X-ray diffraction (XRD) pattern of nanocomposite. The average crystallite size of ZnO NPs was calculated following the Debye-Scherrer formula [Cullity 1978]. TG measurement was carried out in order to determine the mass ratios of ZnO to graphene in composite. TGA curve of GZNC is shown in Figure 3.2b.

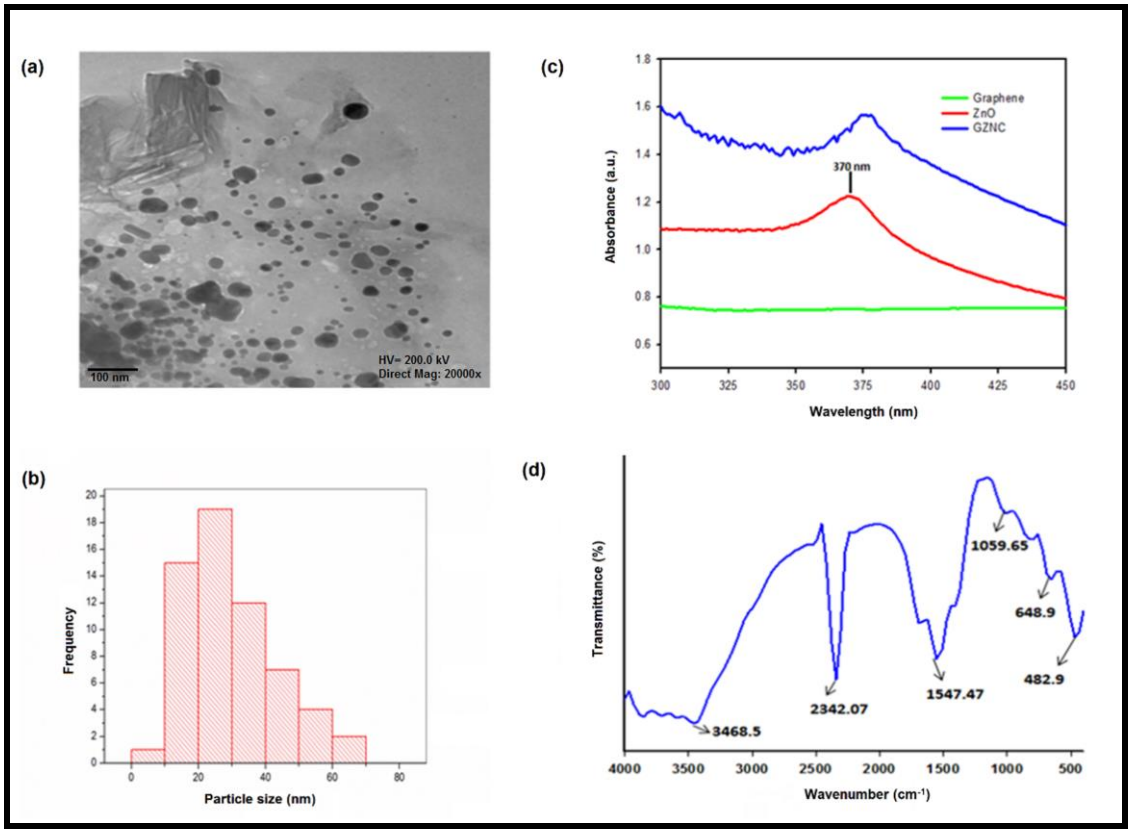


**Figure 3.1** Characterization of graphene/zinc oxide nanocomposite: (a, b) TEM image and particle size analysis of GZNC, (c) UV visible spectra of graphene, zinc oxide and GZNC, (d) FTIR spectra of GZNC.

### 3.3.2 *Enhanced antibacterial activity of GZNC*

The minimum inhibitory concentration (MIC) of GZNC against *S. mutans* and its clinical isolates was found to be 125 µg $ml^{-1}$ whereas MBC was found to be 250 µg $ml^{-1}$.

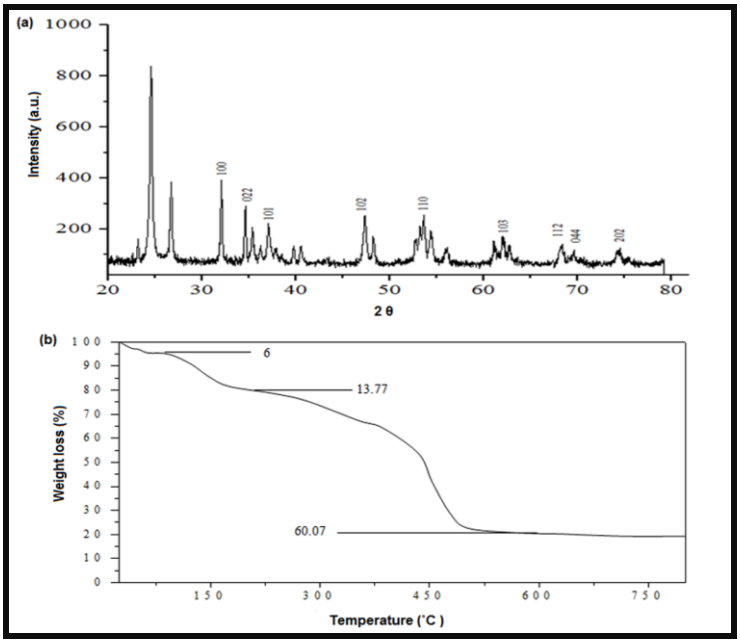


**Figure 3.2** (a) X ray diffraction pattern and (b) TG curve of GZNC.

### 3.3.3 *Effect on adherence*

The effect of sub inhibitory concentrations of GZNC on sucrose dependent adherence of all three strains is represented in Figure 3.3a. Sub inhibitory concentration (62.5 µg $ml^{-1}$) GZNC reduced the adherence of SM 497, SM 34 and SM 06 by 46%, 68% and 69% respectively (Results were statistically significant with P- values ≤ 0.05).

### 3.3.4 *Concentration dependent inhibition of biofilm*

Inhibition of biofilm formation by GZNC was in a dose dependent manner. Figure 3.3b embodies the effect of composite on biofilm formation. It was shown that 62.5 µg $ml^{-1}$ concentration of composite reduced biofilm formation by 80%, 44% and 29% in SM 497, SM 34 and SM 06 respectively (Results were statistically significant with P- values ≤ 0.05).

### 3.3.5 *Effect on viability of bacterial cells*

XTT assay was performed to detect the amount of viable cells present after treatment with composite. There was almost similar decrease in viability as compared to control in SM 497, SM 34 and SM 06 which was 37% , 31% and 38% respectively on treatment of 62.5 µg $ml^{-1}$ of GZNC. The reduction of viable cells was found to be concentration dependent on GZNC treatment (Figure 3.3c).

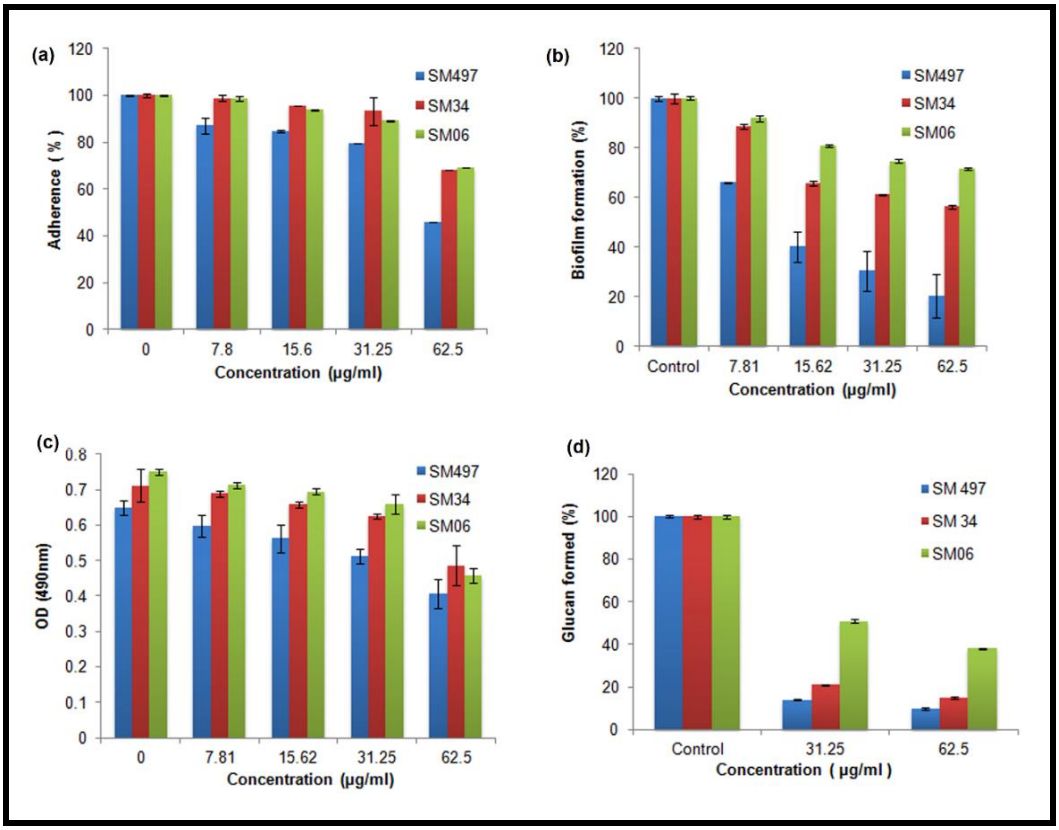


**Figure 3.3** inhibitory effects of sub-MIC concentrations of GZNC on: (a) sucrose dependent adherence, (b) biofilm formation, (c) viability (XTT assay), (d) Glucan formation. Each value is an average of triplicate and each bar indicate ± standard deviation (n =3).

### 3.3.6. *Effect on water insoluble glucan production*

The effect of different concentration of GZNC on synthesis of water insoluble glucans was evaluated (Figure 3.3d). There was 90%, 85% and 60% reduction in case of SM 497, SM 34 and SM 6 respectively (Results were statistically significant with P- values ≤ 0.05).

### 3.3.7 *Significant decrease in acid production*

Sub inhibitory concentration of GZNC was found to be efficient in reduction of acidogenicity of all three strains (Table 3.1). On treatment of GZNC, pH of media in SM 497 changed from 4.87 to 5.27, in SM06 the change in pH was from 4.41 to 5.06 and in SM 34 it changed from 4.39 to 6.67.

### 3.3.8 *Effect on growth*

The effect of sub inhibitory concentration of GZNC on growth of *S. mutans* was studied. There was no significant difference in growth curves of all strains as compared to their respective controls (Figure 3.4).

**Table 3.1** Effect of graphene/zinc oxide nanocomposite (GZNC) on acid production of *Streptococcus mutans* and clinical isolates

| | **pH±S.D. (onset)** | **pH±S.D. (control after 24 hrs)** | **pH±S.D. (treated after 24 hrs)** |
|---|---|---|---|
| **#SM 497[a]** | 7.37±0.09 | 4.87±1.14 | 5.27±0.06 |
| ***SM 06[b]** | 7.38±1.03 | 4.41±0.07 | 5.06±1.27 |
| ***SM 34[c]** | 7.37±0.08 | 4.39±1.23 | 6.67±0.09 |

# [a] SM 497 (MTCC strain), *[b] SM 06, [c] SM 34 (clinical isolates) [Islam *et al.* 2008]

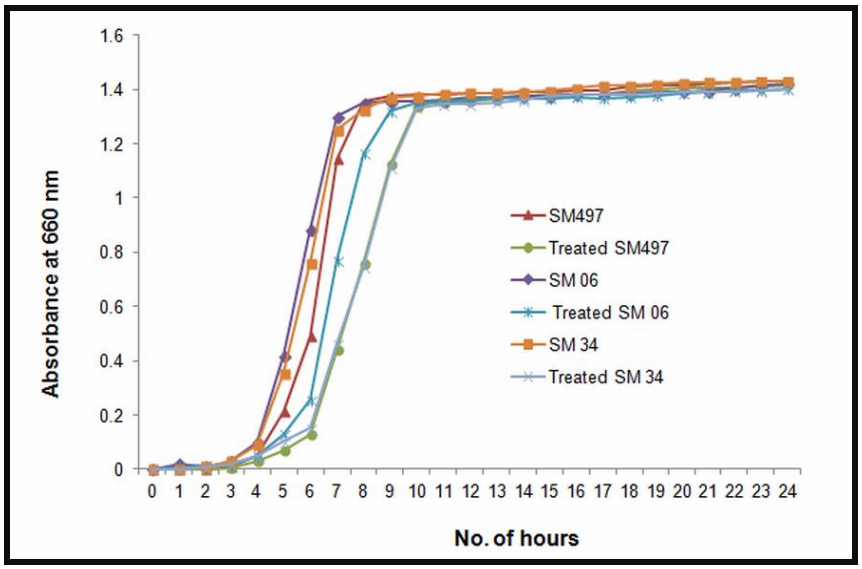


**Figure 3.4** The growth curves of treated and untreated SM 497, SM 06 and SM 34 cells over 24 hours.

### 3.3.9 *Significant reduction in EPS production*

EPS production in presence and absence of GZNC was evaluated by using Congo red dye, which binds to glucose containing polymers. Biofilm formation by *S. mutans* was tested by growing the organism in Brain heart infusion agar supplemented with Congo red in presence and absence of GZNC. When the colonies were grown without GZNC in the medium, the organisms appeared as dry crystalline black colonies, indicating the production of exopolysaccharide (Figure 3.5a). Whereas when the organisms were grown in presence of sub inhibitory concentration of GZNC organisms continued to grow, but GZNC treatment has decreased the synthesis of exopolysaccharides, indicated by the decrease in dry crystalline black colonies. To further verify the reduction in EPS, amount of attached Congo red was calculated by Congo red binding assay which directly relates to amount of EPS formed. Results showed almost 51 % reductions in EPS production on treatment with sub inhibitory concentration of GZNC (Figure 3.5b).

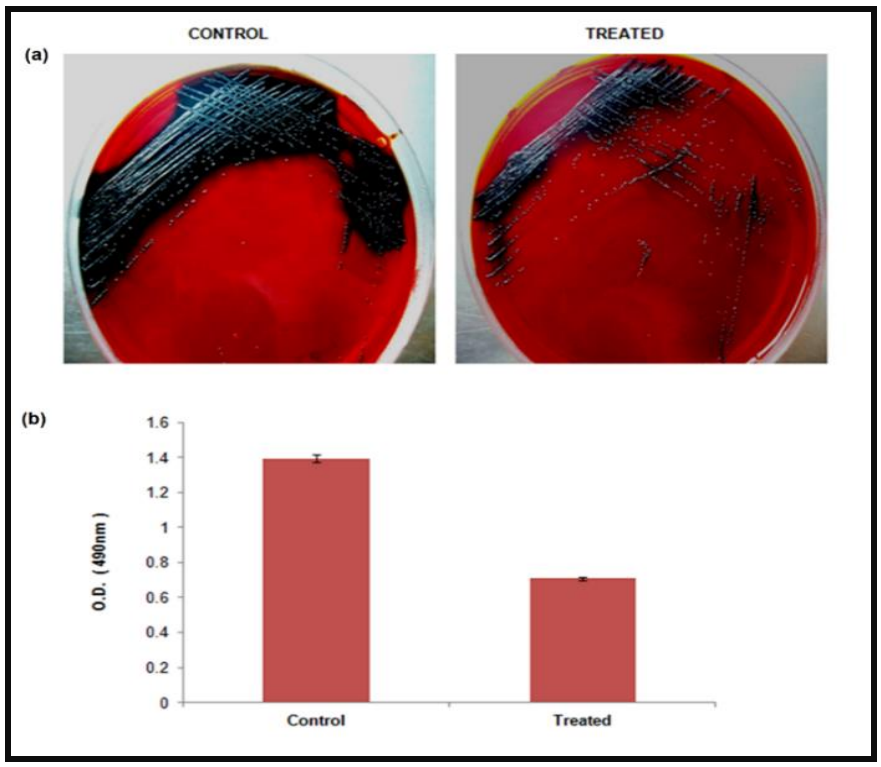


**Figure 3.5** (a) Congo red agar method: control plate showing more black crystalline colonies as compared to treated (b) Congo red binding assay: showing considerable decrease in amount of exopolysaccharide. Each value is an average of triplicate and each bar indicate ± standard deviation (n =3).

### 3.3.10 *Microscopic exploration of GZNC treated biofilm*

SEM and CLSM were performed to explore the architecture of cells in biofilm in presence of GZNC. In SEM image of control sample (Figure 3.6a) *S. mutans* cells can be seen embedded in the extracellular polysaccharides while in treated sample (Figure 3.6b). The cells were highly dispersed indicating reductions in extracellular polysaccharides. In CLSM analysis, majority of cells were live in non-treated samples and a green mat was visible with chains of *Streptococcus* interacting with each other (Figure 3.6c) while in treated cells were scattered all around with poor interaction representing reduction in biofilm (Figure 3.6d, e).

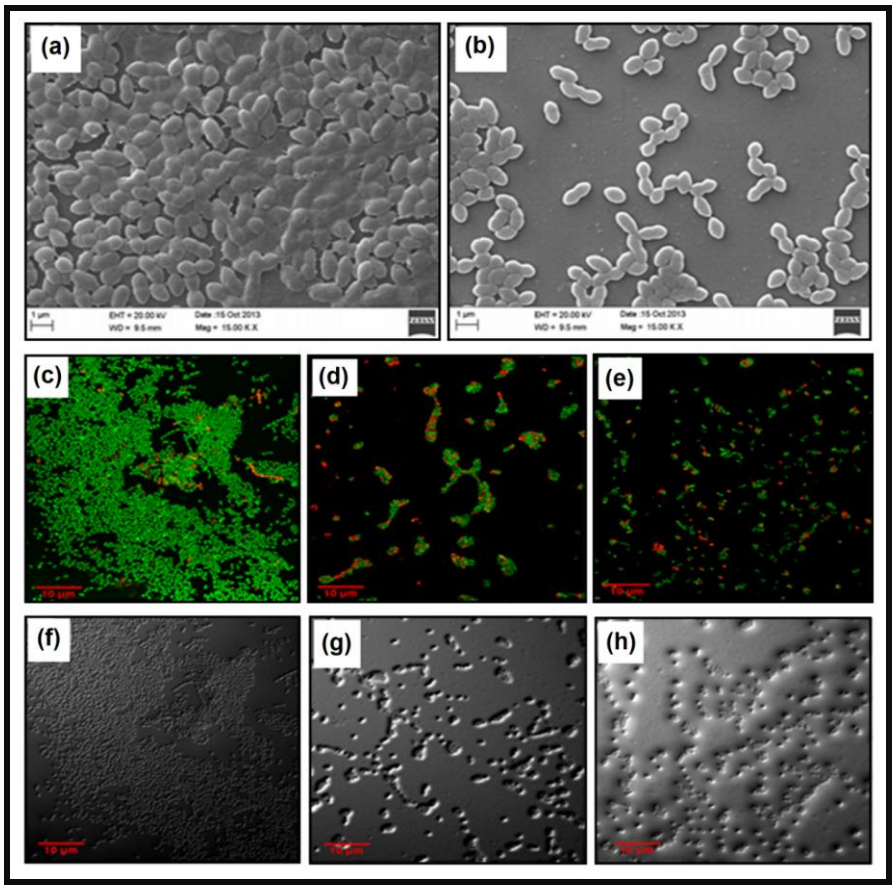


**Figure 3.6** Effect of GZNC on biofilm architecture: SEM image of *S. mutans* biofilm in (a) absence and (b) presence of GZNC, CLSM image of *S. mutans*: (c, f) Control biofilm, (d, g) 32.2 µg $ml^{-1}$ GZNC treated biofilm, (e, f) 62.5µg $ml^{-1}$ GZNC treated biofilm.

### 3.3.11 *Production of reactive oxygen species (ROS)*

Figure 3.7 represent the production of cellular ROS. GZNC showed a noticeable increase of cellular ROS in four hours as compared to control. Moreover, after 12 h considerable increase in ROS was determined with respect to control.

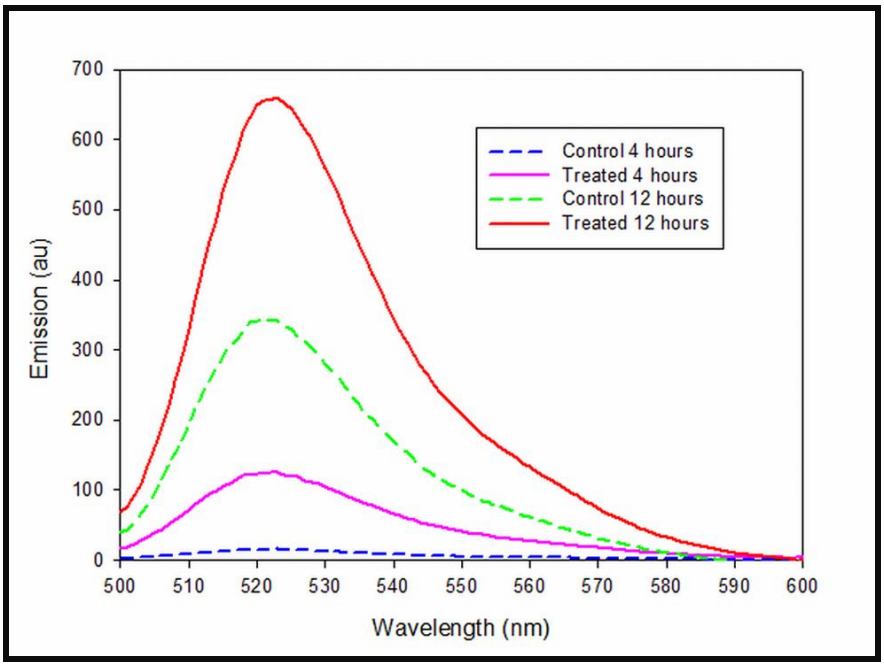


**Figure 3.7** Formation of reactive oxygen species in presence of GZNC.

### 3.3.12 *Cytotoxicity assay and intracellular uptake of GZNC*

Figure 3.8 shows the effect of GZNC on viability of HEK 295 cells. The effect was in dose dependent manner. There was almost 80% viability on treatment of cells with 200 µg/ml of GZNC which is 3 times higher concentration as used for antibiofilm experiment. Even at very high concentration of GZNC (up to 400µg $ml^{-1}$), the viability of cell was above 50% in 24 h of incubation (Results were statistically significant with P- values $\leq$ 0.05). Fluorescence of control sample and treated cells was observed by confocal laser scanning microscopy. Figure 3.9 shows the uptake of GZNC in HEK-293 cells. Enhanced fluorescence was seen in treated cells as compared to control. Cell membranes were seen to be damaged at higher dose of GZNC (400 µg $ml^{-1}$).

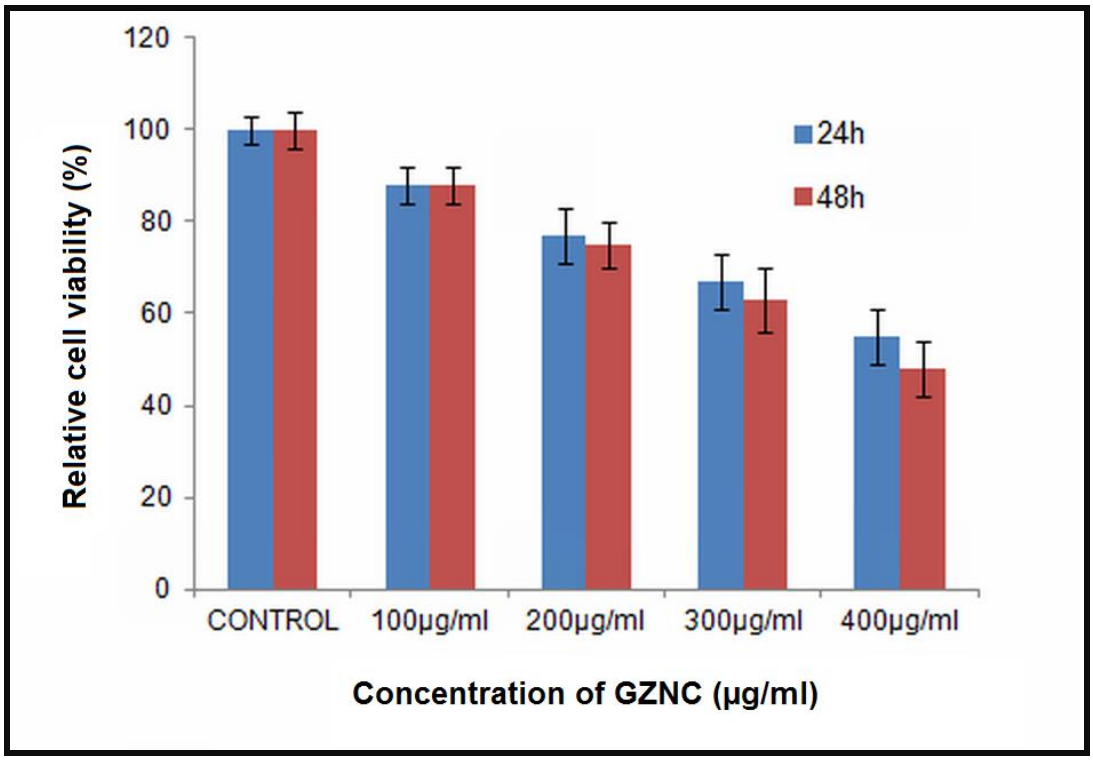


**Figure 3.8**. *In vitro* cytotoxicity assay (MTT) on HEK-293 cell line. Each value is an average of triplicate and each bar indicate ± standard deviation (n =3).

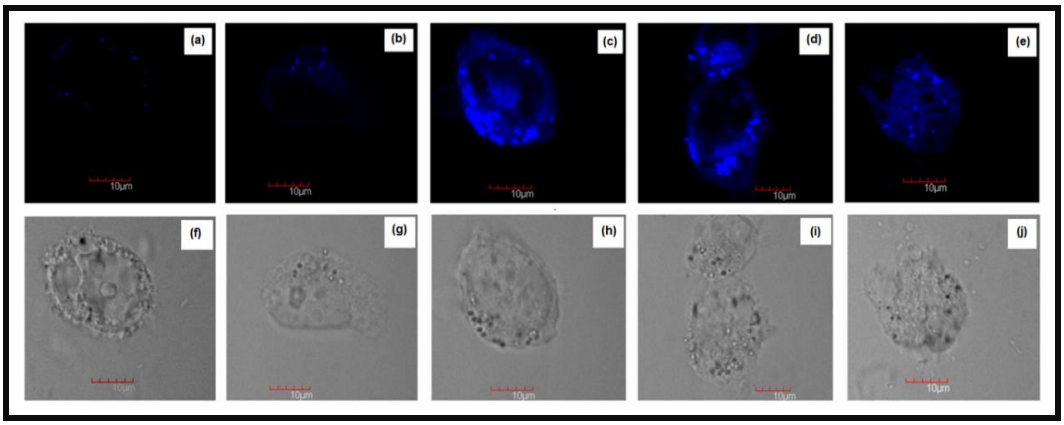


**Figure 3.9** CLSM image showing internalization of nanoparticle and its effect on HEK-293 cells (a, f) control, (b, g) 100µg $ml^{-1}$, (c, h) 200µg $ml^{-1}$, (d, i) 300µg $ml^{-1}$, (e, j) 400µg $ml^{-1}$.

### 3.3.13 *Characterization and antibiofilm properties GZNC coated teeth surface*

Figure 3.10a and 3.10c show the photograph of uncoated and coated teeth. The deposition GZNC was characterized by SEM, Figure 3.10b represent the uncoated acrylic tooth

surface while in figure 3.10d, a uniform coating was observed over the entire tooth surface. Further to quantify biofilm formed on surface of teeth, crystal violet assay was performed. GZNC-coated tooth reduced biofilm formation by 85% (Figure 3.10i), as compared to the uncoated tooth surface photographic images of crystal violet stained tooth surface clearly showed the inhibition of biofilm formation (Figure 3.10 j-m). These results were also supported by SEM imaging (Figure 3.10 e-f). Considerable reduction of *S. mutans* biofilm was observed on coated tooth (Figure 3.10e, f) as compared to the control tooth in which dense colonization was observed (Figure 3.10g, h).

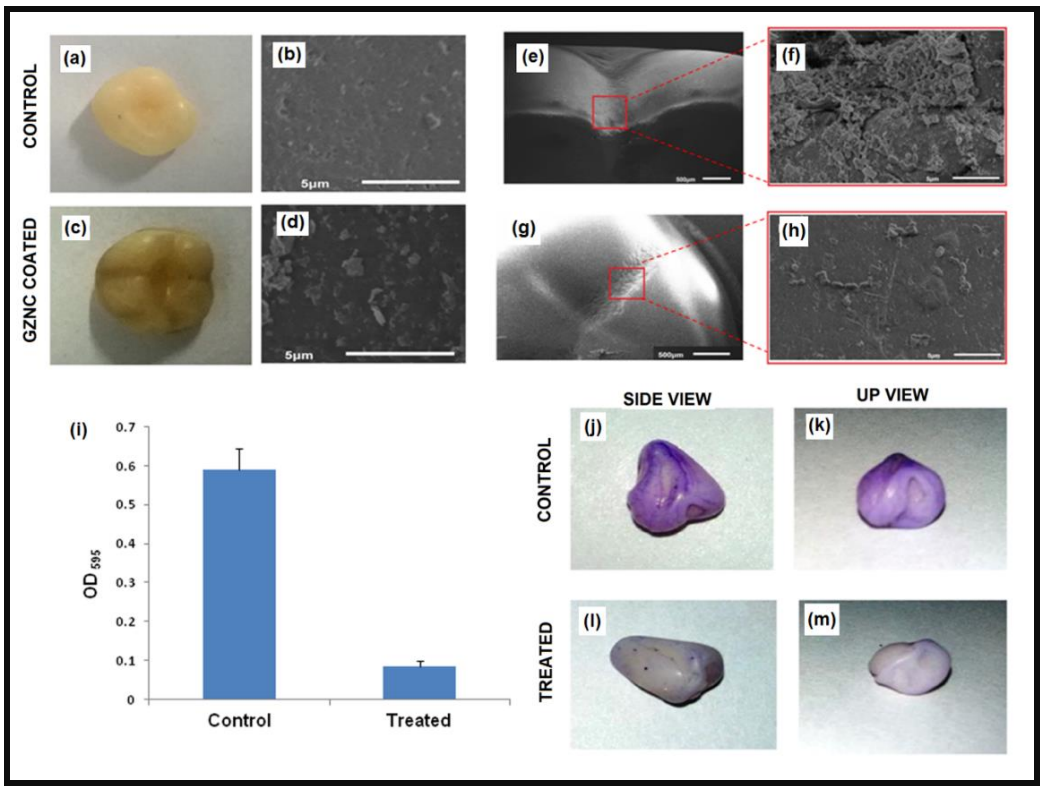


**Figure 3.10** (a) Photograph of non-coated and (c) GZNC coated acrylic teeth; SEM images of surface of teeth (b) control and (d) coated; Region from where SEM analysis for biofilm formation was done (e) control and (g) treated; Magnified view of selected regions: (f) In control showing well defined biofilm architecture and (h) almost negligible biofilm on treated; (i) Quantification of the biofilm biomass; Photograph of crystal violet stained (j, k) Control tooth and (l, m) treated tooth.

### 3.4 Discussion

Oral biofilms play a crucial role in development of dental caries and other periodontal diseases. *Streptococcus mutans* is one of the primary etiological agents in dental caries [Kŕol *et al.* 2014].The pathogenesis of *S. mutans* depends on various virulence factors including adherence, biofilm formation acidogenicity, aciduracity, and synthesis of exopolysaccharide [Hasan *et al.* 2015]. Nanotechnology has opened new horizon for the development of novel nanomaterial to combat chronic infections caused by biofilms. In present report, we explored the potential of graphene/zinc oxide nanocomposite (GZNC) against cariogenic properties of *Streptococcus mutans* and examined the antibiofilm behaviour of artificial acrylic tooth surface coated with GZNC graphene/zinc oxide nanocomposite. The synthesis of GZNC was performed using chemical method and a schematic representation of nucleation of zinc oxide nanoparticle on functionalized graphene oxide is illustrated in Figure 3.11.

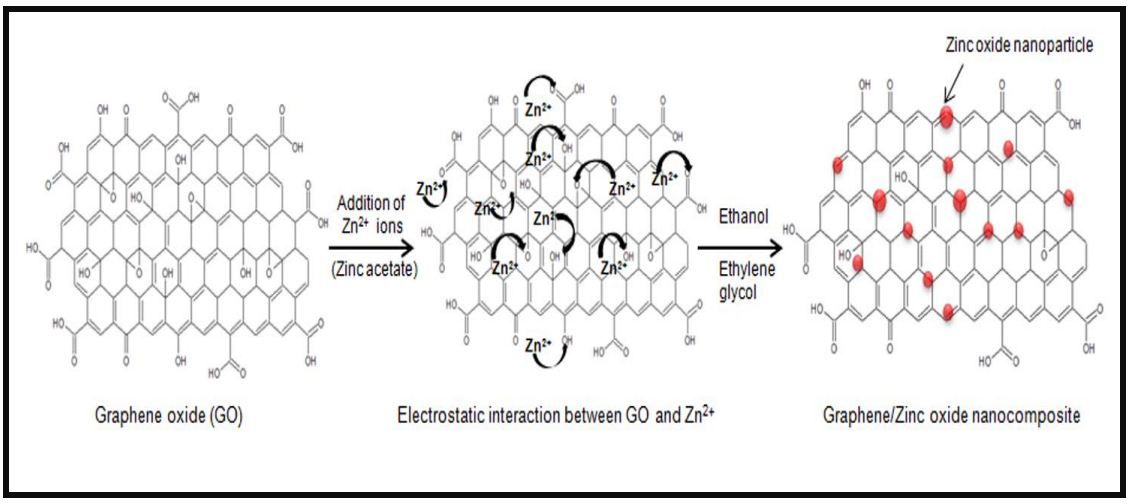


**Figure 3.11** Schematic representation of mechanism of nucleation of zinc oxide nanoparticle on surface of functionalized graphene sheet.

The presence of sharp characteristic absorption peak in UV-visible spectrum of GZNC at ~ 370 nm clearly indicated the formation of good crystalline ZnO nanostructures. In addition the red shift in GZNC curve as compared to pure ZnO shows increased $\pi$-electron concentration and structural ordering and may be ascribed to the chemical bonding (Zn-O-C bond) of zinc oxide and graphene [Hu *et al.* 2010; Liu *et al.* 2012] . TEM results confirmed the attachment of zinc oxide with GO platelets and ZnO

nanoparticle. FTIR spectra of GZNC showed strong absorption bands around 3468.5 $cm^{-1}$, 2342.07 $cm^{-1}$, 1547.47$cm^{-1}$, 1059.65 $cm^{-1}$, 648.9 $cm^{-1}$ and 482.9 $cm^{-1}$. The band at 3468.5 cm-1 may be assigned to O-H bond stretching of adsorbed water molecule. The absorption band at 1547.47 $cm^{-1}$ can be assigned to the stretching vibration of C=C of graphene and another at 1059.65 $cm^{-1}$ can be assigned at the stretching vibration of C–O of graphene [Wu *et al.* 2013].

The presence of Zn-O bond is supported by peak ~482.9 $cm^{-1}$ [Bora *et al.* 2013]. The Powder X-ray diffraction (XRD) pattern of nanocomposite is analysis confirmed that the GZNC consists of cubic ZnO. The average crystallite size of ZnO NPs was calculated following the Debye-Scherrer formula [Cullity 1978]. The calculated average particle size was found to be ~14.76 nm. In TGA curve the weight loss of 6.0 % occurring at about 65 °C is associated to adsorbed water. Pyrolysis of the labile oxygen-containing functional groups at about 200 °C accounts for 13.77 % of weight loss. The thermal decomposition observed in the temperature range 200–500 °C with 60.07% of weight loss attributed to the pyrolysis of the carbon skeleton.

The antibacterial effect of GZNC is much better than ZnO nanoparticle alone where MIC and MBC are reported to be 500 ± 306.18 µg $ml^{-1}$ and 500µg $ml^{-1}$ respectively [Hernández-Sierra *et al.* 2008]. Thus, reflecting that graphene is enhancing the antibacterial property of ZnO nanoparticles. It is also clear from our results that the killing of planktonic cells of *S. mutans* is irrespective of clinical and reference strain. In view of above results it is evident that the nanostructure formed by interaction of ZnO with graphene is providing a unique nano-interface for interacting with microbes as compared to ZnO alone.

The focus of this study was to reduce biofilm rather suppressing the population of *S. mutans* in oral cavity; further studies were performed on sub inhibitory concentrations of composite. Adherence of bacteria to the tooth surface is an important step in biofilm formation and reduction in adherence could serve as preventive step in biofilm formation [Hasan *et al.* 2012]. There is considerable decrease in sucrose dependent adherence on treatment of sub inhibitory concentrations of GZNC in all three strains. *S. mutans* secrete exopolysaccharide (glucans) in presence of sucrose which help in clumping and adherence of cells. This implies that composite is reducing the polysaccharide mediated adherence of bacteria.

Biofilm formation on the tooth surface is the main reason behind the initiation of dental caries. The role of *S. mutans* biofilm in initiation of cariogenesis is well documented [Loesche 1989; Hasan *et al*. 2015]. In the presence of GZNC there was substantial decrease in biofilm forming abilities of *S. mutans* and its clinical isolates. XTT and growth curve results revealed nanocomposite is inhibiting the virulence trait without affecting the bacterial viability.

Acid production and acid tolerance are considered to be the main physiological factors linked with cariogenic potential of *Streptococcus mutans* [Krol *et al.* 2014]. GZNC was found to be efficient in reducing the acid production in both reference and clinical strains. Reducing the acid production is one of the cariostatic effects and may also influence biofilm forming abilities of *S. mutans* [Welin-Neilands & Svensater 2007]. Water insoluble glucans play a significant role in adhesive interaction as compared to water soluble glucans. A considerable reduction in insoluble glucans was observed in presence of GZNC. Lowering in amounts of insoluble glucans could influence the process of biofilm formation by disturbing physical integrity and stability, affecting the diffusion properties and reducing the binding sites for *Streptococcus mutans*. The malformed exopolysaccharide matrix containing less insoluble glucans may also be more susceptible to the influences of antimicrobials and other environmental attacks [Wang *et al.* 2013].

The production of exopolysaccharide (EPS) is one of the key virulence factors of cariogenicity as it is produced by bacteria for the formation, spread and maintenance of biofilms. EPS mediate the adhesion of biofilms to surfaces, provide mechanical stability and transiently immobilize cells [Flemming & Wingender 2010]. The result of Congo red binding assay exhibited that nanocomposite is reducing the EPS production which is pre-requisite for formation and maintenance of biofilm. SEM and CLSM images were in concordance with the above discussed results validating that GZNC is inhibiting the formation of *S. mutans* biofilm.

The antibacterial properties of many nanoparticles have been attributed to the production of reactive oxygen species, such as $TiO_2$ [Su *et al.* 2009], Ag NPs [Vecitis *et al.* 2010]. GZNC showed a noticeable increase of cellular ROS. The internalization of zinc oxide nanoparticles in bacteria is inducing the production of reactive oxygen species (ROS). The production of reactive oxygen species in bacteria can affect DNA may also affect the total cellular machinery of bacteria [Xie *et al.* 2011].

Our study confirms GZNC to be very effective against some of the main caries causing virulence factors of *S. mutans*. The antibiofilm property of GZNC may be attributed to wrapping of graphene sheets on bacterial surface which reduce the cell to cell interaction and further cause the deposition of ZnO nanoparticle on bacterial surface leading to high concentration of zinc ions in cell. Moreover, the leaching of $Zn^{2+}$ ions from nanoparticles may inhibiting the active transport and metabolism of sugars. Zinc has also been reported to reduce acid production by *S. mutans* and has an ability to inhibit glucosyltransferase activity [Aydin Sevinc & Hanley 2010].

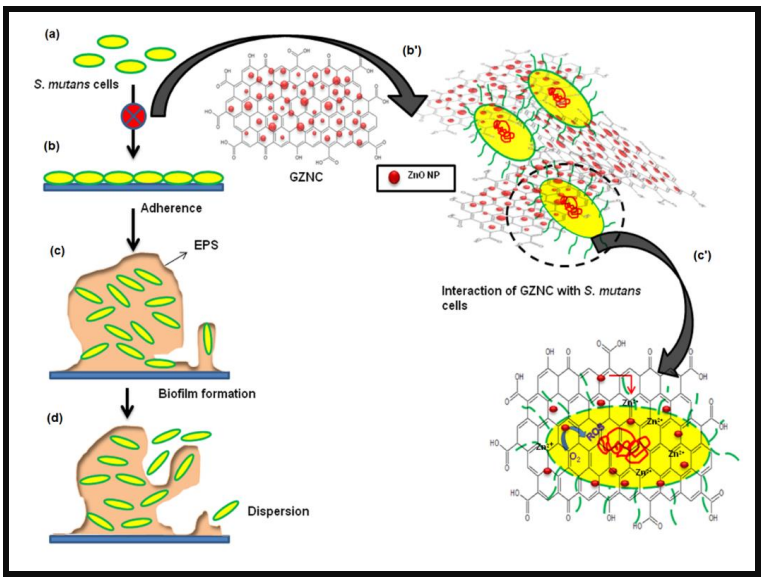


**Figure 3.12** Schematic representation of proposed mechanism of antibiofilm activity of GZNC: (a-d) Steps of biofilm formation in absence of any inhibitory agent ; (a) *S. mutans* cells, (b) Cells adhere to the surface, (c) Biofilm formation and production of exopolysaccharide (EPS), (d) Dispersal of biofilm, (a, b',c') GZNC inhibits the adherence of *S. mutans* consequently blocking all further steps of biofilm formation; (b') GZNC wrap around *S. mutans* surface making direct contact with Zinc oxide nanoparticle thus inhibiting cell to cell contact (c') Entry of Zinc oxide nanoparticle in cell leading to the production of reactive oxygen species, further leaching of $Zn^{2+}$ ions from zinc oxide nanoparticle inhibiting virulence factors of *S. mutans* and also assisting in antibiofilm action.

Based on above discussion we have proposed the mechanism of antibiofilm activity of GZNC against *S. mutans* as described in Figure 3.12. Biofilm formation in *S. mutans* is

complex process and more investigation is needed to further understand the mechanism of biofilm inhibition in presence of graphene/ zinc oxide nanocomposite.

Despite potential antibacterial activity, the use of nanoparticle as therapeutic is limited because of their cytotoxicity against mammalian cells [Yen *et al.* 2009]. Graphene oxide has already been investigated to be non-toxic even at very higher concentrations [Chang *et al.* 2011]. On the other hand due to aggregation and other factors zinc oxide nanoparticles have been reported to be toxic to mammalian cells at even low concentration [Yuan *et al.* 2010]. Our results clearly indicate that graphene/zinc oxide nanocomposite show negligible toxicity against HEK-293 cell line at used concentration. These observations may confirm the promising antibacterial and antibiofilm activity of GZNC.

Dental implants are widely accepted for replacing natural teeth. A considerable proportion of medical implants are cause of device related infection [Costerton *et al.* 2005]. Moreover these infections are difficult to eradicate because bacteria that cause these infections live in well- developed biofilms. *S. mutans* biofilm is one of the causes of failure of dental implant [Busscher *et al.* 2010]. Oral implant related biofilms can cause inflammation of peri-implant tissues which may be a direct cause of periodontal disease [Heuer *et al.* 2007]. In general the most effective way to prevent biofilm formation on implants is to prohibit the initial bacterial adhesion as biofilm are relatively difficult to remove after formation. Therefore these infections may be greatly reduced through improving antimicrobial and antibiofilm properties of implant surface by means of surface modification [Zhao *et al.* 2009].

Acrylic teeth are choice of dental prosthesis. The basic ingredient of Acrylic teeth is poly-methyl methacrylate (PMMA) resin. PMMA resins are resilient plastics formed by joining multiple methyl methacrylate molecules. A cross linking agent is added which serves as a bridge that unites two polymer chains [Stoia *et al.* 2011]. In this manner it yields a net like structure that provides increased resistance to deformation. So these teeth have greater fracture toughness, easier to adjust. Thus, our focus was to observe the ability of nanoparticle coated acrylic tooth to inhibit biofilm formation. Acrylic teeth were coated by GZNC using sonochemistry. Sonochemical irradiation has been demonstrated as a successful technique for the synthesis and deposition of nanoparticles on/into glass, polymer supports, and fabrics as well as tooth surface [Pol *et al.* 2005;

Eshed *et al.* 2013].The results revealed a significant inhibition of biofilm formation on the surface of coated teeth as compared to non-coated suggesting GZNC as a potential coating material for dental implant.

Our study concludes graphene/zinc oxide nanocomposite as effective antibacterial and antibiofilm agent against *S. mutans*. Moreover, it shows a significant reduction in biofilm and cariogenic properties of *S. mutans* in presence of sub inhibitory concentration of GZNC. This is the first study where GZNC has been investigated as a potential coating material for dental implants. GZNC coated acrylic tooth surface successfully inhibited the *S. mutans* biofilm (85%) formation. Furthermore, the lower toxicity of our nanocomposite makes it an effective coating agent for dental implants. However, future work on the stability and practical implication of this nanocomposite is clearly required before it can actually be implemented.

## 4.1 Introduction

Dental caries are characterized by dissolution of tooth enamel and are cause of public health concern [Nakano *et al*. 2007; Falsetta *et al*. 2014]. Major factor influencing the dental decay is an assault of tooth surface by oral microbial biofilms [Selwitz *et al*. 2007; Nance *et al*. 2013]. *S. mutans* is considered to be one of the main etiological agents of dental caries and is best known biofilm forming oral bacterium [Loesche 1989; Hasan *et al*. 2015]. Acid production by fermentation of dietary carbohydrate (acidogenesis), formation of exopolysaccharide, biofilm formation along with its ability to survive in an acidic environment (aciduracity) are some of the prominent characteristics which help *Streptococcus mutans* in their cariogenic process [Koo *et al*. 2003; Krol *et al*. 2014]. Eradication of dental biofilm is very difficult and only mechanical cleaning like brushing or flossing the teeth is not sufficient. Thus, to improve the oral health it is important to formulate approaches that can inhibit or delay the biofilm formation.

Fluorides and its various preparations are of great importance in dentistry [Marquis *et al*. 2003]. In its ionic form fluoride prevents the demineralization and helps in remineralization of tooth enamel [Featherstone 1999]. Fluoride also exerts effects on biological activity of caries causing bacteria. They reduce the ability of plaque forming bacteria to produce acid and can impair glycolysis by inhibition of enolase activity [Hamilton 1977]. Furthermore, they work on membrane associated proton pump ($H^+$-ATPase) by inhibiting it and in turn reducing the cellular level of ATP [Sutton *et al*. 1987; Eshed *et al*. 2013].

It is believed that topical application of fluoride on tooth surface leads to the formation of calcium fluoride like material which act as the reservoir of fluoride ions and during caries challenge it releases fluoride at low pH in plaque and protects the tooth's surface from caries [Rošin-Grget & Lincir 2001; Rølla & Saxegaard 1990]. Nevertheless, the limited concentration of calcium ion in mouth results in the formation of only limited amount of calcium fluoride like deposits after topical application of conventional fluoride formulations [Saxegaard & Rolla 1989].

Nanoscale based approaches are being widely used and have been proven to be more effective in the elimination of biofilms and in inhibition of dental caries [Eshed *et al*. 2013; Kulshrestha *et al*. 2014; Hernández-Sierra *et al*. 2008]. Their high surface to

volume ratio provides them with unique properties which can be exploited for the development of new therapies and drugs [Raghupati *et al*. 2011]. Sun and Chow have demonstrated that calcium fluoride nanoparticle ($CaF_2$-NPs) rinse can increase the level of fluoride ions in the oral fluid and in another study the strength and the fluoride release capacity of dental composite having $CaF_2$-NPs have been shown [Sun and Chow 2008; Xu *et al*. 2008]. However, there are no studies focusing on the direct effect of $CaF_2$-NPs on caries causing virulence factors like exopolysaccharide production, biofilm formation, aciduracity and acidogenesis of *S. mutans* as well as its effect on demineralization of dental enamel.

The main objective of this study was to formulate calcium fluoride nanoparticles ($CaF_2$-NPs) and to evaluate its effect on some of the major virulence factors of *S. mutans*. Furthermore, we have investigated $CaF_2$-NPs effect on caries development in *in vivo* model to evaluate its use as a topical applicant for prevention of dental caries.

### 3.2 Experimental Overview

Calcium fluoride nanoparticles ($CaF_2$-NPs) were synthesized using methodology described in section 2.2.3.3. Characterization of nanoparticle was performed by UV-visible spectroscopy (2.2.4.1), TEM (2.2.4.2), SEM (2.2.4.3), XRD (2.2.4.6) and FTIR (2.2.4.4). The minimum inhibitory concentration and minimum bactericidal concentration of $CaF_2$-NPs were evaluated method outlined in section 2.2.5. The effect of sub inhibitory concentrations of $CaF_2$-NPs on virulence traits of *S. mutans* viz. adherence, biofilm formation, exopolysaccharide production, water soluble and insoluble glucans and glycolytic pH drop was investigated by methodology described in sections 2.2.5, 2.2.7, 2.2.8.1, 2.2.12 and 2.2.14 respectively. The effect of sub inhibitory concentrations of $CaF_2$-NPs on the dispersion of preformed biofilm was assessed using method given in section 2.2.9. The growth pattern of *S. mutans* in presence of sub inhibitory concentrations of $CaF_2$-NPs was evaluated by method provided in section 2.2.11. TEM and CLSM analysis were performed to investigate the effect of $CaF_2$-NPs on the cells and biofilm architecture of *S. mutans* respectively, methodology is described in section 2.2.17. Moreover, the effect of $CaF_2$-NPs on expression of gene involved in *S. mutans* virulence pathway was also studied by quantitative RT-PCR as outline in section 2.2.18. The oral toxicity of these nanoparticles and their anti-cariogenic effect *in vivo* was evaluated by

method given in section 2.2.20. Cytotoxicity assay was also performed on HEK-293 cell line (section 2.2.21).

## 4.3 Results

### 4.3.1 *Characterization of calcium fluoride nanoparticles*

TEM analysis of $CaF_2$-NPs was performed to determine its morphology and size (Figure 4.1a). The particles were found to be in the nanometre range with average particle size of 15-25 nm (Figure 4.1b). SEM image (Figure 4.1d) of nanoparticle revealed the morphology of synthesized nanoparticle. UV-visible spectroscopy of the nanoparticle is represented in Figure 4.1c. FTIR spectrum of $CaF_2$-NPs showed a strong band at ~3400$cm^{-1}$, 1678$cm^{-1}$, 430 $cm^{-1}$ (Figure 4.1e). Furthermore, Figure 4.1f is a typical XRD pattern of $CaF_2$-NPs.

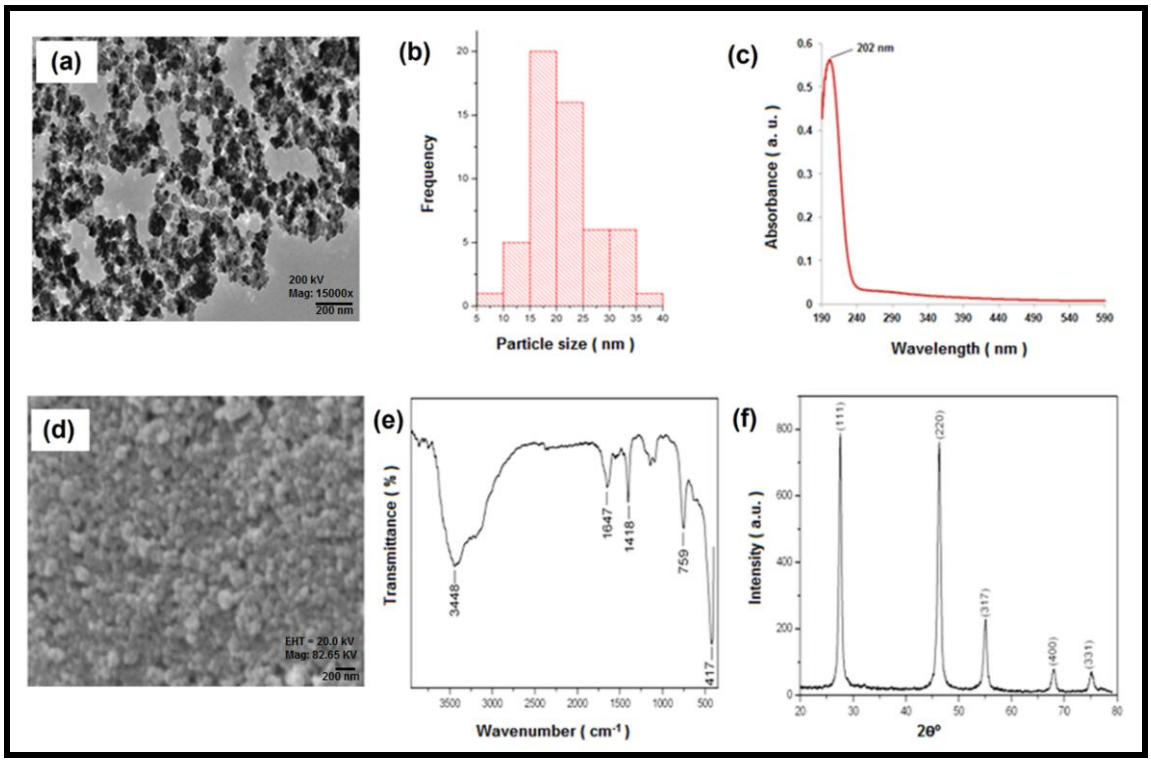


**Figure 4.1** Characterization of $CaF_2$-NPs: (a) Transmission electron microscopy image of $CaF_2$-NPs, (b) Particle size ~ 15-25 nm, (c) UV visible spectrum of $CaF_2$-NPs, (d) Scanning electron microscopy image, (e) FTIR spectrum, and (e) XRD pattern of $CaF_2$-NPs.

### 4.3.2 *Effect on bacterial viability*

The minimum inhibitory concentration of $CaF_2$-NPs on *S. mutans* was found to be > 64 mg/ml.

### 4.3.3 *Significant reduction in biofilm*

Biofilm formation ability of *S. mutans* in presence of different concentration (4, 2, 1 mg $ml^{-1}$) of $CaF_2$-NPs was evaluated using crystal violet assay (Figure 4.2a). There was almost 89%, 71% and 62% reduction in biofilm forming ability of *S. mutans* as compared to control when treated with 4 mg $ml^{-1}$, 2mg $ml^{-1}$ and 1mg $ml^{-1}$ concentration of nanoparticles respectively. With the decrease in nanoparticles concentrations there is gradual increase in its biofilm formation ability. This suggests a concentration dependent reduction in biofilm formation.

### 4.3.4 *Effect on EPS production*

A considerable decrease in EPS production in *S. mutans* in the presence of $CaF_2$-NPs was observed and the reduction is in a concentration dependent manner (Figure 4.2b). A 90 %, 65% and 64% decrease in EPS production by *S. mutans* was observed when treated with 4 mg $ml^{-1}$, 2mg $ml^{-1}$ and 1mg $ml^{-1}$ of $CaF_2$-NPs respectively, as compared to untreated sample. The highest EPS production was seen in control when no nanoparticles were present. When nanoparticle concentration increased, the EPS production decreased.

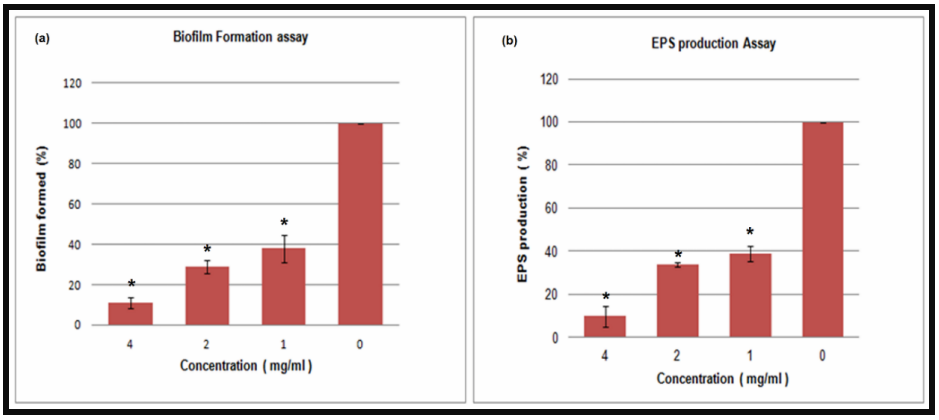


**Figure 4.2** Inhibitory effect of sub-MIC concentration of $CaF_2$-NPs (a) Biofilm formation (b) EPS production. Data are mean ± S.D. (n=3), statistical significance as compared with the untreated control ($p< 0.05$) denoted by an asterisk (*).

### 4.3.5 *Growth curve pattern*

Growth curve was used to investigate the effect of $CaF_2$-NPs on *S. mutans* growth. The results displayed a typical sigmoidal pattern and there was no significant variation between control and treated samples (Figure 4.3). The results clearly indicated that bacterial growth is not hindered at concentration of nanoparticle used in the study.

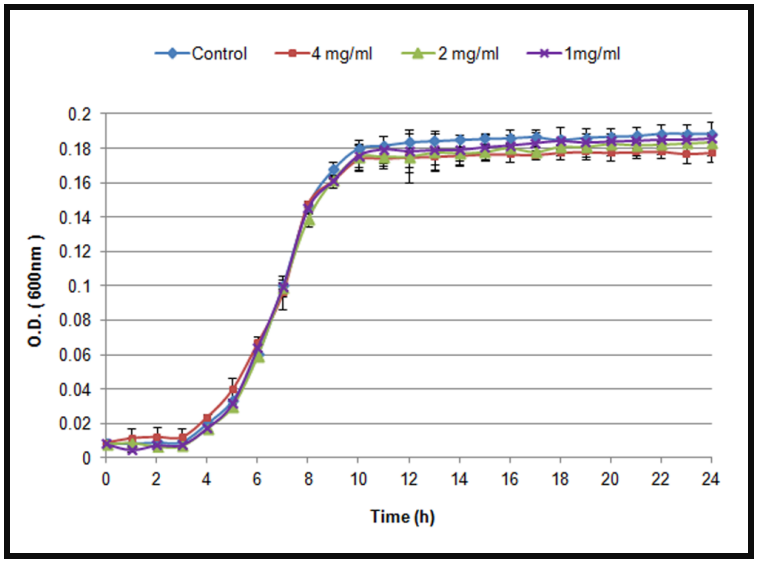


**Figure 4.3** Growth curves of $CaF_2$-NPs treated and untreated *S. mutans* (O.D values, 1:10 times diluted). The data represent mean ± S.D.

### 4.3.6 *Effect on adherence*

The inhibitory effect of different concentration of $CaF_2$-NPs on initial adherence of *S. mutans* is shown in Figure 4.4 (a). There was 70%, 57% and 44% inhibition of attachment of *S. mutans* to the glass surface in presence of 4mg $ml^{-1}$, 2mg $ml^{-1}$ and 1 mg $ml^{-1}$ concentrations of $CaF_2$-NPs respectively.

### 4.3.7 *Dispersion of preformed biofilm*

Different concentrations of $CaF_2$-NPs were used to evaluate their effect on treatment of preformed biofilm of *S. mutans* (Figure 4.4b).There was 11% , 7% and 5% reduction of preformed biofilm on treatment with 4mg $ml^{-1}$, 2mg $ml^{-1}$ and 1 mg $ml^{-1}$ concentrations of $CaF_2$-NPs respectively.

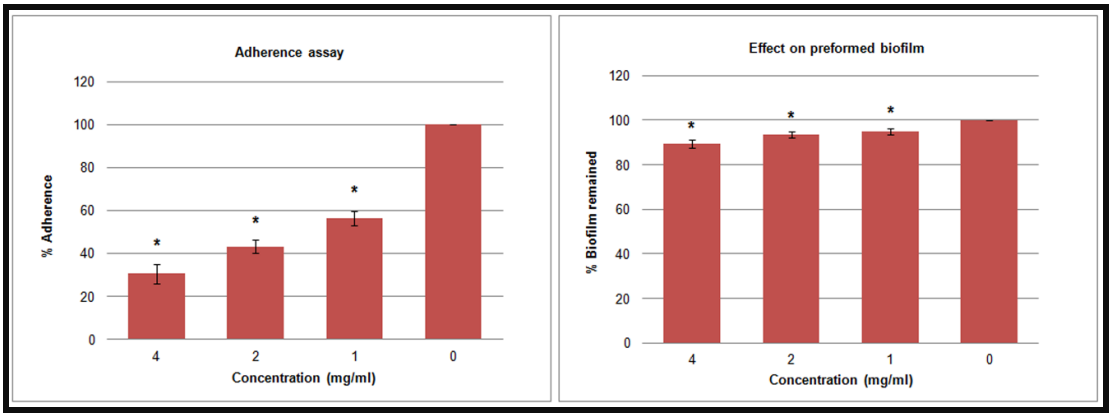


**Figure 4.4** Inhibitory effect of sub-MIC concentration of $CaF_2$-NPs (a) Adherence assay (b) Preformed biofilm reduction. Data are mean ± S.D. (n=3), statistical significance as compared with the untreated control ($p< 0.05$) denoted by an asterisk (*).

### 4.3.8 *Reduction in glucan production*

A significant reduction in both insoluble glucan and soluble glucan production was observed in *S. mutans* when treated with $CaF_2$-NPs (Figure 4.5). Almost 90% reduction was observed in treated sample as compared to control. Soluble and insoluble glucans both were reduced to the same extent in the present experiment.

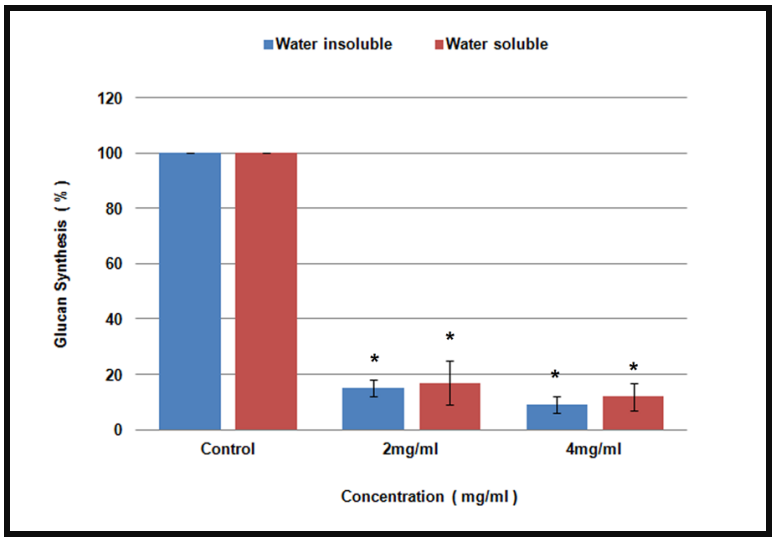


**Figure 4.5** Inhibitory effect of $CaF_2$-NPs on synthesis of water soluble polysaccharide and water insoluble polysaccharide (Glucans). Data are mean ± S.D. (n=3), statistical significance as compared with the untreated control ($p< 0.05$) denoted by an asterisk (*).

### 4.3.9 *Decrease in rate of acid production and stress tolerance*

As shown in Figure 4.6, the acid tolerance ability of *S. mutans* was inhibited appreciably in the presence of $CaF_2$-NPs. The onset pH of 7.2 dropped to 4.5 in control while in treated samples (4 mg $ml^{-1}$) final pH was 5.2. Furthermore, the rate of initial pH drop in 10 min was calculated to be 0.14 $min^{-1}$ to 0.09 $min^{-1}$ in case of control and treated samples respectively, demonstrating pronounced reduction in the acid production ability of *S. mutans.*

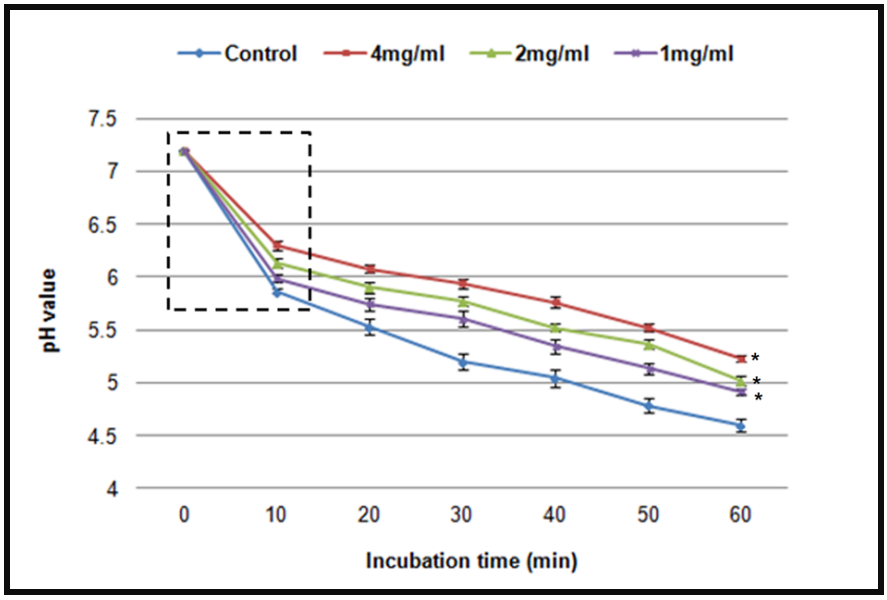


**Figure 4.6** Effect on sub-MIC levels of $CaF_2$-NPs on glycolytic pH-drop (the values enclosed in box corresponds to the initial rate of pH drop). Data are mean ± S.D. (n=3), statistical significance as compared with the untreated control ($p < 0.05$) denoted by an asterisk (*).

### 4.3.10 *Expression profile of virulence gene*

Quantitative RT-PCR was performed to gain insight into the effect of $CaF_2$-NPs treatment on the expression of virulence genes (*gtfC, vicR, ftf, comDE, spaP*) in *S. mutans*. An entire set of genes was down regulated after treatment with nanoparticles (Figure 4.7). The expression *spaP* decreased by 80% ant that of *vicR* and *comDE* genes by > 50%. The decrease in expression of *gtfC* gene was 32% and a suppression of 14% was observed in the expression of *ftf* gene.

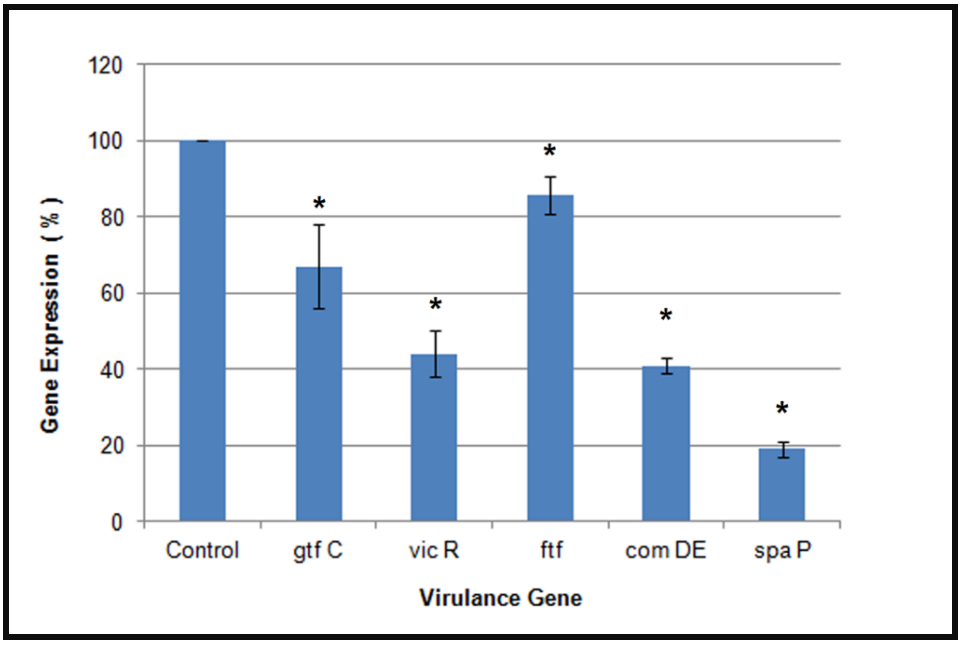


**Figure 4.7** Expression profile of various genes of *S. mutans* in response to treatment of sub-MIC concentration of $CaF_2$-NPs. The data presented were generated from at least three independent sets of experiments (Data is mean ± Standard deviation) Statistical significance as compared with the untreated control ($p< 0.05$) denoted by an asterisk (*).

### 4.3.11 *Impairment of biofilm architecture visualized through confocal microscopy*

Confocal laser scanning microscopy (CLSM) images of *S. mutans* illustrate an apparent obliteration of biofilm architecture in the presence of $CaF_2$-NPs without affecting its growth (Figure 4.8). The upper panel shows the control sample images while lower three panel represent images of biofilms when treated with various concentrations of $CaF_2$-NPs. In control images (Figure 4.8a-d) majority of cells shows green fluorescence with a mat of *S. mutans* cells showing rich biofilm architecture while in treated samples (Figure 4.8e-h) cells were highly dispersed and alive, which depicted inhibition of biofilm formation and not the viability.

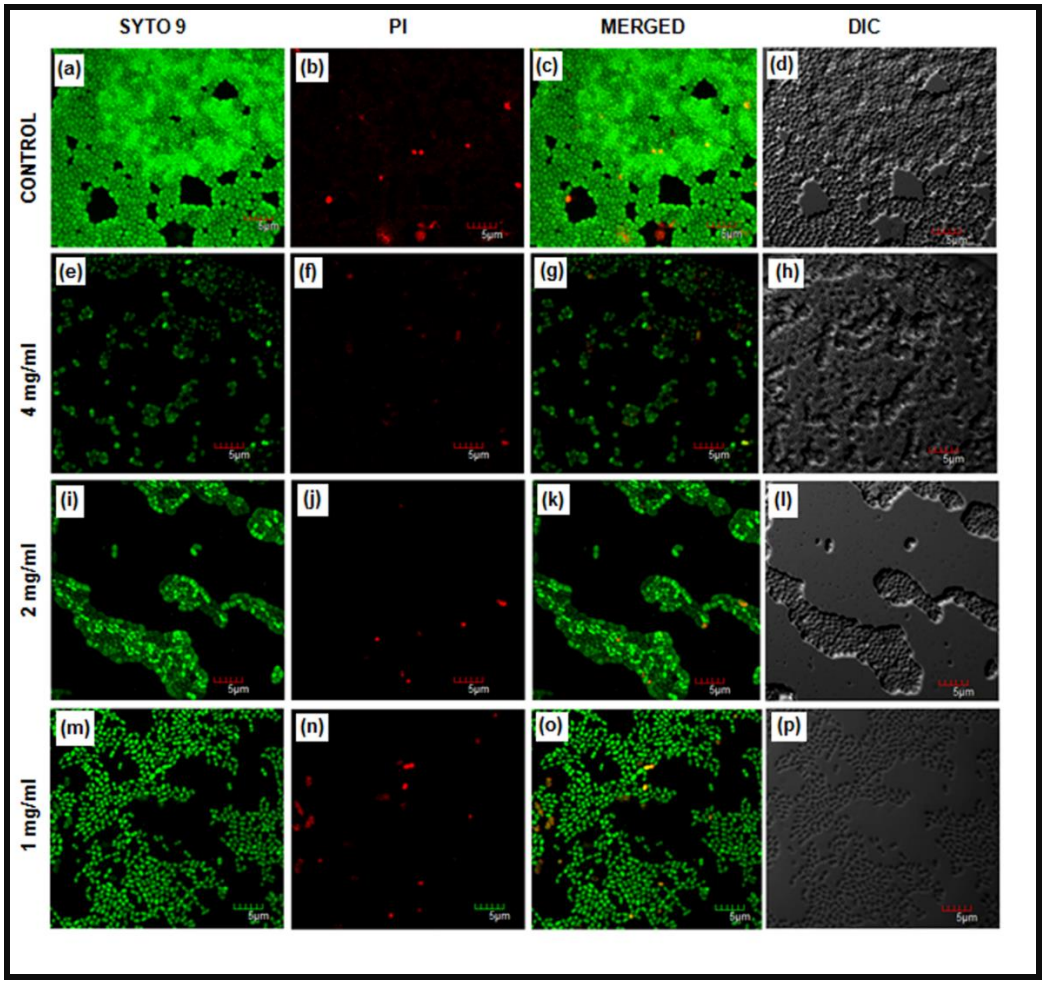


**Figure 4.8** Effect of $CaF_2$-NPs on biofilm architecture: Confocal laser scanning micrographs of control biofilm (a, b, c, d), micrographs of treated biofilm 4mg/ml (e, f, g, h), 2mg/ml (i, j, k, l), 1 mg/ml (m, n, o, p).

### 4.3.12 *Insignificant effect on cell wall*

TEM analysis was performed to visualize the effect of nanoparticle on the cell wall of *S. mutans* (Figure 4.9). In control, the cell wall is intact with the healthy intracellular content of bacterium (Figure 4.9a) on the contrary in image of treated samples (Figure 4.9b) little damage was observed (indicated by red arrows) but the damage was not prominent and majority of cells were having intact membrane. The results suggest that there was insignificant damage to cell walls in the presence of $CaF_2$-NPs.

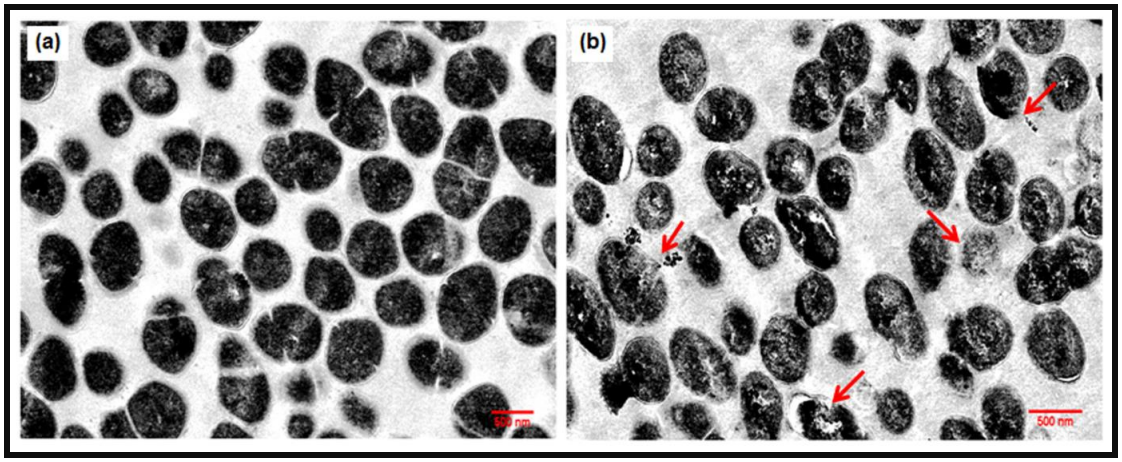


**Figure 4.9** Transmission electron microscopy images of *Streptococcus mutans*: (a) control (b) treated with sub-MIC concentration of $CaF_2$-NPs (Magnification of 4000X).

### 4.3.13 *Cytotoxicity*

Relative cell viability of HEK-293 cell line in presence of $CaF_2$-NPs is shown in Figure 4.10. Almost 100% viability was observed at all concentration (4 mg $ml^{-1}$, 2 mg $ml^{-1}$ and 1 mg $ml^{-1}$). Thus test concentration of $CaF_2$-NPs are nontoxic to HEK-293 cell line.

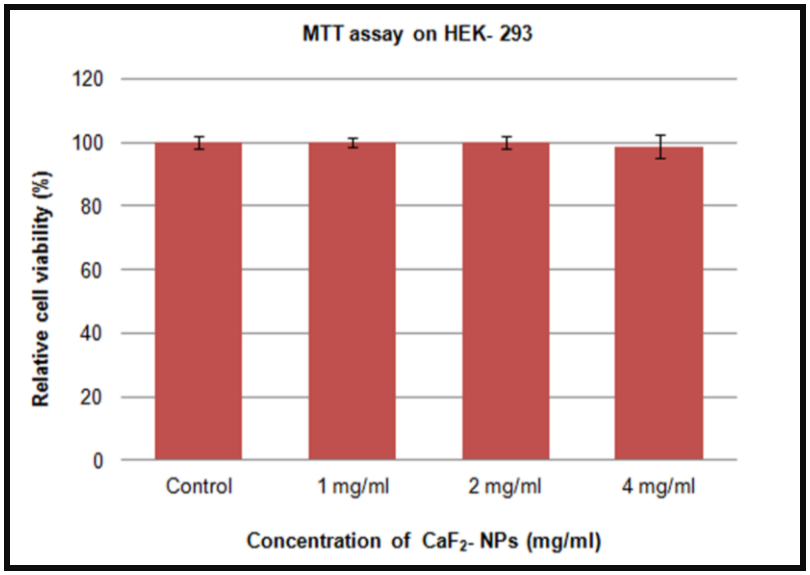


**Figure 4.10** *In vitro* cytotoxicity assay (MTT) on HEK-293 cell line.

### 4.3.14 *Oral toxicity profile*

No mortality was observed after oral toxicity assay and animals did not exhibit any behavioural or weight changes. Thus, indicating that nanoparticles were absolutely non-toxic to the animals used in this study.

### 4.3.15 *In vivo Caries reduction*

The weekly recovery of *S. mutans* cells over 5 weeks post treatment is presented in Table 4.1. There was a substantial decrease in the recovery of *S. mutans* cells from rats treated with nanoparticles as compared to the untreated group (control). It was also found that there was significant reduction of caries score in rats treated with $CaF_2$-NPs as compared to the control. Figure 4.11 shows the reduction in smooth as well as sulcal surface caries after treatment. The overall reduction in smooth surface caries was comparable to sulcal surface caries post treatment. The severity of smooth surface caries was reduced to 52.6 % (slight), 72.1% (moderate) and 70.7% (extensive) as compared to sulcal surface caries where they were reduced by 50.8% (slight), 65.6% (moderate) and 69.5% (extensive). However, the reduction in the extensive caries was found to be pronounced over slight and moderate caries.

**Table 4.1** Recovery of *S. mutans* on the following weeks after inoculation ($\times 10^4$ CFU)

| Weeks | Control | Treated |
|---|---|---|
| **1** | 110.77± 5.06 | 127.56 ± 4.44 |
| **3** | 127.67 ± 2.12 | 110.83 ± 6.01 |
| **6** | 148.06 ± 6.73 | 95.77 ± 2.82 |
| **8** | 166.35 ± 7.04 | 88.89 ± 4.56 |
| **10** | 188.08 ± 7.02 | 74.08 ± 3.87 |

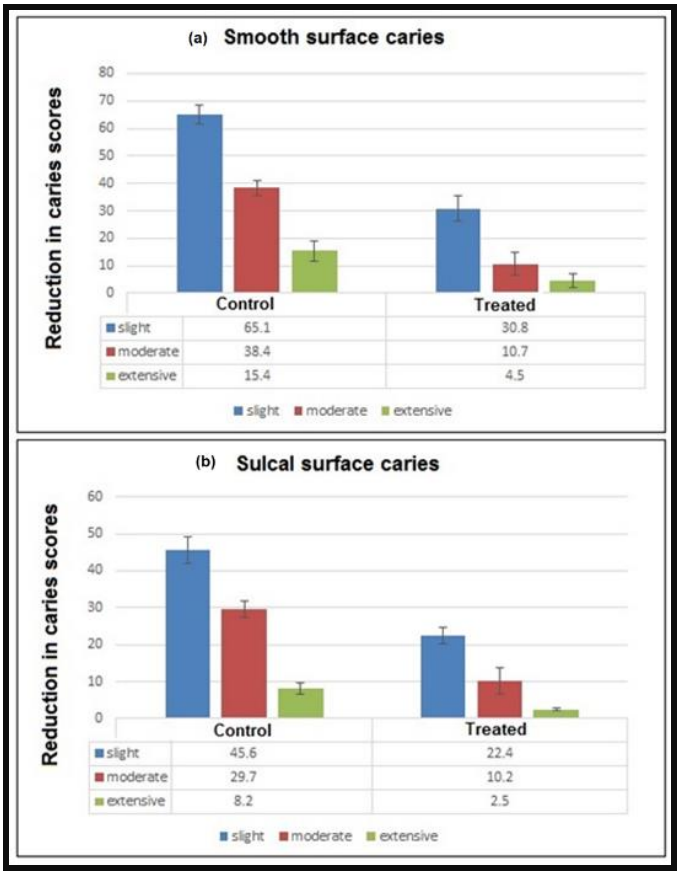


**Figure 4.11** Effect of sub- MIC level of $CaF_2$-NPs on dental caries development in rats; Data represents mean± S.D. of Keyes' score.

### 4.3.16 *Scanning electron micrograph of untreated and treated rats teeth*

The SEM analysis of the rats teeth clearly depicted the demineralization of the dental margins in untreated group Figure 4.12a while the groups treated with $CaF_2$-NPs showed smooth dental margins as clearly shown in Figure 4.12a'. Furthermore, the Figure 4.12b, c and Figure 4.12b', c' show the dental surface of untreated and treated tooth respectively. It was observed that in untreated samples the surface of the tooth has an evident biofilm embedded in the glucan pool, whereas in the treated groups the dental surface was found clear from any such exopolysaccharide projections as previously detectible in control.

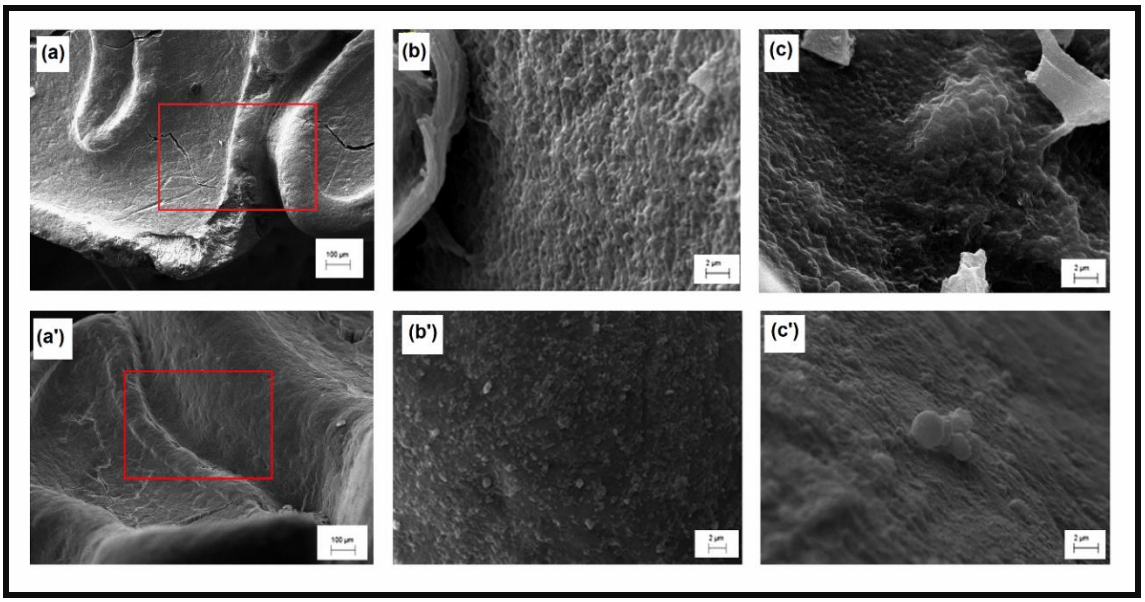


**Figure 4.12** SEM analysis of rats' teeth to evaluate the effect of $CaF_2$-NPs on caries development and extent of demineralization in treated (lower panel) and untreated groups (upper panel): (a) Untreated rat tooth showing caries (magnification 200X), (b, c) magnified view of marked region showing biofilm of *S. mutans* on untreated tooth (magnification 10X), (a') $CaF_2$-NPs treated tooth (magnification 200X), (b', c') magnified view of marked region of a treated tooth (magnification 10X).

### 4.4 Discussion

*S. mutans* is the key organism of dental caries and its cariogenic potentials are well documented [Islam *et al*. 2008; Dmitriev *et al*. 2011]. Control of its virulence factors like exopolysaccharide production, biofilm formation, aciduracity and acidogenesis and enhancement of remineralization of tooth enamel are major approaches which can be used for combating dental caries. In the present study, we have reported $CaF_2$-NPs to be very effective in suppressing *S. mutans* biofilm and other virulence factor (exopolysaccharide formation, acidogenesis, aciduracity).

$CaF_2$-NPs were prepared using a co-precipitation method a type of liquid- phase methods. The main advantages of using liquid phase methods are simple methodology and high surface activity of produced nano-materials [Omolfajr 2011]. Transmission electron microscopy (TEM) and scanning electron microscopy (SEM) results revealed the shape and size of nanoparticles. The particles are not fully dispersed but are agglomerated. The larger particles in SEM image exhibit several spherical purtubances on their surface

implying that these larger particles are formed by fusion of smaller particle during their preparation process [Pandurangappa & Lakshminarasappa 2011]. $CaF_2$-NPs show characteristic absorption peaks in UV range. The origin of these bands is due to the nanosize of particle. It has been suggested that large surface to volume ratio of nanoparticle results in the development of voids on the surface and inside the agglomerated nanoparticles. These voids lead to fundamental adsorption in UV range [Kumar *et al.* 2007]. Furthermore, it is well established that surfaces of nanoparticle comprise of numerous defects like Schottky or Frenkel resulting in absorption of light by nanocrystal [Zang *et al.* 2008]. Thus, absorption band at 202 nm in the present study confirms formation of $CaF_2$- NPs. FTIR spectrum was measured to analyze the structural properties and bonds of $CaF_2$- NPs. Two strong peaks at ~3400 $cm^{-1}$ and ~1678 $cm^{-1}$ in FTIR spectrum are due to H-O-H bending of water molecule. Band at ~ 430 $cm^{-1}$ arise due to hindered rotation of hydroxyl ion [Khan *et al.* 2013]. The XRD pattern of $CaF_2$-NPs matched well with the standard JCPDS card NO 87-0971 which reveals a cubic phase fluorite type structure [Fujihara *et al.* 2002]. The broad peaks in XRD pattern suggest small crystalline size [Pandurangappa & Lakshminarasappa 2011]. The crystaline size was calculated to be ~ 6.8 nm by using scherer`s formula. Moreover, from XRD spectra it can be estimated that the particles are in single phase and pure sample has been synthesised as there is no extra peaks found.

Formation of biofilm is the crucial virulence factor of *S. mutans* by virtue of which it causes dental caries [Hamada & Slade 1980; Nance *et al*. 2013]. Biofilm are adherent bacterial communities embedded in the hydrated matrix of exopolysaccharide and exhibiting a complex three dimensional structure [Costerton *et al*. 1999; Selwitz 2007]. The cells in biofilms behave differently in their functionalities as compared to their planktonic counterparts [Fux *et al*. 2003]. Biofilm architecture imparts bacteria with the ability to resist antibiotic and lead to persistent bacterial infection [Mah & O'Toole 2001]. $CaF_2$-NPs were found to substantially decrease the biofilm formation after 24 hours of incubation. EPS (Exopolysaccharide) is essential for the formation, maintenance and spread of biofilm and it is one of the key virulence factors of *S. mutans* [Flemming & Wingender 2010]. A considerable reduction in EPS production in the presence of $CaF_2$-NPs may be associated with the diminution of biofilm forming ability of *S. mutans*.

Moreover, the similarity in the growth curve of treated and control samples indicated that $CaF_2$-NPs reduced biofilm formation without affecting bacterial viability.

Attachment of *S. mutans* cells to the adhering surface is significant steps in the process of caries formation and its deterrence could be a prophylaxis against its virulence [Islam *et al.* 2008]. Adherence occurs mainly by virtue of the hydrophobic interactions between the cells and the adhering surface. The marked inhibition in adherence after short term exposure of sub inhibitory concentrations of $CaF_2$-NPs shows that nanoparticles are modifying the physical properties of cell surface which intern reducing the hydrophobic interactions between *S. mutans* and adhering surface. Moreover, very less reduction in preformed biofilm on treatment with $CaF_2$-NPs suggest that these nanoparticle are best suited in prophylactic treatment of dental caries. Glucan is the main exopolysaccharide produced by *S. mutans* and are integral components in the sucrose dependent colonization of *S. mutans* biofilm on the tooth surface. It is elicited from the data that there is a phenomenal reduction in glucan synthesis. Almost equal reduction was observed in both water soluble and water insoluble glucans. This indicates that $CaF_2$-NPs are acting on the GTFs and impairing their enzymatic activity, thus the reduction in EPS production was due to malfunctioning of GTFs.

Acid production and acid tolerance are cardinal virulence factors which attributes to the cariogenic ability of *S. mutans* [Kuramitsu 1993]. Pursuing these abilities *S. mutans* easily survives in stress condition and impose stress on other species of cariogenic plaque eventually evolves out as dominant species. Furthermore, the sustained pH values below pH 5.4 aids in the demineralization of enamel and development of dental caries [Banas 2004].

The rate of pH drop reflects acidogenic capacities of the cells, while final pH values of the suspensions represent acid tolerance [Gregoire *et al*. 2010]. In the present study the results show a significant drop in the final pH of the suspension in the presence of $CaF_2$-NPs suggesting deterioration in the acid tolerance capacity of *S. mutans*. Along with this the rate of pH drop was decreased in the presence of $CaF_2$-NPs as compared to control which implies the impairment of acid production capacity.

It is evident that $CaF_2$-NPs are acting against some of the major virulence factors of *S. mutans*. One of the reasons behind this anti biofilm property of $CaF_2$-NPs may be the

release of fluoride ions. Fluoride ions have been reported to act directly or in the form of metal complexes to inhibit many enzymes [Li 2003]. In *S. mutans*, fluoride ions combine with H ions forming HF molecule, which can eventually inhibit the glycolytic enzymes like Enolases [Sutton *et al*. 1987; Eshed *et al*. 2013]. In addition, a fluoride ion hinders the proton extrusion by F-ATPases through lending a proton back into the cell [Li 2003; Svensäter *et al*. 2000]. Thus, it is possible that suppression of the acid and glucan production ability in the presence of $CaF_2$-NPs is due to release of fluoride ions from the nanoparticles.

Gene expression profile of selected genes of *S. mutans* revealed a considerable reduction in gene expression in the presence of $CaF_2$-NPs. *spaP* (Ag I/II or P1) is a protein of the antigen I/II family is crucial in *S. mutans* for initial adhesion to tooth surface [Khan *et al*. 2010]. Down regulation of this gene in *S. mutans* probably results in poor adhesion and reduced ability to form biofilm on smooth surfaces. Gene *vic R* is a two component regulatory system and is known to regulate a set of gene encoding for important surface proteins which are critical for sucrose dependent adherence to a smooth tooth surface [Hasan *et al*. 2012]. Thus suppression of these two genes may further lead to inhibition of adhesion and may be a cause of anticariogenic action. In addition, *gtf C* and *ftf* which encode GTFC and FTF enzyme that catalyse the cleavage of sucrose to synthesize extracellular glucan and fructan polysaccharides [He *et al*. 2012], were also down-regulated. The reduction in aforesaid genes will thereby suppress the exopolysaccharide synthesis pathway eventually inhibiting the biofilm formation. Furthermore, *com DE* which is a part of the quorum sensing cascade of *S. mutans* was also suppressed considerably. It has been shown to regulate genetic competence, acid tolerance, and biofilm formation [Yung-Hua *et al*. 2002]. Hence, down regulation of this gene will not only attenuate internal communication system, but also adversely affect the acid tolerance potential of *S. mutans*. As the gene examined are only selected set of genes of *S. mutans* genome, additional assessment of other virulence gene is further required to get a broader spectrum of effect of $CaF_2$-NPs on cariogenic potentials of *S. mutans*.

The findings of the present study indicated that anti biofilm effect of $CaF_2$-NPs against *S. mutans* is a combination of both the suppression in enzymatic activity associated with glucan synthesis and of gene involved in adhesion, acid production, acid tolerance and quorum sensing. Interaction of $CaF_2$-NPs with enzymes and suppression of genes are

interlinked to each other at different steps of regulatory network. This may lead to impairment of the whole metabolic network, eventually forbidding bacterial pathogenesis.

Confocal laser scanning microscopy results were in consistence with the above discussed results. A disruption of biofilm architecture was observed by CLSM in the presence of sub-MIC concentrations of $CaF_2$-NPs. In control sample a green mat is clearly visible which shows that the cells are interacting with each other and forming a healthy biofilm while in treated samples there were more live cells as compared to dead cells, but less biofilm was formed suggesting that at tested concentrations there was a tremendous decrease in biofilm formation ability of *S. mutans*. Moreover, TEM images of *S. mutans* are exhibiting insignificant destruction of peptidoglycan layer and there is no damage to the cells which validate that $CaF_2$-NPs is not affecting bacterial viability.

Further, the use of animal models to study the *S. mutans*-host interactions under controlled conditions demonstrated that the daily topical exposure $CaF_2$-NPs dramatically affected the ability of *S. mutans* to colonize the tooth surfaces, consequently inhibiting the development of smooth surface caries and sulcal surface carious lesions.

These nanoparticles were able to lodge themselves deep in the cavity and could release calcium fluoride in a sustained manner to mineralize the cavity. However, the depth of slight caries was not deep enough to lodge the nanoparticles within them. This is the probable reason for the reduction of extensive caries over the slight and moderate caries. The *in vivo* effect of $CaF_2$-NPs was also confirmed by the scanning electron micrographs demonstrating a reduced demineralization and biofilm formation on tooth surfaces treated with $CaF_2$-NPs. It has been reported that topical application of fluoride on tooth surface results in the formation of calcium fluoride like material which act as the reservoir of fluoride ions that when released, protect the tooth's surface and help in remineralisation [Rošin-Grget & Linčir 2001; Rølla & Saxegaard 1990]. Hence, the reduction in caries may be due to attachment of nanoparticle on the tooth surface and sustained release of fluoride ions [Sun & Chow 2008; Xu *et al*. 2008] from $CaF_2$-NPs, which not only helps in the suppression of virulence traits of *S. mutans* but also promote remineralisation.

Despite the potential benefits of using nanoparticle it is necessary to be concerned about their probable harmful effects to human health. In present study the most likely harmful effect may be the entry of nanoparticles in the human gastrointestinal tract. $CaF_2$-NPs

were found to be non-cytotoxic to human normal cell line (HEK-293) and there was no oral toxicity. Thus, substantiating no detrimental effect to human normal cells. Apart from that there is diverse microbial ecosystem in human intestine and metabolic activities of these microbes directly actuate human health [Rajilić-Stojanović *et al*. 2007]. Hence, it is important to address the interaction of gut microbes with $CaF_2$-NPs and whether these interactions are deleterious, positive, or insignificant. Consequently, further research is required in this aspect before using $CaF_2$-NPs in therapeutics.

In conclusion, the present study validates the anti-cariogenic potential of $CaF_2$-NPs against *S. mutans*. These nanoparticles appears to be ideal for prevention of dental caries with no oral toxicity. Moreover, they are non-cytotoxic to normal human cell line (HEK-293). Thus, $CaF_2$-NPs could possibly be used as topical applicant on tooth surface and as a potential therapeutic agent against *S. mutans* to inhibit caries related problems.

## 5.1 Introduction

Bacterial biofilm are posing a global health concern as they are highly resistant to antibiotics and are cause of several chronic infections [Costerton *et al.* 1999; de la Fuente-Núnez *et al.* 2013]. Biofilms are a well-organized association of bacteria embedded in the pool of self- produced polymeric matrix [Høiby *et al.* 2010]. They have tendency to grow on surfaces of medical implants such as sutures, catheters, dental implants and cause infections which can only be treated by their removal. Thus, not only increasing the cost of treatment, but also imposing mental stress to patients [Costerton *et al.* 2005; Høiby *et al.* 2011]. Alternate strategies for inhibition of biofilm and its control are urgently needed. Nanoparticle based antimicrobials have been widely studied in recent years [Hernández-Sierra *et al.* 2008; Eshed *et al.* 2012]. In particular, silver nanoparticles (Ag-NPs) and their composites have gained major attentions as they possess exceptional antibacterial properties, broad antimicrobial spectrum and negligible tendency to induce bacterial resistance [Radziga *et al.* 2013; Gupta *et al.* 2014; Rai *et al.* 2014]. The suggested mechanisms behind the antibacterial activity of Ag-NPs are slow and sustained release of $Ag^+$ ions, direct damage to cell wall and production of reactive oxygen species (ROS) [Prabhu & Poulose 2012].

The major drawback of nanoparticles is colloidal instability and tendency to aggregate which reduce their antibacterial efficacy. Loading of nanoparticle on the supporting matrix is one of the strategies to avoid this problem [Zhou *et al.* 2013]. Graphene oxide (GO) has emerged as an excellent supporting material for nanoparticles. GO contain a single atomic $sp^2$ hybridized carbon layer with various functional groups like hydroxyl, epoxy, carbonyl, carboxyl on both accessible sides which are reducible [Zhang *et al.* 2012]. Furthermore, it is highly hydrophilic and readily forms stable colloidal dispersions. Hence, it acts as a good matrix for growing and stabilizing nanoparticles [Ocsoy *et al.* 2013; Kulshrestha *et al.* 2014]. However, widely used reducing agents like Sodium borohydride ($NaBH_4$), hydrazine are highly toxic and poisonous. They have both biological and environmental hazard [Wang *et al.* 2011]. Moreover, these processes are time consuming and cost ineffective as handling of hazardous waste generated may significantly increase the production cost on an industrial scale. Green synthesis of nanoparticles is an eco-friendly method and has potentials to replace chemical and physical methods [Mohanpuria *et al.* 2008]. Plant extracts offer a superior platform for

the formation of nanoparticle because along with being non-toxic they also act as natural capping agents. They are cheap and easily available. Furthermore, they contain large quantities of secondary metabolite which can be used as reducing and stabilizing agent [Kharissova *et al.* 2013; Philip *et al.* 2011; Patra *et al.* 2015]. *Lagerstroemia speciosa* (L.) Pers. (LS) plant belongs to the family Lythraceae and has been known to possess medicinal properties [Chan *et al.* 2014; Park *et al.* 2014]. Its leaf extract has been widely studied for its therapeutic properties and have recently been used in formation of silver nanoparticles [Sundararajan *et al.* 2014]. Although antioxidant and antibacterial properties of floral extract of LS have been reported, but there are no studies on its use in nano-material formation.

It is the first report where we have bio-fabricated silver nanoparticle onto the surface of graphene oxide using a floral extract of *Lagerstroemia speciosa* (L.) plant and have obtained a highly dispersed and stable graphene oxide-silver nanocomposite (GO-Ag). The method is simple and have no environmental and biological hazards. Recently, many stable silver nanocomposites have been developed by researchers with GO sheets utilizing both chemical and biological synthesis [Upadhyay *et al.* 2014; Tang *et al.* 2013; Shao *et al.* 2015]. But there are scarce reports on the antibiofilm efficacy of these composites. In view of this fact, our study highlight the potentials of GO-Ag as an antibiofilm agent on both gram-negative (*Enterobacter cloacae*) and gram-positive (*Streptococcus mutans*) bacteria and provide an in-depth analysis on its mode of action in both the bacteria.

### 5.2 Experimental Overview

The synthesis of GO and green synthesis of graphene oxide silver nanocomposite was performed using methodology described in section 2.2.3.1 and section 2.2.3.4 respectively. The characterization of GO and GO-Ag was done by UV-visible spectroscopy (2.2.4.1), TEM (2.2.4.2), XRD (2.2.4.5) and EDX (2.2.4.6). The sub-MIC concentrations of GO and GO-Ag against *S. mutans* and *E. cloacae* were estimated by method outlined in section 2.2.5. The effect of sub-MIC concentration of GO and GO-AG on biofilm forming abilities of both the strains were evaluated by crystal violet assay described in section 2.2.7. Growth curve pattern of *S. mutans* and *E. cloacae* was investigated in presence of sub-MIC concentrations of GO and GO-Ag by method

provided in section 2.2.11. Furthermore, effect of sub inhibitory concentration of GO-Ag on cell membrane integrity of both the strains was evaluated (Section 2.2.15). Amount of ROS produced in the presence of sub-MIC concentration of GO-Ag in both the strains was also estimated (section 2.2.16). SEM and CLSM analysis of GO-Ag treated biofilms was performed using methodology outlined in section 2.2.17. Moreover, the effect of GO-Ag on expression of gene involved in *S. mutans* virulence pathway was studied by quantitative RT-PCR as outline in section 2.2.18. Cytotoxicity assay was also performed on HEK-293 cell line (section 2.2.21).

## 5.3 Results

### 5.3.1 *Characterization of GO-Ag*

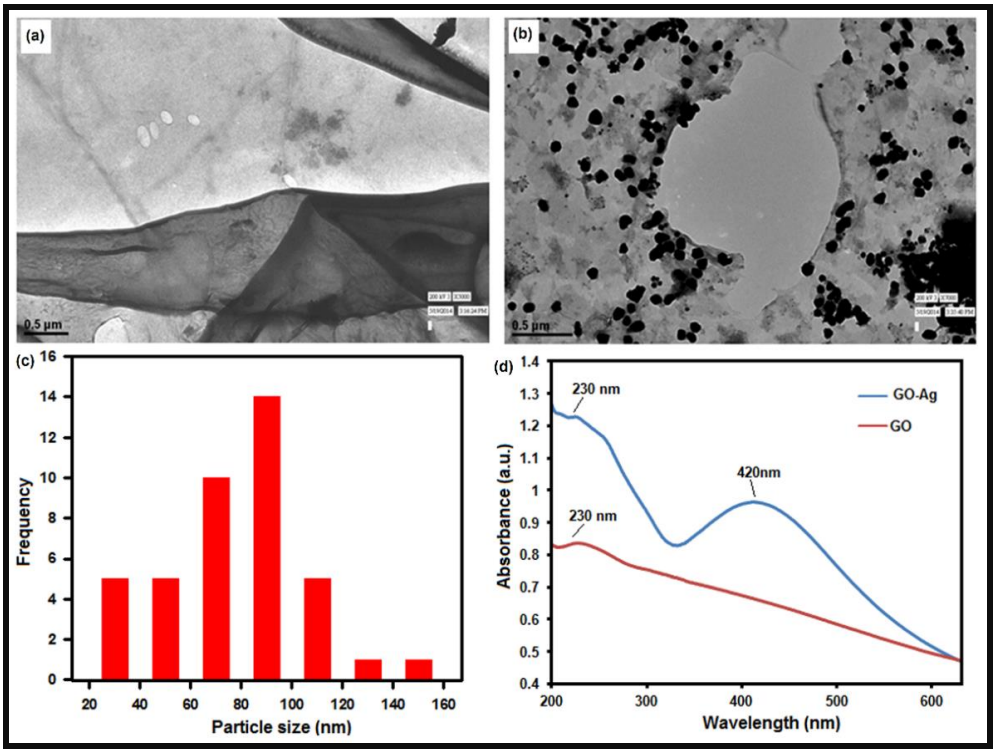


**Figure 5.1** Characterization of GO-Ag (a) TEM image of GO (b) TEM image of GO-Ag (c) Particle size distribution of silver nanoparticles (d) UV-vis spectra of GO and GO-Ag.

The TEM micrograph of GO (Figure 5.1a) displayed a single layer of graphene oxide sheet. While image of GO-Ag (Figure 5.1b) revealed well dispersed silver nanoparticle embellished on the surface of GO nanosheets. The average size of silver nanoparticle was in range of 60-100 nm (Figure 5.1c). Formation silver nanoparticle on the surface of GO

was monitored using UV- visible spectroscopy (Figure 5.1d). Figure 5.2a depicts the X-Ray diffraction pattern of GO. The sharp diffraction peak of GO was observed at 9.8º. While in XRD pattern of GO-Ag (Figure 5.2b) along with peak at 9.8º a broad peak appeared at 24.26º. Energy-dispersive X-ray spectroscopy (EDX) was used to analyse the chemical composition of GO and GO-Ag. Peaks corresponding to C and O were observed in spectrum of GO (Figure 5.3a) while spectrum of GO-Ag shows peaks corresponding to C, O and Ag (Figure 5.3b).The inset tables give the weight percent and atomic percent of elements present in both the compound.

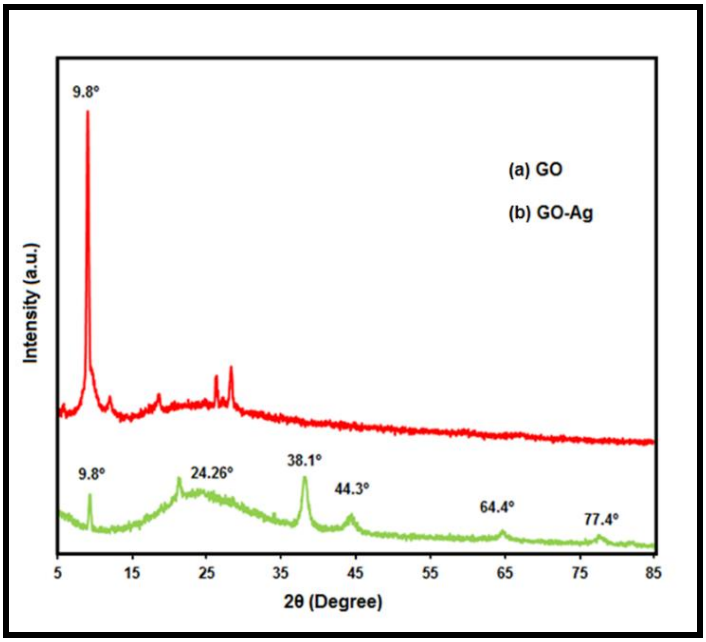


**Figure 5.2** XRD pattern of (a) GO and (b) GO-Ag.

### 5.3.2 *Antibacterial concentrations of GO-Ag nanocomposite*

The MIC values of GO-Ag were much lower in *E. cloacae* as compared to *S. mutans* although the MIC value of GO was same for both the strains (Table 5.1). The MBC of GO-Ag for *E. cloacae* and *S. mutans* were 94 µg $ml^{-1}$ and 188 µg $ml^{-1}$ respectively (Figure 5.4). As the antibacterial concentrations were different for both the categories of bacteria so we used different sub inhibitory concentrations of GO-Ag in *E. cloacae* (24 µg $ml^{-1}$ and 12 µg $ml^{-1}$) and *S. mutans* (47 µg $ml^{-1}$ and 24 µg $ml^{-1}$) for further experiments.

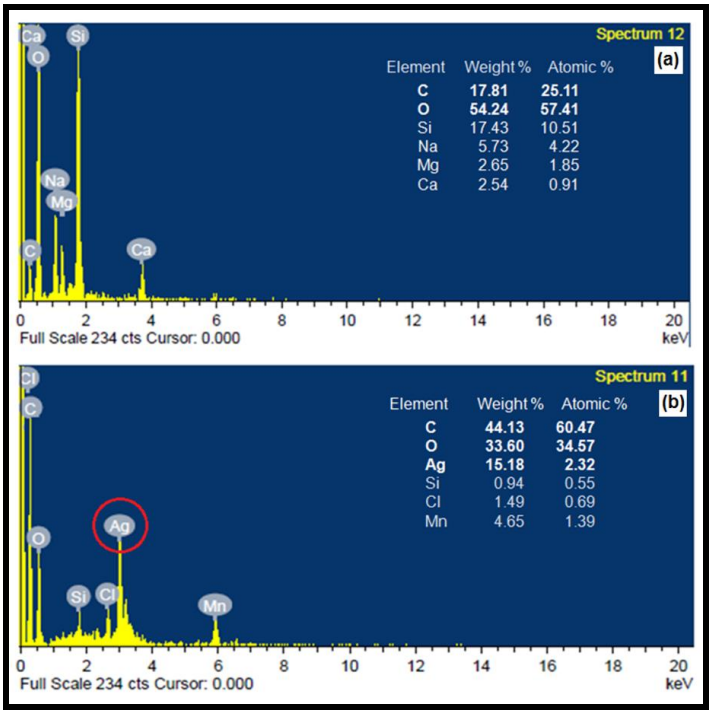


**Figure 5.3** EDX spectra of (a) GO and (b) GO-Ag.

**Table 5.1** MIC values of GO and GO-Ag

| S. No. | Nanoparticle | *S. mutans* | *E. cloacae* |
|---|---|---|---|
| **1)** | Graphene oxide | >1500 µg/ml | >1500 µg/ml |
| **2)** | Graphene oxide - silver nanocomposite | 94 µg/ml | 47 µg/ml |

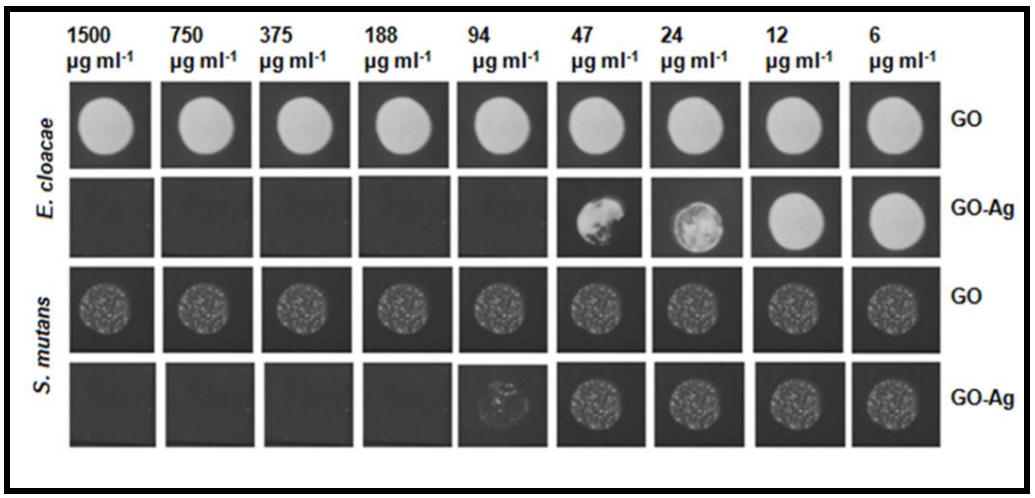


**Figure 5.4** MBC of GO and GO-Ag against *S. mutans* and *E. cloacae*

### 5.3.3 *Inhibitory effect on biofilm forming abilities Streptococcus mutans and Enterobacter cloacae*

There were 90% and 49% reduction in the presence of 24 µg $ml^{-1}$ and 12 µg $ml^{-1}$ of GO-Ag respectively in *E. cloacae*, while, at the same concentrations GO reduced the biofilm to 35% and 20% (Figure 5.5b). Similarly, 89% and 34% reduction was observed in *S. mutans* biofilm when treated with 47 µg $ml^{-1}$ and 24 µg $ml^{-1}$ of GO-Ag respectively, however, in the presence of same concentrations of GO there was only 18% and 15% reduction in *S. mutans* biofilm (Figure 5.5a).

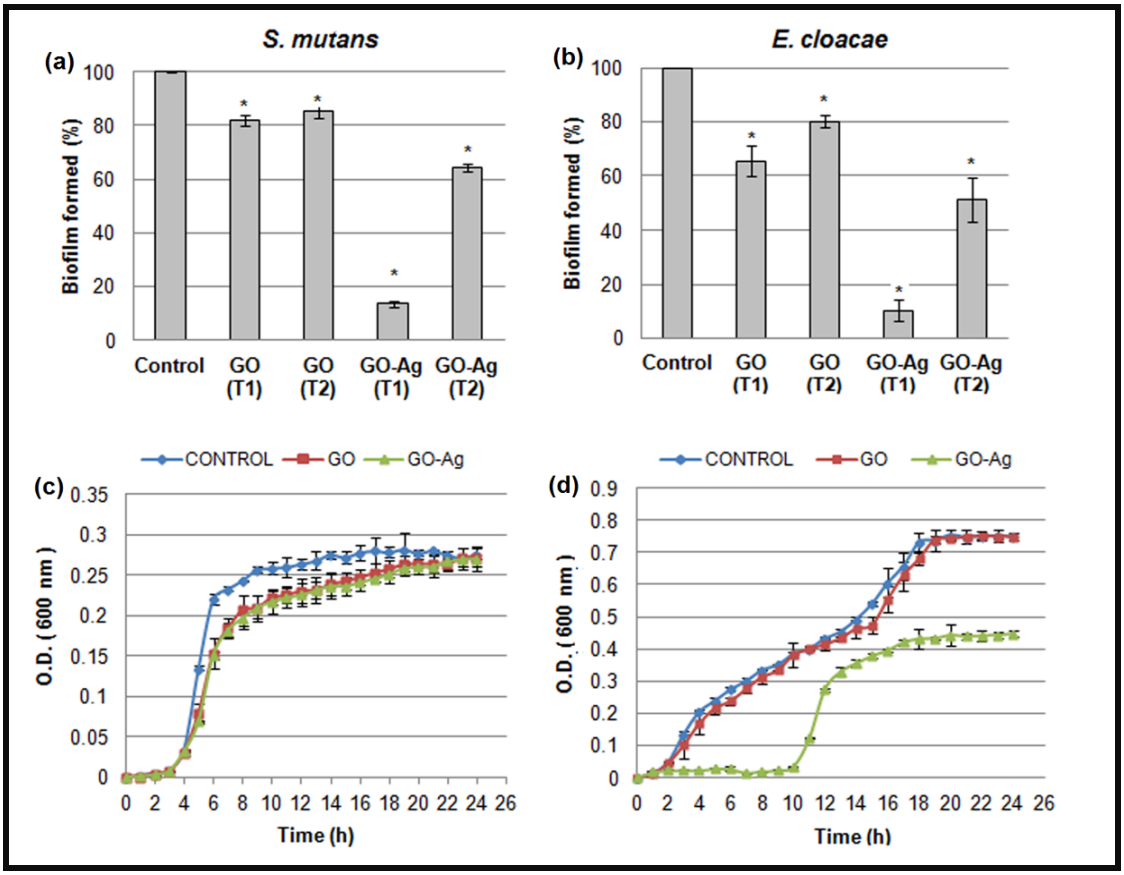


**Figure 5.5** (a) Effect of sub inhibitory concentrations of GO and GO-Ag on *S. mutans* biofilm formation, where T1 is 47 µg $ml^{-1}$ and T2 is 24 µg $ml^{-1}$ (b) Effect of sub inhibitory concentrations of GO and GO-Ag on *E. cloacae* biofilm formation ,where T1 is 24 µg$ml^{-1}$ and T2 is12 µg $ml^{-1}$ (c) Effect of GO and GO-Ag on growth curve pattern of *S. mutans* (d) Effect of GO and GO-Ag on growth curve pattern of *E. cloacae* (* means p value <0.05).

### 5.3.4 *Effect on growth curve*

Growth curve assay was performed in the presence of sub inhibitory concentrations of GO and GO-Ag. There was no change in pattern of growth curve in *S. mutans* (Figure 5.5c), while in *E. cloacae* the growth pattern of GO-Ag treated bacteria was altered considerably, a delay in exponential phase was observed (Figure 5.5d).

### 5.3.5 *Protein leakage assay*

Further, the effect of GO-Ag on cell membrane integrity was evaluated by protein leakage assay. Figure 5.6a revealed that in *E. cloacae* after 4h of treatment amount of protein released was 0.13 mg $ml^{-1}$ while in *S. mutans* it was only 0.03 mg $ml^{-1}$ which is negligible.

### 5.3.6 *Reactive oxygen species production*

Reactive oxygen species detection assay revealed the amount of reactive oxygen species (ROS) generated in *E. cloacae* was much higher than *S. mutans* after 12 h of incubation (Figure 5.6b).

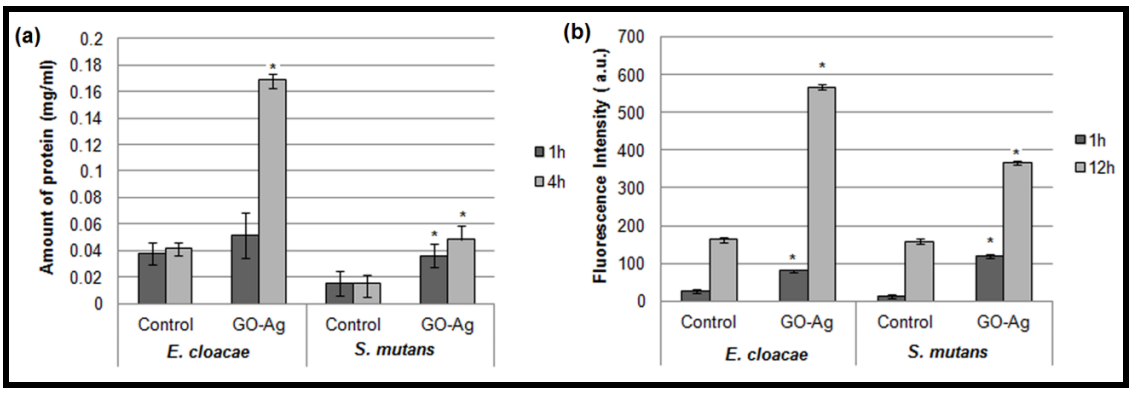


**Figure 5.6** (a) Effect of GO-Ag on cell membrane integrity of *S. mutans* and *E. cloacae* (b) Amount of reactive oxygen species generation by GO-Ag in *S. mutans* and *E. cloacae* (Data is mean ± Standard deviation, * represent p value < 0.05).

### 5.3.7 *Microscopic analysis of biofilms*

The scanning electron micrographs of *S. mutans* and *E. cloacae* are shown in Figure 5.7. Upper panel represents the effect of GO and GO-Ag (47 µg $ml^{-1}$) on *S. mutans* biofilm (Figure 5.7a, b) while the lower panel displays the effect of GO and GO-Ag (24 µg $ml^{-1}$)

on *E. cloacae* biofilm (Figure 5.7e, f). The results depict a substantial decrease in biofilm architecture on treatment of GO-Ag in both the cases. Furthermore, the magnified view of cells of biofilm show no changes in cell morphology of *S. mutans* in the presence of GO-Ag (Figure 5.7c, d). However, GO-Ag treated *E. cloacae* displayed a damage in cell wall and decreased intracellular density (Figure 5.7g, h). Confocal microscopy analysis was performed on both the bacterial biofilms by using SYTO 9 (green fluorescence, live) and PI (Red fluorescence, dead). Images of SYTO9/PI stained biofilms of and EC15 in shown in Figure 5.8.

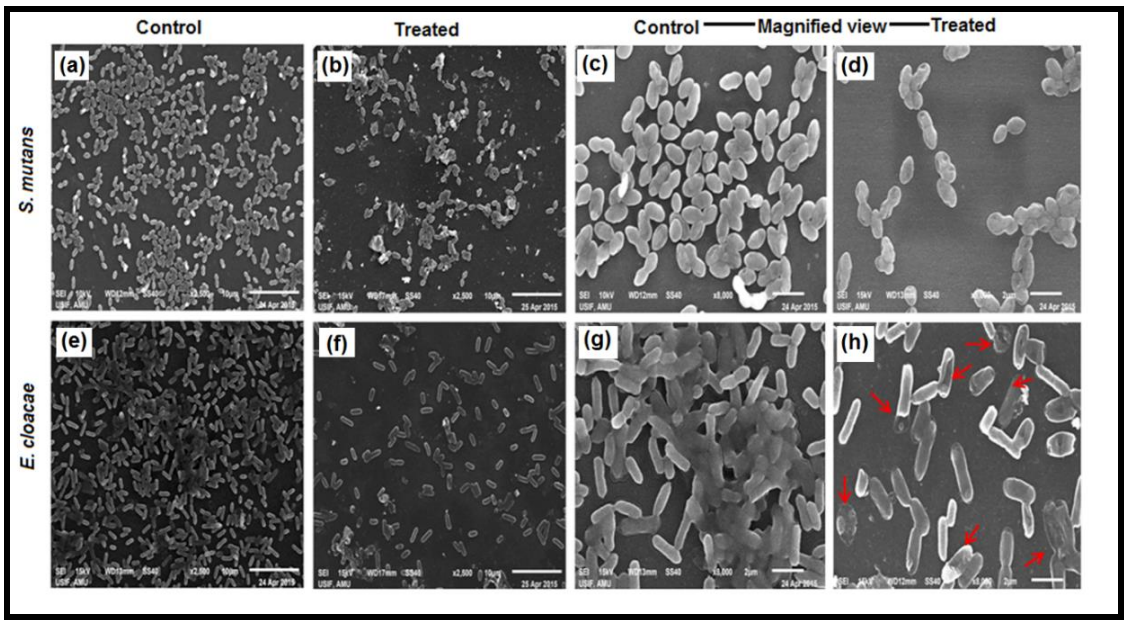


**Figure 5.7** Scanning electron microscopy images of biofilm treated with sub inhibitory concentration of GO-Ag: (a, b) inhibition of *S. mutans* biofilm, (e, f) inhibition of *E. cloacae* biofilm, (c) magnified view of *S. mutans* in control biofilm, (d) magnified view of *S. mutans* in treated biofilm showing no change in cell wall integrity, (g) magnified view of *E. cloacae* in control biofilm, (h) magnified view of *E. cloacae* in treated biofilm, red arrow depicting loss of intracellular component.

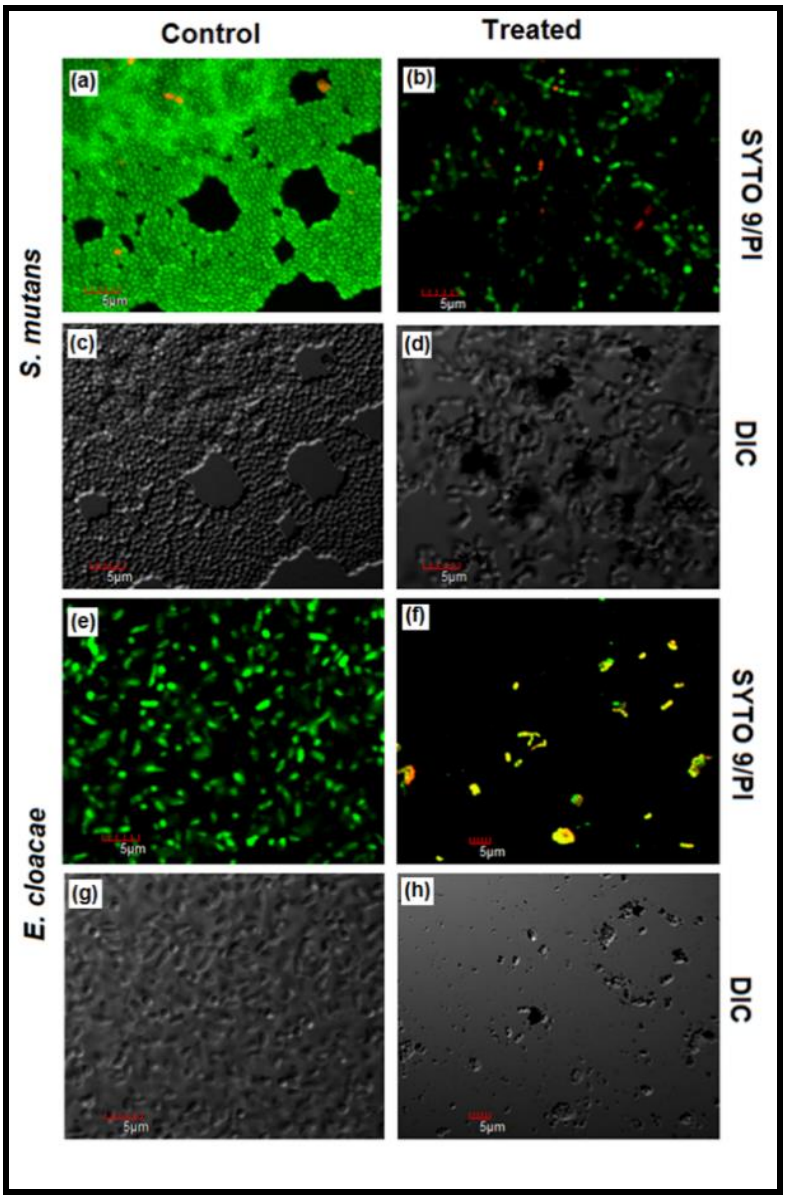


**Figure 5.8** Confocal laser scanning microscopy images stained with SYTO9 (green, live) and PI (red, dead): (a, c) control biofilm of *S. mutans*, (b, d) treated biofilms of *S. mutans*, (e, g) control biofilms of *E. cloacae*, (f, h) treated biofilms of *E. cloacae*, Scale bar = 5µm.

### 5.3.8 *Quantitative RT- PCR analysis*

Figure 5.9 shows the gene expression profile of three important genes of *S. mutans* (*com DE*, *spa P* and *vic R*) which play major role in process of biofilm formation. There was downregulation in gene expression of all these genes.

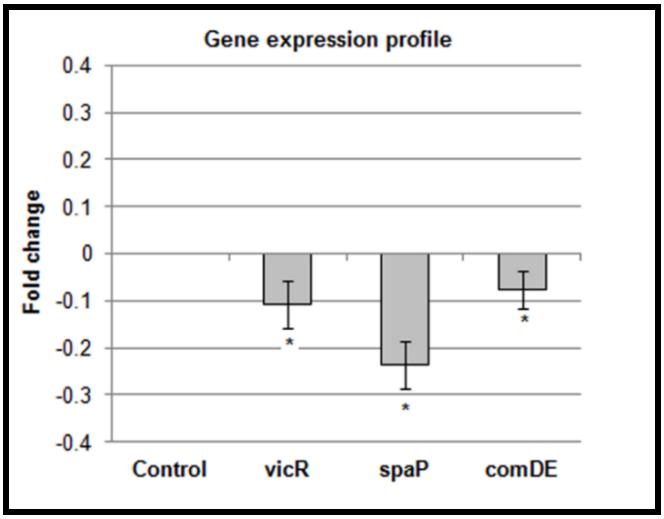


**Figure 5.9** Gene expression profile of specific genes involved in the formation of *S. mutans* biofilm. Quantitative RT-PCR was carried out in triplicate. Data presented were generated from at least four independent sets of experiments (Data is mean ± Standard deviation, * represent p value < 0.05).

### 5.3.9 *Cytotoxicity on HEK -293 cell line*

MTT assay was performed to assess the effect of GO-Ag on HEK-293 cell line (Figure 5.10). The $IC_{50}$ value of GO-Ag was 750µg $ml^{-1}$ while it was 1500µg $ml^{-1}$ for GO. This value was much higher than the concentrations used in present study suggesting that these nanoparticle are non-toxic to human normal cell line at antibacterial concentrations of these nanoparticles (94 µg $ml^{-1}$ in *S. mutans* and 47 µg $ml^{-1}$ in *E. cloacae*).

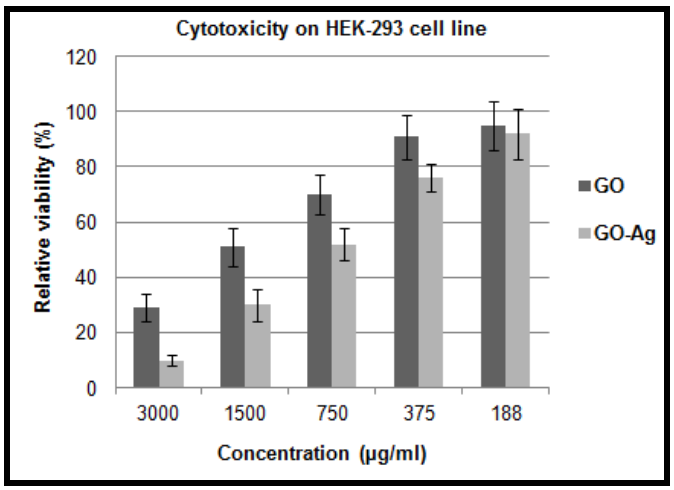


**Figure 5.10** Effect of GO and GO-Ag on viability of HEK-293 cell line.

## 5.4 Discussion

Plant extracts have been known to possess large amount of secondary metabolites which can act as reducing and capping agents for nanoparticles [Kharissova *et al.* 2013; Philip *et al.* 2011; Patra *et al.* 2015]. The green synthesis of nanoparticle is environment friendly mode and is less hazardous [Mohanpuria *et al.* 2008]. In the present study graphene oxide-silver nanocomposite (GO-Ag) was synthesized by simultaneous reduction and stabilization of silver nanoparticle on to the surface of graphene oxide using *Lagerstroemia speciosa* floral extract. The schematic representation of the process of GO-Ag preparation is shown in Figure 5.11.

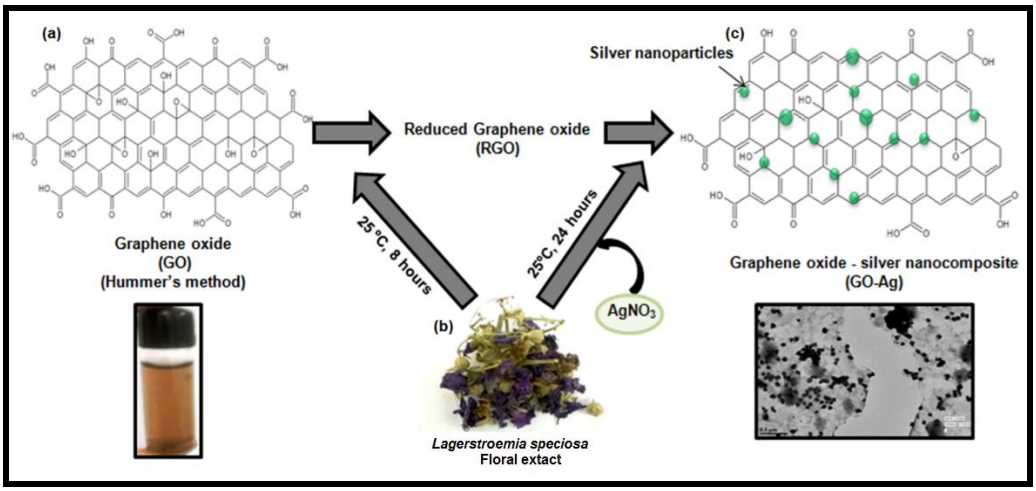


**Figure 5.11** Schematic representation of green synthesis of GO-Ag: (a) Graphene oxide was prepared by Hummers method, (b) plant extract was used to reduce GO to RGO, (c) silver nanoparticle was reduced and stabilized onto the surface of GO with help of plant extract.

Morphological aspects of GO and GO-Ag were analysed using Transmission electron microscopy (TEM). The average size of silver nanoparticle was in range of 60-100 nm. The results validate that graphene oxide is acting as a supporting agent for silver nanoparticle and also reducing the agglomeration of nanoparticles [Zhou *et al.* 2013]. Formation silver nanoparticle on the surface of GO was monitored using UV- visible spectroscopy. A peak was observed at 230 nm in UV-visible spectrum of GO which is characteristic peak of GO due to $\pi-\pi^*$ transitions of the aromatic C−C bonds [Shao *et al.* 2015]. The UV-visible spectrum of GO-Ag showed an additional peak at 420 nm along with peak at 230 nm. The peak at 420 nm corresponds to surface plasmon resonance peak

of silver nanoparticle [Chevirona *et al.* 2014], suggesting the formation of silver nanoparticles onto the surface of graphene oxide. Broadening and shifting of the XRD peak of GO to around 24º suggest the formation of reduced graphene oxide [Seema *et al.* 2012]. Furthermore, sharp peaks at 38.1º, 44.3º, 64.4º and 77.4º in XRD pattern of GO-Ag can be assigned to the (111), (200), (220), and (311) diffraction cubic crystal planes of Ag (JCPDS No. 04-0783), demonstrating the formation of metallic silver nanoparticles [Ma *et al.* 2011]. The strong signal of silver in the EDX analysis of GO-Ag along with carbon and oxygen confirms the formation of silver nanoparticle on graphene oxide sheets.

The minimum inhibitory concentration (MIC) and minimum bactericidal concentrations (MBC) were estimated for gram-positive and gram-negative bacterial species by taking *Streptococcus mutans* and *Enterobacter cloacae* as model organisms. It has been demonstrated that enhanced antibacterial activity of graphene nanocomposites are due to nonspecific binding abilities of GO sheets to microbes [Park *et al.* 2010]. Thus, stabilization of silver nanoparticle onto the GO sheets provide better platform for interaction of nanoparticle with microbes [Xu *et al.* 2011]. Silver nanoparticles are well known for their antibacterial properties although exact mechanism has not yet been reported. It has been suggested that production of reactive oxygen species (ROS) and release of silver ions are the main antibacterial properties of silver nanoparticles which may lead to oxidative stress and cellular damage [Shao *et al.* 2015]. Furthermore, the difference in antibacterial concentrations of GO-Ag for gram-negative and gram-positive bacteria may be attributed to the difference in cell wall composition with gram-positive bacteria having multi-layered peptidoglycan on their surface [Tang *et al.* 2013]. Thus, higher concentration of GO-Ag was required to kill *S. mutans* as compared to *E. cloacae*.

The best way of to deal with the biofilm related infections is the prophylaxis treatment of biofilm [Lynch *et al.* 2008; Anghel *et al.* 2012]. Keeping this in view the biofilm forming abilities of both the bacteria were assessed in the presence of GO-Ag. It is apparent from the results that GO is acting as an inimitable nano-interface for interaction of microbe with silver nanoparticles and thus, considerably inhibiting the biofilm formation [Kulshrestha *et al.* 2014; Tang *et al.* 2013].

It is important to investigate whether the effect on biofilm is due to inhibition of biofilm forming pathway or because of the killing of planktonic cells. From the growth curve data

it may be elucidated that the reduction in biofilm in *E. cloacae* is due to *killing* of its planktonic cells. These results of cell membrane integrity assay were in accordance with the growth curve assay suggesting that GO-Ag is affecting the planktonic cells of *E. cloacae* by cell mebrane disruption which may be the reason of decreased biofilm formation. On contrary, *S. mutans* possess multilayer peptidoglycan which renders GO-Ag unable to damage its, thus, the inhibition in its biofilm formation is due to some other factors.

Reactive oxygen species (ROS) production is one of the primary mechanisms by virtue of which nanoparticle effects the bacterial cell functioning [Premanathan *et al.* 2011]. When the ROS production by nanoparticles exceeds the capacity of cellular antioxidant defence system, it can cause oxidative stress which can further initiate lipid per oxidation, thus damaging the cell membrane and eventually leading to cell death [Lovrić *et al.* 2005; Khan *et al.* 2012]. Hence, it can be elucidated from present results that amount of ROS produced by GO-Ag in *S. mutans* is not exceeding its antioxidant system subsequently not affecting its membrane integrity but in *E. cloacae* there is higher amount of ROS which is causing oxidative stress and cell death. It is apparent from SEM results that *E. cloacae* cells are killed by pit formation in their cell wall while *S. mutans* are not directly damaged by GO-Ag and there is only reduction in biofilm. A considerable reduction of biofilm architecture was visualized by CLSM in *S. mutans* but there was no effect on viability of cells as indicated by green fluorescence of Syto-9. In *E. cloacae* there was a decrease in biofilm but the cell viability was affected as yellow fluorescence was visible due to entry of both the dyes. The microscopic analysis results were in accordance with the previous results validating that inhibition of biofilm in *E. cloacae* in presence of GO-Ag is because of loss of viability of planktonic cells while in *S. mutans* the cells are viable after treatment with sub inhibitory concentrations of GO-Ag and the biofilm inhibition may be due the release of silver ions which can affect the biofilm cascade on genetic level.

In the presence of GO-Ag there was downregulation of expression of important genes associated with process of biofilm formation of *S. mutans*. Gene *spaP* (Ag I/II) helps in sucrose independent initial adherence of *S. mutans* while *vicR* is a two component regulatory system and have been reported to regulate genes which are necessary for sucrose dependent adherence of *S. mutans* [Hasan *et al.* 2012; Khan *et al.* 2010]. Thus,

down regulation of these genes will affect the adherence of *S. mutans* to the surface which is first step of biofilm formation. *comDE* plays a crucial role in quorum sensing cascade of *S. mutans* [Hasan *et al.* 2014; Li *et al.* 2002]. Its downregulation will suppress the regulation of genetic tolerance, acid production and biofilm formation. From the results it became apparent that in *S. mutans* the inhibition in biofilm in presence of GO-Ag is due to effect on biofilm associated genes cascade.

In conclusion, we demonstrate a simple and environment friendly approach for synthesis of well dispersed silver nanoparticle onto the surface of graphene oxide by using flower extract of *Lagerstroemia speciosa* (L.) Pers. The sub inhibitory concentrations of nanocomposite were found to inhibit biofilm formation of both gram-negative and gram-positive bacteria but the mechanism of inhibition of biofilm is different in both the microbes. Moreover, nanocomposite was found to be non-toxic against HEK-293 cell line at used concentrations. Hence, GO-Ag may be assigned as potential prophylaxis for biofilm based infections although further research is required to elucidate specific biofilm inhibition pathway by proteomics and metabolomics approaches.

In present study we have developed nanoparticles and nanomaterials which efficiently inhibited the bacterial biofilm formation. The graphene/ zinc oxide nanocomposite (GZNC) was found to substantially impede biofilm and other cariogenic properties of *S. mutans*. Also the concentrations of GZNC used in the study were non-toxic to HEK-293 cell line. Moreover, there was remarkable reduction in biofilm on GZNC coated acrylic tooth surface. Thus, GZNC emerged out as an alternate therapeutic agent against *S. mutans* biofilm based infections and may be used as a potential coating agent for dental implants. Although further research is required for its stability and toxicity before industrial implication.

The *in vitro* studies showed that in the presence of sub inhibitory concentrations of calcium fluoride nanoparticles ($CaF_2$-NPs) *S. mutans* displayed a considerable reduction in its cariogenic properties (adherence, biofilm formation, exopolysaccharide production, acid production and acid tolerance properties). Furthermore, *in vivo* experiments revealed a significant reduction in dental caries. Hence, $CaF_2$-NPs have its perspectives as a promising topical applicant on tooth surface to curtail dental caries.

The synthesis of silver nanoparticle onto the surface of graphene oxide was performed by environment friendly approach using floral extract of *Lagerstroemia speciosa* (L.) Pers. The sub inhibitory concentrations of graphene oxide silver nanocomposite (GO-Ag) were found to inhibit the formation of biofilm in both gram-positive and gram-negative bacteria. There was loss of viability in gram-negative bacteria while in gram-positive bacteria the inhibition of biofilm was due to its effect on the biofilm formation cascade. Thus, GO-Ag may have its application as a potential prophylaxis for biofilm associated infections although further studies are required to elucidate the specific biofilm inhibition pathway.

Abranches J, Miller JH, Martinez AR, Simpson-Haidaris PJ, Burne RA, Lemos JA. The collagen-binding protein Cnm is required for *Streptococcus mutans* adherence to and intracellular invasion of human coronary artery endothelial cells. ***Infect Immun***. 2011; 79: 2277-84.

Ahmed MA, Ceronifrom D. Musculoskeletal Postoperative Infections due to *Enterobacter cloacae* complex: A New Reality. ***J Med MicrobDiagn***. 2013; 3**:** 2161-0703.1000128.

Akhavan O, Ghaderi E. Toxicity of graphene and graphene oxide nanowalls against bacteria. ***ACS nano***. 2010; 4**:** 5731-6.

Alipour M, Suntres ZE. Liposomal antibiotic formulations for targeting the lungs in the treatment of *Pseudomonas aeruginosa*. ***Ther Deliv***. 2014; 5**:** 409-27.

Amato SM, Brynildsen MP. Nutrient transitions are a source of persisters in *Escherichia coli* biofilms. ***PloS one***. 2014; 9**:** e93110.

Andersson S. Characterization of bacterial biofilms for wastewater treatment. 2009.

Anghel I, Grumezescu AM, Andronescu E, Anghel AG, Ficai A, Saviuc C, Grumezescu V, Vasile BS, Chifiriuc MC. Magnetite nanoparticles for functionalized textile dressing to prevent fungal biofilms development. ***Nanoscale Res Lett***. 2012; 7: 1-6.

Ansari MA, Khan HM, Khan AA, Sultan A, Azam A. Characterization of clinical strains of MSSA, MRSA and MRSE isolated from skin and soft tissue infections and the antibacterial activity of ZnO nanoparticles. ***World J Microb Biot***. 2012; 28: 1605-13.

Applerot G, Lellouche J, Perkas N, Nitzan Y, Gedanken A, Banin E. ZnO nanoparticle-coated surfaces inhibit bacterial biofilm formation and increase antibiotic susceptibility. ***Rsc Adv***. 2012; 2: 2314-21.

Archer NK, Mazaitis MJ, Costerton JW, Leid JG, Powers ME, Shirtliff ME. *Staphylococcus aureus* biofilms: properties, regulation, and roles in human disease. ***Virulence***. 2011; 2: 445-59.

Arciola CR, Campoccia D, Speziale P, Montanaro L, Costerton JW. Biofilm formation in *Staphylococcus* implant infections. A review of molecular mechanisms and implications for biofilm-resistant materials. ***Biomaterials***. 2012; 33: 5967-82.

Armstead AL, Li B. Nanomedicine as an emerging approach against intracellular pathogens. ***Int J Nanomed***. 2011; 6: 3281.

Aydin Sevinç B, Hanley L. Antibacterial activity of dental composites containing zinc oxide nanoparticles. ***J Biomed Mater Res Part B: Appl Biomat***. 2010; 94: 22-31.

Baek Y-W, An Y-J. Microbial toxicity of metal oxide nanoparticles (CuO, NiO, ZnO, and $Sb_2O_3$) to *Escherichia coli*, *Bacillus subtilis*, and *Streptococcus aureus*. ***Sci Total Environ***. 2011; 409: 1603-8.

Banas JA. Virulence properties of *Streptococcus mutans*. ***Front Biosci***. 2004; 9: 1267-77.

Beloin C, Roux As, Ghigo JM. *Escherichia coli* biofilms. ***Bacterial Biofilms***: Springer, 2008. 249-89.

Beyth N, Houri-Haddad Y, Domb A, Khan W, Hazan R. Alternative Antimicrobial Approach: Nano-Antimicrobial Materials. ***J Evid Based Complementary Alter Med***. 2015; 2015.

Beyth N, Yudovin-Farber I, Bahir R, Domb AJ, Weiss EI. Antibacterial activity of dental composites containing quaternary ammonium polyethylenimine nanoparticles against *Streptococcus mutans*. ***Biomaterials***. 2006; 27: 3995-4002.

Biswas S, Bowler ICJW, Bunch C, Prendergast B, Webster DP. *Streptococcus mutans* infective endocarditis complicated by vertebral discitis following dental treatment without antibiotic prophylaxis. ***J Med Microbiol***. 2010; 59: 1257-9.

Blecher K, Nasir A, Friedman A. The growing role of nanotechnology in combating infectious disease. ***Virulence***. 2011; 2**:** 395-401.

Bora T, Lakshman KK, Sarkar S, Makhal A, Sardar S, Pal SK, Dutta J. Modulation of defect-mediated energy transfer from ZnO nanoparticles for the photocatalytic degradation of bilirubin. ***Beilstein J Nanotech***. 2013; 4: 714-25.

Bowen WH, Koo H. Biology of *Streptococcus mutans*-derived glucosyltransferases: role in extracellular matrix formation of cariogenic biofilms.***Caries Res***. 2011; 45: 69-86.

Bowling FL, Jude EB, Boulton AJM. MRSA and diabetic foot wounds: contaminating or infecting organisms? ***Cur Diab Rep***. 2009; 9: 440-4.

Brown AN, Smith K, Samuels TA, Lu J, Obare SO, Scott ME. Nanoparticles functionalized with ampicillin destroy multiple-antibiotic-resistant isolates of *Pseudomonas aeruginosa* and *Enterobacter aerogenes* and methicillin-resistant *Staphylococcus aureus.* ***App Environ Microbiol***. 2012; 78: 2768-74.

Buffet-Bataillon S, Tattevin P, Bonnaure-Mallet M, Jolivet-Gougeon A. Emergence of resistance to antibacterial agents: the role of quaternary ammonium compounds--a critical review. ***Int J Antimicrob Agents***. 2012; 39: 381-9.

Burns JL, Gibson RL, McNamara S, Yim D, Emerson J, Rosenfeld M, Hiatt P, McCoy K, Castile R, Smith AL. Longitudinal assessment of *Pseudomonas aeruginosa* in young children with cystic fibrosis. ***J Infect Dis***. 2001; 183: 444-52.

Busscher HJ, Rinastiti M, Siswomihardjo W, Van der Mei HC. Biofilm formation on dental restorative and implant materials. ***J Dent Res***. 2010; 89: 657-65.

Carlson C, Hussain SM, Schrand AM, K. Braydich-Stolle L, Hess KL, Jones RL, Schlager JJ. Unique cellular interaction of silver nanoparticles: size-dependent generation of reactive oxygen species. ***J Phy Chem B***. 2008; 112: 13608-19.

Castor TP. Phospholipid nanosomes. ***Curr Drug Deliv***. 2005; 2: 329-40.

Chan EWC, Tan LN, Wong SK. Phytochemistry and Pharmacology of *Lagerstroemia speciosa*: A Natural Remedy for Diabetes. ***Int J Herb Med***. 2014; 2: 100-5.

Chang Y, Yang S-T, Liu J-H, Dong E, Wang Y, Cao A, Liu Y, Wang H. *In vitro* toxicity evaluation of graphene oxide on A549 cells. ***Toxicol Lett***. 2011; 200: 201-10.

Characklis WG. Biofilm development: a process analysis. *Microbial Adhesion and Aggregation, ed. KC Marshall*. 2012**:** 137-57.

Chen CP, Chen CT, Tsai T. Chitosan Nanoparticles for Antimicrobial Photodynamic Inactivation: Characterization and *In Vitro* Investigation. ***Photochem Photobiol***. 2012; 88: 570-6.

Chen X, Schauder S, Potier N, Van Dorsselaer A, Pelczer I, Bassler BL, Hughson FM. Structural identification of a bacterial quorum-sensing signal containing boron. ***Nature***. 2002; 415: 545-9.

Cheviron P, Gouanvé F, Espuche E. Green synthesis of colloid silver nanoparticles and resulting biodegradable starch/silver nanocomposites. ***Carb polymers***. 2014; 108: 291-8.

Costerton JW, Montanaro L, Arciola CR. Biofilm in implant infections: its production and regulation. ***Int J Artificial Org***. 2005; 28: 1062-8.

Costerton JW, Stewart PS, Greenberg EP. Bacterial biofilms: a common cause of persistent infections. ***Science***. 1999; 284: 1318-22.

Couvreur P, Vauthier C. Nanotechnology: intelligent design to treat complex disease. ***Pharm Res***. 2006; 23: 1417-50.

Cullity BD. Elements of. *X-ray diffraction*. 1978.

Cunha MnV, Sousa SlA, Leitao JH, Moreira LM, Videira PA, Sá-Correia, I. Studies on the involvement of the exopolysaccharide produced by cystic fibrosis-associated isolates of the *Burkholderia cepacia* complex in biofilm formation and in persistence of respiratory infections. ***J Clin Microbiol***. 2004; 42: 3052-8.

Dai K, Lu L, Liang C, Dai J, Zhu G, Liu Z, Liu Q, Zhang Y. Graphene oxide modified ZnO nanorods hybrid with high reusable photocatalytic activity under UV-LED irradiation. ***Mater Chem Phys***. 2014; 143: 1410-6.

Dalben M, Varkulja G, Basso M, Krebs VLJ, Gibelli MA, Van Der Heijden I, Rossi F, Duboc G, Levin AS, Costa SF. Investigation of an outbreak of *Enterobacter cloacae* in a neonatal unit and review of the literature. ***J Hosp Infect***. 2008; 70: 7-14.

de Faria AF, Martinez DSfT, Meira SMM, de Moraes ACM, Brandelli A, Souza Filho AG, Alves OL. Anti-adhesion and antibacterial activity of silver nanoparticles supported on graphene oxide sheets. ***Colloids Surf B: Biointerfaces***. 2014; 113: 115-24.

de la Fuente-Núñez C, Reffuveille F, Fernández L, Hancock RE. Bacterial biofilm development as a multicellular adaptation: antibiotic resistance and new therapeutic strategies. ***Curr Opi Microbiol***. 2013; 16: 580-9.

De SoetJJ, Nyvad B, Kilian M. Strain-Related Acid Production by Oral *Streptococci*. ***Caries Res***. 2000; 34:486-90.

Denizot F, Lang R. Rapid colorimetric assay for cell growth and survival: modifications to the tetrazolium dye procedure giving improved sensitivity and reliability. ***J Immunol Methods***. 1986; 89: 271-7.

Dmitriev A, Mohapatra SS, Chong P, Neely M, Biswas S, Biswas I. CovR-controlled global regulation of gene expression in *Streptococcus mutans*. ***PloS one***. 2011; 6: e20127.

Dubois M, Gilles KA, Hamilton JK, Rebers P, Smith F. Colorimetric method for determination of sugars and related substances. ***Anal Chem***. 1956; 28: 350-6.

Dusane DH, Zinjarde SS, Venugopalan VP, McLean RJC, Weber MM, Rahman PKSM. Quorum sensing: implications on rhamnolipid bio surfactant production. ***Biotechnol Gen Eng Rev***. 2010; 27: 159-84.

EjrnæsK. Bacterial characteristics of importance for recurrent urinary tract infections caused by *Escherichia coli*. ***Dan Med Bull***. 2011; 58: B4187.

Ellis MW, Schlett CD, Millar EV, Crawford KB, Cui T, Lanier JB, Tribble DR. Prevalence of nasal colonization and strain concordance in patients with community-associated *Staphylococcus aureus* skin and soft-tissue infections. ***Infection Control***. 2014; 35: 1251-6.

Eshed M, Lellouche J, Banin E, Gedanken A. $MgF_2$ nanoparticle-coated teeth inhibit *Streptococcus mutans* biofilm formation on a tooth model. ***J Mater Chem B***. 2013; 1: 3985-91.

Eshed M, Lellouche J, Matalon S, Gedanken A, Banin E. Sonochemical coatings of ZnO and CuO nanoparticles inhibit *Streptococcus mu*tans biofilm formation on teeth model. ***Langmuir***. 2012; 28: 12288-95.

Espitia PJP, SoaresNdFtF, dos Reis Coimbra JSl, de Andrade NlJ, Cruz RS, Medeiros EAA. Zinc oxide nanoparticles: synthesis, antimicrobial activity and food packaging applications. ***Food Bioprocess Technol***. 2012; 5: 1447-64.

Falsetta ML, Klein MI, Colonne PM, Scott-Anne K, Gregoire S, Pai C-H, Gonzalez-Begne M, Watson G, Krysan DJ, Bowen WH. Symbiotic relationship between *Streptococcus mutans* and *Candida albicans* synergizes virulence of plaque biofilms in vivo. ***Infect Immun***. 2014; 82: 1968-81.

Farokhzad OC, Langer R. Impact of nanotechnology on drug delivery. ***ACS nano***. 2009; 3: 16-20.

Featherstone JDB. Prevention and reversal of dental caries: role of low level fluoride. ***Community Dent Oral Epidemiol***. 1999; 27: 31-40.

Filoche S, Wong L, Sissons CH. Oral biofilms: emerging concepts in microbial ecology. ***J Dent Res***. 2010; 89: 8-18.

Flemming H-C, Wingender J. The biofilm matrix. ***Nat Rev Microbiol***. 2010; 8:623-33.

Foster TJ, Geoghegan JA, Ganesh VK, HöökM. Adhesion, invasion and evasion: the many functions of the surface proteins of *Staphylococcus aureus.* ***Nat Rev Microbiol***. 2014; 12: 49-62.

Friedman AJ, Phan J, Schairer DO, Champer J, Qin M, Pirouz A, Blecher-Paz K, Oren A, Liu PT, Modlin RL. Antimicrobial and anti-inflammatory activity of chitosan-alginate nanoparticles: a targeted therapy for cutaneous pathogens. ***J Invest Dermatol***. 2013; 133: 1231-9.

Fujihara S, Kadota Y, Kimura T. Role of organic additives in the sol-gel synthesis of porous $CaF_2$ anti-reflective coatings. ***J Sol-Gel Sci Tech***. 2002; 24: 147-54.

Fux CA, Costerton JW, Stewart PS, Stoodley P. Survival strategies of infectious biofilms. ***Trends Microbiol***. 2005; 13: 34-40.

Fux CA, Stoodley P, Hall-Stoodley L, Costerton JW. Bacterial biofilms: a diagnostic and therapeutic challenge. 2003.

Goldstone JR, Popat R, Fletcher MP, Crusz AS, Diggle PS. Quorum sensing and social interactions in microbial biofilms. *Microbial Biofilms. Current Research and Applications. Caister Academic Press, Norfolk, UK*. 2012**:** 1-24.

Gomes C, Moreira RG, Castell-Perez E. Poly (DL-lactide-co-glycolide) (PLGA) Nanoparticles with Entrapped trans-Cinnamaldehyde and Eugenol for Antimicrobial Delivery Applications. ***J Food Sci***. 2011; 76: N16-N24.

Gregoire S, Singh AP, Vorsa N, Koo H. Influence of cranberry phenolics on glucan synthesis by glucosyltransferases and *Streptococcus mutans* acidogenicity. ***J Appl Microbiol***. 2007; 103: 1960-8.

Gu H, Hou S, Yongyat C, De Tore S, Ren D. Patterned biofilm formation reveals a mechanism for structural heterogeneity in bacterial biofilms. ***Langmuir***. 2013; 29: 11145-53.

Gupta K, Barua S, Hazarika SN, Manhar AK, Nath D, Karak N, Namsa ND, Mukhopadhyay R, Kalia VC, Mandal M. Green silver nanoparticles: enhanced antimicrobial and antibiofilm activity with effects on DNA replication and cell cytotoxicity. ***Rsc Adv***. 2014; 4: 52845-55.

Habimana O, Semião AJC, Casey E. The role of cell-surface interactions in bacterial initial adhesion and consequent biofilm formation on nanofiltration/reverse osmosis membranes. ***J Memb Sci***. 2014; 454: 82-96.

Hajipour MJ, Fromm KM, Ashkarran AA, de Aberasturi DJ, de Larramendi IR, Rojo T, Serpooshan V, Parak WJ, Mahmoudi M. Antibacterial properties of nanoparticles. ***Trends Biotechnol***. 2012; 30: 499-511.

Hamada S, Slade HD. Biology, immunology, and cariogenicity of *Streptococcus mutans*. ***Microbiol Rev***. 1980; 44: 331.

Hamilton IR. Effects of fluoride on enzymatic regulation of bacterial carbohydrate metabolism. ***Caries Res***. 1977; 11: 262-91.

Hardie JM. Oral microbiology: current concepts in the microbiology of dental caries and periodontal disease. ***British Dent J***. 1992; 172: 271-8.

Hasan S, Danishuddin M, Adil M, Singh K, Verma PK, Khan AU. Efficacy of *E. officinalis* on the cariogenic properties of *Streptococcus mutans*: a novel and alternative approach to suppress quorum-sensing mechanism. ***PloS one***. 2012; 7: e40319.

Hasan S, Danisuddin M, Khan AU. Inhibitory effect of *Zingiber officinale* towards *Streptococcus mutans* virulence and caries development: *in vitro* and *in vivo* studies. ***BMC Microbiol***. 2015; 15 (1):1

Hasan S, Singh K, Danisuddin M, Verma PK, Khan AU. Inhibition of major virulence pathways of *Streptococcus mutans* by quercitrin and deoxynojirimycin: a synergistic approach of infection control. ***PloS one***. 2014; 9: e91736.

Hassett DJ, Korfhagen TR, Irvin RT, Schurr MJ, Sauer K, Lau GW, Sutton MD, Yu H, Hoiby N. *Pseudomonas aeruginosa* biofilm infections in cystic fibrosis: insights into pathogenic processes and treatment strategies. ***Expert Opin Ther Targets***. 2010; 14: 117-30.

He Z, Wang Q, Hu Y, Liang J, Jiang Y, Ma R, Tang Z, Huang Z. Use of the quorum sensing inhibitor furanone C-30 to interfere with biofilm formation by *Streptococcus mutans* and its luxS mutant strain. ***Int J Antimicrob Agents***. 2012; 40: 30-5.

Heim KP, Crowley PJ, Brady LJ. An intramolecular interaction involving the N terminus of a streptococcal adhesin affects its conformation and adhesive function. ***J Biol Chem***. 2013; 288: 13762-74.

Hernandez-Delgadillo R, Velasco-Arias D, Diaz D, Arevalo-Niño K, Garza-Enriquez M, De la Garza-Ramos MA, Cabral-Romero C. Zerovalent bismuth nanoparticles inhibit *Streptococcus mutans* growth and formation of biofilm. ***Int J Nanomed***. 2012; 7: 2109.

Hernández-Sierra J F, Ruiz F, Pena DCC, Martínez-Gutiérrez F, Martínez AE, GuillénAdJsP , Tapia-Pérez H, Castañón GM. The antimicrobial sensitivity of *Streptococcus mutans* to nanoparticles of silver, zinc oxide, and gold. ***Nanomed Nanotechnol Bio Med***. 2008; 4: 237-40.

Heuer W, Elter C, Demling A, Neumann A, Suerbaum S, Hannig M, Heidenblut T, Bach FW, Stiesch-Scholz M. Analysis of early biofilm formation on oral implants in man. ***J Oral rehab.*** 2007; 34: 377-82.

Høiby N, Bjarnsholt T, Givskov M, Molin Sr, Ciofu O. Antibiotic resistance of bacterial biofilms. ***Int J Antimicrob Agents***. 2010; 35: 322-32.

Høiby N, Johansen HK, Moser C, Song Z, Ciofu O, Kharazmi A. *Pseudomonas aeruginosa* and the *in vitro* and *in vivo* biofilm mode of growth. ***Microb Infec***. 2001; 3: 23-35.

Høiby N,Ciofu O, Johansen HK, SongZ-j, Moser C, JensenPØ, MolinS, Givskov M, Tolker-Nielsen T, Bjarnsholt T. The clinical impact of bacterial biofilms. ***Int J Oral Sci***. 2011; 3: 55.

Hong SH, Lee J, Wood TK. Engineering global regulator Hha of *Escherichia coli* to control biofilm dispersal. ***Microb Biotechnol***. 2010; 3: 717-28.

Hu W, Peng C, Luo W, Lv M, Li X, Li D, Huang Q, Fan C. Graphene-based antibacterial paper. ***ACS nano***. 2010; 4: 4317-23.

Huang L, Dai T, Xuan Y, Tegos GP, Hamblin MR. Synergistic combination of chitosan acetate with nanoparticle silver as a topical antimicrobial: efficacy against bacterial burn infections. ***Antimicrob Agents Chemother***. 2011; 55: 3432-8.

Huang R, Li M, Gregory RL. Bacterial interactions in dental biofilm. ***Virulence***. 2010; 2: 435-44.

Huang Z, Zheng X, Yan D, Yin G, Liao X, Kang Y, Yao Y, Huang D, Hao B. Toxicological effect of ZnO nanoparticles based on bacteria. ***Langmuir***. 2008; 4140-4.

Huh AJ, Kwon YJ. "Nanoantibiotics": a new paradigm for treating infectious diseases using nanomaterials in the antibiotics resistant era. ***J Control Release.*** 2011; 156: 128-45.

Hummers Jr WS, Offeman RE. Preparation of graphitic oxide. ***J Am Chem Soc***. 1958; 80: 1339.

Huse HK, Kwon T, Zlosnik JEA, Speert DP, Marcotte EM, Whiteley M. *Pseudomonas aeruginosa* enhances production of a non-alginate exopolysaccharide during long-term colonization of the cystic fibrosis lung. 2013.

Hwang J-H, Lee J-H, Hwang J-H, Chung KM, Lee E-J, Yoon Y-J, Moon M-K, Kim J-S, Won K-S, Lee C-S. Comparison of Arbekacin and Vancomycin in Treatment of Chronic Suppurative Otitis Media by Methicillin Resistant *Staphylococcus aureus.* ***J Korean Med Sci*****.** 2015; 30: 688-93.

Iannitelli A, Grande R, Stefano AD, Giulio MD, Sozio P, Bessa LJ, Laserra S, Paolini C, Protasi F, Cellini L. Potential antibacterial activity of carvacrol-loaded poly (DL-lactide-co-glycolide) (PLGA) nanoparticles against microbial biofilm. ***Int J Mol Sci***. 2011; 12: 5039-51.

Islam B, Khan SN, Haque I, Alam M, Mushfiq M, Khan AU. Novel anti-adherence activity of mulberry leaves: inhibition of *Streptococcus mutans* biofilm by 1-deoxynojirimycin isolated from *Morus alba*. ***J Antimicrob Chemother***. 2008; 62: 751-7.

Jackson DW, Suzuki K, Oakford L, Simecka JW, Hart ME, Romeo T. Biofilm formation and dispersal under the influence of the global regulator CsrA of *Escherichia coli*. ***J Bacteriol***. 2002; 184: 290-301.

Jensen PÃ, Bjarnsholt T, Phipps R, Rasmussen TB, Calum H, Christoffersen L, Moser C, Williams P, Pressler T, Givskov M. Rapid necrotic killing of polymorphonuclear leukocytes is caused by quorum-sensing-controlled production of rhamnolipid by *Pseudomonas aeruginosa*. ***Microbiology***. 2007; 153: 1329-38.

Jin T, Sun D, Su JY, Zhang H, Sue HJ. Antimicrobial efficacy of zinc oxide quantum dots against *Listeria monocytogenes, Salmonella enteritidis,* and *Escherichia coli* O157: H7. ***J Food Sci***. 2009; 74: M46-M52.

Jones ME, Draghi DC, Thornsberry C, Karlowsky JA, Sahm DF, Wenzel RP. Annals of Clinical Microbiology and Antimicrobials. ***Ann Clin Microbiol Antimicrob***. 2004; 3: 14.

Jung C-J, Yeh C-Y, Shun C-T, Hsu R-B, Cheng H-W, Lin C-S, Chia J-S. Platelets enhance biofilm formation and resistance of endocarditis-inducing s*treptococci* on the injured heart valve. ***Int J Infect Dis***. 2012; 205: 1066-75.

Kasraei S, Sami L, Hendi S, AliKhani M-Y, Rezaei-Soufi L, Khamverdi Z. Antibacterial properties of composite resins incorporating silver and zinc oxide nanoparticles on *Streptococcus mutans* and *Lactobacillus.* ***Restor Dent Endod***. 2014; 39: 109-14.

Kenawy E-R, Worley SD, Broughton R. The chemistry and applications of antimicrobial polymers: a state-of-the-art review. ***Biomacromolecules***. 2007; 8: 1359-84.

Khan AU, Nordmann P. NDM-1-producing *Enterobacter cloacae* and *Klebsiella pneumoniae* from diabetic foot ulcers in India. ***J Med Microbiol***. 2012; 61: 454-6.

Khan EM, Alam F, Parveen A, Naqvi AH. Structural, Optical and Dielectric Properties of Alkaline Earth Metal (Sr0. 05, Mg0. 05 and Ba0. 05) Doped $CaF_2$ Nanoparticles and Their Microscopic Analysis. ***J Adv Microscopy Res***. 2013; 8: 45-52.

Khan R, Zakir M, Khanam Z, Shakil S, Khan AU. Novel compound from *Trachyspermum ammi* (Ajowan caraway) seeds with antibiofilm and anti-adherence activities against *Streptococcus mutans*: a potential chemotherapeutic agent against dental caries. ***J Appl Microbiol***. 2010; 109: 2151-9.

Khan S, Alam F, Azam A, Khan AU. Gold nanoparticles enhance methylene blue-induced photodynamic therapy: a novel therapeutic approach to inhibit *Candida albicans* biofilm. ***Int J Nanomedicine***. 2010; 7: 3245.

Kharissova OV, Dias HR, Kharisov BI, Pérez BO, Pérez VMJ. The greener synthesis of nanoparticles. ***Trends Biotechnol***. 2013; 31**:** 240-8.

Kim S-M, Lee H-W, Choi Y-W, Kim S-H, Lee J-C, Lee Y-C, Seol S-Y, Cho D-T, Kim J. Involvement of curli fimbriae in the biofilm formation of *Enterobacter cloacae.* ***J Microbiol***. 2012; 50: 175-8.

Kim Y-M, Shimizu R, Nakai H, Mori H, Okuyama M, Kang M-S, Fujimoto Z, Funane K, Kim D, Kimura A. Truncation of N-and C-terminal regions of *Streptococcus mutans* dextranase enhances catalytic activity. ***J Appl Microbiol***. 2011; 91: 329-39.

Knetsch MLW, Koole LH. New strategies in the development of antimicrobial coatings: the example of increasing usage of silver and silver nanoparticles. ***Polymers***. 2011; 3:340-66.

Koo H, Hayacibara MF, Schobel BD, Cury JA, Rosalen PL, Park YK, Vacca-Smith AM, Bowen WH. Inhibition of *Streptococcus mutans* biofilm accumulation and polysaccharide production by apigenin and tt-farnesol. ***J Antimicrob Chemother***. 2003; 52: 782-9.

Koo H, Xiao J, Klein MI, Jeon JG. Exopolysaccharides produced by *Streptococcus mutans* glucosyltransferases modulate the establishment of microcolonies within multispecies biofilms. ***J Bacteriol***. 2010; 192: 3024-32.

Kostakioti M, Hadjifrangiskou M, Hultgren SJ. Bacterial biofilms: development, dispersal, and therapeutic strategies in the dawn of the post antibiotic era. ***Cold Spring Harb Perspect Med***. 2013; 3: a010306.

Król JE, Biswas S, King C, Biswas I. SMU. 746-SMU. 747, a putative membrane permease complex, is involved in aciduricity, acidogenesis, and biofilm formation in *Streptococcus mutans*. ***J Bacteriol***. 2014; 196: 129-39.

Kulshrestha S, Khan S, Meena R, Singh BR, Khan AU. A graphene/zinc oxide nanocomposite film protects dental implant surfaces against cariogenic *Streptococcus mutans*. ***Biofouling***. 2014; 30: 1281-94.

Kumar GA, Chen CW, Ballato J, Riman RE. Optical characterization of infrared emitting rare-earth-doped fluoride nanocrystals and their transparent nanocomposites. ***Chem Mater***. 2007; 19: 1523-8.

Kumari A, Yadav SK, Yadav SC. Biodegradable polymeric nanoparticles based drug delivery systems. ***Colloids Surf B Biointerfaces***. 2010; 75: 1-18.

Kuramitsu HK. Virulence factors of mutans streptococci: role of molecular genetics. ***Crit Rev Oral Biol* Med**. 1993; 4: 159-76.

LaFleur MD, Kumamoto CA, Lewis K. *Candida albicans* biofilms produce antifungal-tolerant persister cells. ***Antimicrob Agents Chemother***. 2006; 50: 3839-46.

Lang NP, Mombelli A, Attström R.Oral biofilms and calculus.*Clinical Periodontology and Implant Dentistry. Oxford, UK: Blackwell Munksgaard*. 2008**:** 197-205.

Lara HH, Ayala-Núnez NV, Turrent LDCI, Padilla CR. Bactericidal effect of silver nanoparticles against multidrug-resistant bacteria. ***World J Microbiol Biotechnol***. 2010; 26: 615-21.

Larson RM. Merits and modifications of scoring rat dental caries by Keye's™ method. *Proceedings of the Symposium on Animal Models in Cariology. Washington, DC: Information Retrieval, Special Supplement to Microbiology Abstracts*. Vol. 195, 1981. 203.

Lebeaux D, Ghigo J-M, Beloin C. Biofilm-related infections: bridging the gap between clinical management and fundamental aspects of recalcitrance toward antibiotics. ***Microbiol Mol Biol Rev***. 2014; 78: 510-43.

Leid JG, Costerton JW, Shirtliff ME, Gilmore MS, Engelbert M. Immunology of Staphylococcal biofilm infections in the eye: new tools to study biofilm endophthalmitis. ***DNA Cell Biol***. 2002; 21: 405-13.

Lellouche J, Friedman A, Lahmi R, Gedanken A, Banin E. Antibiofilm surface functionalization of catheters by magnesium fluoride nanoparticles. ***Int J Nanomedicine***. 2012; 7:1175.

Lellouche J, Kahana E, Elias S, Gedanken A, Banin E. Antibiofilm activity of nanosized magnesium fluoride. ***Biomaterials***. 2009; 30: 5969-78.

Lembre P, Lorentz Cc, Di Martino P, *Exopolysaccharides of the biofilm matrix: A complex biophysical world*. 2012: INTECH Open Access Publisher.

Lew DP, Waldvogel FA. Osteomyelitis. ***Lancet***. 2004; 364: 369-79.

Lewis K. Persister cells, dormancy and infectious disease. ***Nat Rev Microbiol***. 2007; 5: 48-56.

Li D, Shibata Y, Takeshita T, Yamashita Y. A novel gene involved in the survival of *Streptococcus mutans* under stress conditions. ***Appl Environ Microbiol***. 2014; 80: 97-103.

Li L. The biochemistry and physiology of metallic fluoride: action, mechanism, and implications. ***Crit Rev Oral Biol* Med**. 2003; 14: 100-14.

Li Q, Mahendra S, Lyon DY, Brunet L, Liga MV, Li D, Alvarez PJJ. Antimicrobial nanomaterials for water disinfection and microbial control: potential applications and implications. ***Water Res***. 2008; 42: 4591-602.

Li W-R, Xie X-B, Shi Q-S, Zeng H-Y, You-Sheng OUY, Chen Y-B. Antibacterial activity and mechanism of silver nanoparticles on *Escherichia coli*. ***Appl Microbiol Biotechnol***. 2010; 85: 1115-22.

Li Y, Burne RA. Regulation of the gtfBC and ftf genes of *Streptococcus mutans* in biofilms in response to pH and carbohydrate. ***Microbiology***. 2001; 147: 2841-8.

Li Y-H, Tang N, Aspiras MB, Lau PCY, Lee JH, Ellen RP, Cvitkovitch DG. A quorum-sensing signaling system essential for genetic competence in *Streptococcus mutans* is involved in biofilm formation. ***J Bacteriol***. 2002; 184: 2699-708.

Lichter JA, Rubner MF. Polyelectrolyte multilayers with intrinsic antimicrobial functionality: the importance of mobile polycations. ***Langmuir***. 2009; 25: 7686-94.

Liou J-W, Chang H-H. Bactericidal effects and mechanisms of visible light-responsive titanium dioxide photocatalystson pathogenic bacteria. *Archivum immunologiae et therapiae experimentalis.*2012; 60: 267-75.

Liu S, Hu M, Zeng TH, Wu R, Jiang R, Wei J, Wang L, Kong J, Chen Y. Lateral dimension-dependent antibacterial activity of graphene oxide sheets. ***Langmuir***. 2012; 28: 12364-72.

Liu S, Zeng TH, Hofmann M, Burcombe E, Wei J, Jiang R, Kong J, Chen Y. Antibacterial activity of graphite, graphite oxide, graphene oxide, and reduced graphene oxide: membrane and oxidative stress. ***ACS nano***. 2011; 5: 6971-80.

Liu Y, He L, Mustapha A, Li H, Hu ZQ, Lin M. Antibacterial activities of zinc oxide nanoparticles against *Escherichia coli* O157: H7. ***J Appl Microbiol.***2009; 107: 1193-201.

Loesche WJ. Role of *Streptococcus mutans* in human dental decay. ***Microbiol Rev***. 1986; 50: 353.

López-Moreno A, Sepúlveda-Sánchez JD, Mercedes Alonso Guzmán E, Le Borgne S. Calcium carbonate precipitation by heterotrophic bacteria isolated from biofilms formed on deteriorated ignimbrite stones: influence of calcium on EPS production and biofilm formation by these isolates. ***Biofouling***. 2014; 30: 547-60.

Lovrić J, Cho SJ, Winnik FoM, Maysinger D. Unmodified cadmium telluride quantum dots induce reactive oxygen species formation leading to multiple organelle damage and cell death. ***Chem Bio***. 2005; 12: 1227-34.

Lynch AS, Robertson GT. Bacterial and fungal biofilm infections. ***Annu Rev Med***. 2008; 59: 415-28.

Ma J, Zhang J, Xiong Z, Yong Y, Zhao XS. Preparation, characterization and antibacterial properties of silver-modified graphene oxide. ***J Mater Chem***. 2011; 21: 3350-2.

Mah T-F. Biofilm-specific antibiotic resistance. ***Future Microbiol***. 2012; 7: 1061-72.

Mah T-FC, O'Toole GA. Mechanisms of biofilm resistance to antimicrobial agents. ***Trends Microbiol***. 2001; 9: 34-9.

Mahmoudi M, Serpooshan V. Silver-coated engineered magnetic nanoparticles are promising for the success in the fight against antibacterial resistance threat. ***ACS nano***. 2012; 6: 2656-64.

Marquis RE, Clock SA, Mota-Meira M. Fluoride and organic weak acids as modulators of microbial physiology. ***FEMS Microbiol Rev***. 2003; 26: 493-510.

Marsh PD. Microbiology of dental plaque biofilms and their role in oral health and caries. ***Dent Clin North Am***. 2010; 54: 441-54.

Mazda Y, Kawada-Matsuo M, Kanbara K, Oogai Y, Shibata Y, Yamashita Y, Miyawaki S, Komatsuzawa H. Association of CiaRH with resistance of *Streptococcus mutans* to antimicrobial peptides in biofilms. ***Mol Oral Microbiol***. 2012; 27: 124-35.

McNeil SE. Unique benefits of nanotechnology to drug delivery and diagnostics. *Characterization of Nanoparticles Intended for Drug Delivery*: Springer, 2011. 3-8.

McNeill K, Hamilton IR. Acid tolerance response of biofilm cells of *Streptococcus mutans.* ***FEMS Microbiol Lett***. 2003; 221: 25-30.

Miller KV, Eisley KM, Shanks RMQ, Lahr RM, Lathrop KL, Kowalski RP, Noecker RJ. Recurrent enterococcal endophthalmitis seeded by an intraocular lens biofilm. ***J Cataract Refract Surg***. 2011; 37: 1355-9.

Minardi D, Cirioni O, Ghiselli R, Silvestri C, Mocchegiani F, Gabrielli E, d'Anzeo G, Conti A, Orlando F, Rimini M. Efficacy of tigecycline and rifampin alone and in combination against *Enterococcus faecalis* biofilm infection in a rat model of ureteral stent. ***J Surg Res***. 2012; 176: 1-6.

Mohammadi G, Valizadeh H, Barzegar-Jalali M, Lotfipour F, Adibkia K, Milani M, Azhdarzadeh M, Kiafar F, Nokhodchi A. Development of azithromycin-PLGA nanoparticles: Physicochemical characterization and antibacterial effect against *Salmonella typhi*. ***Colloids Surf* B *Biointerface*s**. 2010; 80: 34-9.

Mohanpuria P, Rana NK, Yadav SK. Biosynthesis of nanoparticles: technological concepts and future applications. ***J Nanopart Res***. 2008; 10: 507-17.

Murugan K, Usha M, Malathi P, Al-Sohaibani AS, Chandrasekaran M. Biofilm forming multi drug resistant *Staphylococcus* spp. among patients with conjunctivitis. ***Pol J Microbiol***. 2010; 59: 233-9.

Musil I, Jensen V, Schilling J, Ashdown B, Kent T. Case report *Enterobacter cloacae* infection of an expanded polytetrafluoroethylene femoral-popliteal bypass graft: a case report. ***J Med* Case *Rep.***2010; 4:131.

Nakano K, Nomura R, Nemoto H, Mukai T, Yoshioka H, Shudo Y, Hata H, Toda K, Taniguchi K, Amano A. Detection of novel serotype k *Streptococcus mutans* in infective endocarditis patients. ***J Med Microbiol***. 2007; 56: 1413-5.

Nakazato G, Tsuchiya H, Sato M, Yamauchi M. In vivo plaque formation on implant materials. ***Int J Oral Maxillofac Implants***. 1988; 4: 321-6.

Nance WC, Dowd SE, Samarian D, Chludzinski J, Delli J, Battista J, Rickard AH. A high-throughput microfluidic dental plaque biofilm system to visualize and quantify the effect of antimicrobials. ***J Antimicrob Chemother***. 2013; 68: 2550-60.

Nguyen D, Joshi-Datar A, Lepine F, Bauerle E, Olakanmi O, Beer K, McKay G, Siehnel R, Schafhauser J, Wang Y. Active starvation responses mediate antibiotic tolerance in biofilms and nutrient-limited bacteria. ***Science***. 2011; 334: 982-6.

Novick RP, Geisinger E. Quorum sensing in staphylococci. ***Annu Rev Genet***. 2008; 42: 541-64.

Novoselov KS, Geim AK. The rise of graphene. ***Nat Mater***. 2007; 6: 183-91.

Ochekpe NA, Olorunfemi PO, Ngwuluka NC. Nanotechnology and drug delivery part 1: background and applications. ***Trop J Pharm Res***. 2009; 8.

Ocsoy I, Paret ML, Ocsoy MA, Kunwar S, Chen T, You M, Tan W. Nanotechnology in plant disease management: DNA-directed silver nanoparticles on graphene oxide as an antibacterial against *Xanthomonas perforans*. ***ACS nano***. 2013; 7: 8972-80.

Olsen I. Biofilm-specific antibiotic tolerance and resistance. ***Eur J Clin Microbiol Infect Dis***. 2015; 34: 877-86.

Omolfajr N, Nasser S, Mahmood R, Kompany A. Synthesis an d Characterization of $CaF_2$ NPs with Co-precipitation and Hydrothermal Method. ***J Nanomed Nanotechnol***. 2011; 2: 2.

O'Toole G, Kaplan HB, Kolter R. Biofilm formation as microbial development. ***Annu Rev Microbiol.***2000; 54: 49-79.

Paganelli FL, Willems RJ, Leavis HL. Optimizing future treatment of enterococcal infections: attacking the biofilm? ***Trends Microbiol***. 2012; 20: 40-9.

Pal S, Tak YK, Song JM. Does the antibacterial activity of silver nanoparticles depend on the shape of the nanoparticle? A study of the gram-negative bacterium *Escherichia coli*. ***Appl Environ Microbiol***. 2007; 73: 1712-20.

Pandurangappa C, Lakshminarasappa BN. Optical absorption and Photoluminescence studies in Gamma-irradiated nanocrystalline $CaF_2$. ***J Nanomed Nanotechnol***. 2011; 2: 2.

Pandurangappa C, Lakshminarasappa BN. Optical studies of samarium-doped fluoride nanoparticles. ***Philos Mag***. 2011; 91: 4486-94.

Parboosing R, Maguire GEM, Govender P, Kruger HG. Nanotechnology and the treatment of HIV infection.***Viruses***. 2012; 4: 488-520.

Paredes JI, Villar-Rodil S, Martinez-Alonso A, Tascon JMD. Graphene oxide dispersions in organic solvents. ***Langmuir***. 2008; 24: 10560-4.

Park S, Mohanty N, Suk JW, Nagaraja A, An J, Piner RD, Cai W, Dreyer DR, Berry V, Ruoff RS. Biocompatible, Robust Free-Standing Paper Composed of a TWEEN/Graphene Composite. ***Adv Mater***. 2010; 22: 1736-40.

Park SW, Kwon MJ, Yoo JY, Choi H-J, Ahn Y-J. Antiviral activity and possible mode of action of ellagic acid identified in *Lagerstroemia speciosa* leaves toward human rhinoviruses. ***BMC Complement Altern Med***. 2014; 14: 171.

Patra S, Mukherjee S, Barui AK, Ganguly A, Sreedhar B, Patra CR. Green synthesis, characterization of gold and silver nanoparticles and their potential application for cancer therapeutics. ***Mater Sci Eng* C**. 2015; 53:298-309.

Pavlovsky L, Sturtevant RA, Younger JG, Solomon MJ. Effects of Temperature on the Morphological, Polymeric, and Mechanical Properties of *Staphylococcus epidermidis* Bacterial Biofilms. ***Langmuir***. 2015; 31: 2036-42.

Peleg AY, Hooper DC. Hospital-acquired infections due to gram-negative bacteria. ***N Engl J Medicine***. 2010; 362: 1804-13.

Pelgrift RY, Friedman AJ. Nanotechnology as a therapeutic tool to combat microbial resistance. ***Adv Drug Deliv Rev***. 2013; 65: 1803-15.

Pelgrift RY, Friedman AJ. Nanotechnology as a therapeutic tool to combat microbial resistance. ***Adv Drug Deliv Rev***. 2013; 65: 1803-15.

Percival SL, Hill KE, Malic S, Thomas DW, Williams DW. Antimicrobial tolerance and the significance of persister cells in recalcitrant chronic wound biofilms. ***Wound Repair Regen***. 2011; 19:1-9.

Phan TN, Buckner T, Sheng J, Baldeck JD, Marquis RE. Physiologic actions of zinc related to inhibition of acid and alkali production by oral streptococci in suspensions and biofilms. ***Oral Microbiol Immun***. 2004; 19: 31-8.

Philip D, Unni C, Aromal SA, Vidhu VK. Murrayakoenigii leaf-assisted rapid green synthesis of silver and gold nanoparticles. ***Spectrochim Acta A Mol Biomol Spectrosc.*** 2011; 78: 899-904.

Pinto-Alphandary H, Andremont A, Couvreur P. Targeted delivery of antibiotics using liposomes and nanoparticles: research and applications. ***Int J Antimicrob Agents***. 2000; 13: 155-68.

Plotkin BJ, Wu Z, Ward K, Nadella S, Green JM, Rumnani B. Effect of Human Insulin on the Formation of Catheter-Associated *E. coli* Biofilms. ***Open Journal of Urology***. 2014; 2014.

Pol VG, Wildermuth G, Felsche J, Gedanken A, Calderon-Moreno J. Sonochemical deposition of Au nanoparticles on titania and the significant decrease in the melting point of gold. ***J Nanosci Nanotechnol***. 2005; 5: 975-9.

Prabhu S, Poulose EK. Silver nanoparticles: mechanism of antimicrobial action, synthesis, medical applications, and toxicity effects. ***Int Nano Lett***. 2012; 2: 1-10.

Premanathan M, Karthikeyan K, Jeyasubramanian K, Manivannan G. Selective toxicity of ZnO nanoparticles toward Gram-positive bacteria and cancer cells by apoptosis through lipid peroxidation. ***Nanomed Nanotechnol***. 2011; 7: 184-92.

Qvist T, Pressler T, Høiby N, Katzenstein TL. Shifting paradigms of nontuberculous mycobacteria in cystic fibrosis. ***Respir Res***. 2014; 15: 41.

Radzig MA, Nadtochenko VA, Koksharova OA, Kiwi J, Lipasova VA, Khmel IA. Antibacterial effects of silver nanoparticles on gram-negative bacteria: influence on the

growth and biofilms formation, mechanisms of action. ***Colloids Surf B Biointerfaces***. 2013; 102: 300-6.

Raghupathi KR, Koodali RT, Manna AC. Size-dependent bacterial growth inhibition and mechanism of antibacterial activity of zinc oxide nanoparticles. ***Langmuir***. 2011; 27: 4020-8.

Rai M, Kon K, Ingle A, Duran N, Galdiero S, Galdiero M. Broad-spectrum bioactivities of silver nanoparticles: the emerging trends and future prospects. ***Appl Microbiol Biotechnol***. 2014; 98: 1951-61.

Rajilić-Stojanović M, Smidt H, De Vos W M. Diversity of the human gastrointestinal tract microbiota revisited. ***Environ Microbiol***. 2007; 9: 2125-36.

Reisner A, Haagensen JAJ, Schembri MA, Zechner EL, Molin Sr. Development and maturation of *Escherichia coli* KP-12 biofilms. ***Mol Microbiol***. 2003; 48: 933-46.

Ren G, Hu D, Cheng EWC, Vargas-Reus MA, Reip P, Allaker RP. Characterisation of copper oxide nanoparticles for antimicrobial applications. ***Int J Antimicrob Agents***. 2009; 33: 587-90.

Rølla G, Saxegaard E. Critical evaluation of the composition and use of topical fluorides, with emphasis on the role of calcium fluoride in caries inhibition. ***J Dent Res***. 1990; 69: 780-5.

Rošin-Grget K, Linčir I. Current concept on the anticaries fluoride mechanism of the action. ***Coll Antropol***. 2001; 25: 703-12.

Rovers MM, Schilder AGM, Zielhuis GA, Rosenfeld RM. Otitis media. ***Lancet***. 2004; 363: 465-73.

Rowe MC, Withers HL, Swift S. Uropathogenic *Escherichia coli* forms biofilm aggregates under iron restriction that disperse upon the supply of iron. ***FEMS microbiol lett***. 2010; 307: 102-9.

Rudkjøbing VB, Thomsen TR, Alhede M, Kragh KN, Nielsen PH, Johansen UR, Givskov M, Høiby N, Bjarnsholt T. The microorganisms in chronically infected end-stage and non-end-stage cystic fibrosis patients. ***FEMS Immunol Med Microbio.*** 2012; 65: 236-44.

Ruparelia JP, Chatterjee AK, Duttagupta SP, Mukherji S. Strain specificity in antimicrobial activity of silver and copper nanoparticles. ***Acta Biomater***. 2008; 4: 707-16.

Rutherford ST, Bassler BL. Bacterial quorum sensing: its role in virulence and possibilities for its control. ***Cold Spring Harb Perspect Med***. 2012; 2: a012427.

Saxegaard E, Rølla G. Kinetics of acquisition and loss of calcium fluoride by enamel *in vivo*. ***Caries Res***. 1989; 23: 406-11.

Schierle CF, De la Garza M, Mustoe TA, Galiano RD. *Staphylococcal* biofilms impair wound healing by delaying reepithelialization in a murine cutaneous wound model. ***Wound Repair Regen***. 2009; 17: 354-9.

Seema H, Kemp KC, Chandra V, Kim KS. Graphene-$SnO_2$ composites for highly efficient photocatalytic degradation of methylene blue under sunlight. ***Nanotechnology***. 2012; 23: 355705.

Selwitz RH, Ismail AI, Pitts NB. Dental caries. ***Lancet***. 2007; 369: 51-9.

Shao W, Liu X, Min H, Dong G, Feng Q, Zuo S. Preparation, Characterization, and Antibacterial Activity of Silver Nanoparticle-Decorated Graphene Oxide Nanocomposite. ***ACS Appl Mater Interfaces***. 2015; 7: 6966-73.

Sharma S, Lavender S, Woo J, Guo L, Shi W, Kilpatrick-Liverman L, Gimzewski JK. Nanoscale characterization of effect of L-arginine on *Streptococcus mutans* biofilm adhesion by atomic force microscopy. ***Microbiology***. 2014; 160: 1466-73.

Shi L-E, Li Z-H, Zheng W, Zhao Y-F, Jin Y-F, Tang Z-X. Synthesis, antibacterial activity, antibacterial mechanism and food applications of ZnO nanoparticles: a review. ***Food Addit Contam Part A***2014; 31: 173-86.

Silvestry-Rodriguez N, Sicairos-Ruelas EE, Gerba CP, Bright KR. Silver as a disinfectant. ***Rev Environ Contam Toxicol***: Springer, 2007. 23-45.

Smith EG, Spatafora GA. Gene Regulation in *S. mutans* Complex Control in a Complex Environment. ***J Dent Res***. 2012; 91: 133-41.

Solano C, Echeverz M, Lasa Ii. Biofilm dispersion and quorum sensing. ***Curr Opin Microbiol***. 2014; 18: 96-104.

Sondi I, Salopek-Sondi B. Silver nanoparticles as antimicrobial agent: a case study on *E. coli* as a model for Gram-negative bacteria. ***J Colloid Interface Sci***. 2004; 275: 177-82.

Soppimath KS, Aminabhavi TM, Kulkarni AR, Rudzinski WE. Biodegradable polymeric nanoparticles as drug delivery devices. ***J Control Release***. 2001; 70: 1-20.

Stoia AE, Sinescu C, Pielmusi M, Enescu M, Tudor A, Rominu RO, Rominu M. Tensile testing, a method used to demonstrate the effect of organic solvents on acrylic teeth denture base resin bond strength. ***Int J Bio Biomed Engg***. 2011; 5: 9-17.

Su H-L, Chou C-C, Hung D-J, Lin S-H, Pao IC, Lin J-H, Huang F-L, Dong R-X, Lin J-J. The disruption of bacterial membrane integrity through ROS generation induced by nanohybrids of silver and clay. ***Biomaterials***. 2009; 30: 5979-87.

Sullan RMA, Li JK, Crowley PJ, Brady LJ, DufrÃªne YF. Binding Forces of *Streptococcus mutans* P1 Adhesin. ***ACS nano***. 2015; 9: 1448-60.

Sun L, Chow LC. Preparation and properties of nano-sized calcium fluoride for dental applications. ***Dent Mater***. 2008; 24: 111-6.

Sundararajan B, Kumari BDR. Biosynthesis of silver nanoparticles in *Lagerstroemia speciosa* (L.) pers and their antimicrobial activities. ***Int J Pharm Pharm Sci***. 2014; 6: 30-4.

Sutton SV, Bender GR, Marquis RE. Fluoride inhibition of proton-translocating ATPases of oral bacteria. ***Infect Immun***. 1987; 55: 2597-603.

Svensäter G, Sjögreen B, Hamilton IR. Multiple stress responses in *Streptococcus mutans* and the induction of general and stress-specific proteins. ***Microbiology***. 2000; 146: 107-17.

Takei S, Hotomi M, Yamanaka N. Minimal biofilm eradication concentration of antimicrobial agents against nontypeable *Haemophilus influenzae* isolated from middle ear fluids of intractable acute otitis media. ***J Infect Chemother***. 2013; 19: 504-9.

Tang J, Chen Q, Xu L, Zhang S, Feng L, Cheng L, Xu H, Liu Z, Peng R. Graphene oxide-silver nanocomposite as a highly effective antibacterial agent with species-specific mechanisms. ***ACS Appl MaterInterfaces***. 2013; 5: 3867-74.

Thorsteinsson T, Másson M, Kristinsson KG, Hjálmarsdóttir MA, Hilmarsson H, Loftsson T. Soft antimicrobial agents: synthesis and activity of labile environmentally friendly long chain quaternary ammonium compounds. ***J Med Chem*** 2003; 46: 4173-81.

Toutain CM, Caizza NC, Zegans ME, O'Toole GA. Roles for flagellar stators in biofilm formation by *Pseudomonas aeruginosa*. ***Res Microbiol***. 2007; 158: 471-7.

Tseng BS, Zhang W, Harrison JJ, Quach TP, Song JL, Penterman J, Singh PK, Chopp DL, Packman AI, Parsek MR. The extracellular matrix protects *Pseudomonas aeruginosa* biofilms by limiting the penetration of tobramycin. ***Environ Microbiol***. 2013; 15: 2865-78.

Upadhyay RK, Soin N, Roy SS. Role of graphene/metal oxide composites as photocatalysts, adsorbents and disinfectants in water treatment: a review. ***RSC Adv.*** 2014; 4: 3823-51.

Van Houdt R, Michiels CW. Role of bacterial cell surface structures in *Escherichia coli* biofilm formation. ***Res Microbiol***. 2005; 156: 626-33.

Vecitis CD, Zodrow KR, Kang S, Elimelech M. Electronic-structure-dependent bacterial cytotoxicity of single-walled carbon nanotubes. ***ACS nano***. 2010; 4: 5471-9.

Veerachamy S, Yarlagadda T, Manivasagam G, Yarlagadda PKDV. Bacterial adherence and biofilm formation on medical implants: A review. ***Proc Inst Mech Eng H***. 2014; 228: 1083-99.

Verhoeff M, van der Veen EL, Rovers MM, Sanders EAM, Schilder AGM. Chronic suppurative otitis media: a review. ***Int J Pediatr Otorhinolaryngol***. 2006; 70: 1-12.

Vlamakis H, Chai Y, Beauregard P, Losick R, Kolter R. Sticking together: building a biofilm the *Bacillus subtilis* way. ***Nat Rev Microbiol.***2013; 11: 157-68.

Wang Y, Shi Z, Yin J. Facile synthesis of soluble graphene via a green reduction of graphene oxide in tea solution and its biocomposites. ***ACS Appl Mater Interfaces***. 2011; 3: 1127-33.

Wei Q, Ma LZ. Biofilm matrix and its regulation in *Pseudomonas aeruginosa*. ***Int J Mol Sci***. 2013; 14: 20983-1005.

Wei Y, Perez LJ, Ng W-L, Semmelhack MF, Bassler BL. Mechanism of *Vibrio cholerae* autoinducer-1 biosynthesis. ***ACS Chem Biol***. 2011; 6: 356-65.

Welin-Neilands J, Svensäter G. Acid tolerance of biofilm cells of *Streptococcus mutans*. ***Appl environ microbiol***. 2007; 73: 5633-8.

Whitchurch CB, Tolker-Nielsen T, Ragas PC, Mattick JS. Extracellular DNA required for bacterial biofilm formation. ***Science***. 2002; 295: 1487-.

Wiley L, Bridge DR, Wiley LA, Odom JV, Elliott T, Olson JC. Bacterial Biofilm Diversity in Contact Lens-Related Disease: Emerging Role of *Achromobacter*, *Stenotrophomonas*, and *Delftia* Biofilm Diversity in Contact Lens-Related Disease. ***Invest Ophthalmol Vis Sci***. 2012; 53: 3896-905.

Williamson KS, Richards LA, Perez-Osorio AC, Pitts B, McInnerney K, Stewart PS, Franklin MJ. Heterogeneity in *Pseudomonas aeruginosa* biofilms includes expression of ribosome hibernation factors in the antibiotic-tolerant subpopulation and hypoxia-induced stress response in the metabolically active population. ***J Bacteriol***. 2012; 194: 2062-73.

Wingender J, Neu TR, Flemming H-C, *Microbial extracellular polymeric substances: characterization, structure and function*. 2012: Springer Science & Business Media.

Wu M-C, Deokar AR, Liao J-H, Shih P-Y, Ling Y-C. Graphene-based photothermal agent for rapid and effective killing of bacteria. ***ACS nano***. 2013; 7: 1281-90.

Wu Y, VuliÄ‡ M, Keren I, Lewis K. Role of oxidative stress in persister tolerance. ***Antimicrob Agents Chemother***. 2012; 56: 4922-6.

Wunderink RG, Niederman MS, Kollef MH, Shorr AF, Kunkel MJ, Baruch A, McGee WT, Reisman A, Chastre J. Linezolid in methicillin-resistant *Staphylococcus aureus* nosocomial pneumonia: a randomized, controlled study. ***Clin Infect Dis***. 2012; 54: 621-9.

Xia T, Kovochich M, Brant J, Hotze M, Sempf J, Oberley T, Sioutas C, Yeh JI, Wiesner MR, Nel AE. Comparison of the abilities of ambient and manufactured nanoparticles to induce cellular toxicity according to an oxidative stress paradigm. ***Nano Lett.*** 2006; 6: 1794-807.

Xiao J, Klein MI, Falsetta ML, Lu B, Delahunty CM, Yates 3rd JR, Heydorn A, Koo H. The exopolysaccharide matrix modulates the interaction between 3D architecture and virulence of a mixed-species oral biofilm. ***PLoS Pathog***. 2012; 8:e1002623.

Xie Y, He Y, Irwin PL, Jin T, Shi X. Antibacterial activity and mechanism of action of zinc oxide nanoparticles against *Campylobacter jejuni*. ***Appl environ microbiol***. 2011; 77: 2325-31.

Xu HHK, Moreau JL, Sun L, Chow LC. Strength and fluoride release characteristics of a calcium fluoride based dental nanocomposite. ***Biomaterials***. 2008; 29: 4261-7.

Xu W-P, Zhang L-C, Li J-P, Lu Y, Li H-H, Ma Y-N, Wang W-D, Yu S-H. Facile synthesis of silver@ graphene oxide nanocomposites and their enhanced antibacterial properties. ***J Mater Chem***. 2011; 21: 4593-7.

Yang L, Liu Y, Wu H, Song Z, HÃ¸iby N, Molin Sr, Givskov M. Combating biofilms. ***FEMS Immunol Med Microbiol***. 2012; 65: 146-57.

Yen HJ, Hsu Sh, Tsai CL. Cytotoxicity and immunological response of gold and silver nanoparticles of different sizes. ***Small***. 2009; 5: 1553-61.

Yuan J-H, Chen Y, Zha H-X, Song L-J, Li C-Y, Li J-Q, Xia X-H. Determination, characterization and cytotoxicity on HELF cells of ZnO nanoparticles. ***Colloids Surf B: Biointerfaces***. 2010; 76: 145-50.

Zhang D, Liu X, Wang X. Green synthesis of graphene oxide sheets decorated by silver nanoprisms and their anti-bacterial properties. ***J Inorg Biochem***. 2011; 105: 1181-6.

Zhang L, Pornpattananangkul D, Hu CM, Huang CM. Development of nanoparticles for antimicrobial drug delivery. ***Curr Med Chem***. 2010; 17: 585-94.

Zhang X, Quan Z, Yang J, Yang P, Lian H, Lin J. Solvothermal synthesis of well-dispersed $MF_2$ (M= Ca, Sr, Ba) nanocrystals and their optical properties. ***Nanotechnology***. 2008; 19: 075603.

Zhang Y, Liu S, Wang L, Qin X, Tian J, Lu W, Chang G, Sun X. One-pot green synthesis of Ag nanoparticles-graphene nanocomposites and their applications in SERS, $H_2O_2$, and glucose sensing. ***Rsc Adv***.2012; 2: 538-45.

Zhao L, Chu PK, Zhang Y, Wu Z. Antibacterial coatings on titanium implants. ***J Biomed Mater Res Part B: Appl Biomater***. 2009; 91: 470-80.

Zhao X, Koestler BJ, Waters CM, Hammer BK. Post-transcriptional activation of a diguanylate cyclase by quorum sensing small RNAs promotes biofilm formation in *Vibrio cholerae*. ***Mol Microbiol***. 2013; 89: 989-1002.

Zhou Y, Yang J, He T, Shi H, Cheng X, Lu Y. Highly Stable and Dispersive Silver Nanoparticle-Graphene Composites by a Simple and Low-Energy-Consuming Approach and Their Antimicrobial Activity. ***Small***. 2013; 9: 3445-54.

Zitzmann NU, Berglundh T. Definition and prevalence of peri-implant diseases. ***J Clinic Periodontol***. 2008; 35: 286-91.

Zlosnik JEA, Costa PS, Brant R, Mori PYB, Hird TJ, Fraenkel MC, Wilcox PG, Davidson AGF, Speert DP. Mucoid and non-mucoid *Burkholderiacepacia* complex bacteria in cystic fibrosis infections. ***Am J Respir Crit Care Med***. 2011; 183: 67-72.

# *LIST OF PUBLICATIONS*

1. **Shatavari Kulshrestha**, Shakir Khan, Ramovatar Meena, Braj R. Singh and Asad U Khan. A graphene / zinc oxide nanocomposite film protects implant surfaces against cariogenic *Streptococcus mutans* (**Biofouling: The Journal of Bioadhesion and Biofilm Research,** 2014; 30(10): 1281-1292).

2. **Shatavari Kulshrestha**, Shakir Khan, Sadaf Hasan, Ehtisham Khan, Lama Misba and Asad U. Khan. Calcium fluoride nanoparticles induced suppression of *Streptococcus mutans* biofilm: An *in vitro* and *in vivo* approach (Under revision in **Applied Microbiology and Biotechnology**).

3. **Shatavari Kulshrestha**, Shariq Qayyum and Asad U. Khan. Facile green synthesis of graphene oxide-silver nanocomposite using *Lagerstroemia speciosa* floral extract: A study of its antibiofilm mechanism on *Streptococcus mutans* and *Enterobacter cloacae* (Communicated).

4. Lama Misba, **Shatavari Kulshrestha** and Asad U. Khan. Antibiofilm action of toluidine blue O-Silver nanoparticle conjugate on *Streptococcus mutans*: A mechanism of type I photodynamic therapy (Under preparation).

# *Conferences / Workshops Attended*

- Attended "Science Communication Workshop" Aligarh Muslim University, Aligarh, India, **26 March, 2015**.

- Attended international conference on nanoscience and nanotechnology "Aligarh Nano IV International 2014" organised by Department of Applied Physics, Z.H. College of Engineering & Technology, Aligarh Muslim University, Aligarh, India, **8-10 March, 2014**.

- Presented poster at National Symposium on "New facets of Biotechnology from Genes to Proteins" sponsored by UGC, DST and DBT, Govt. of India, New Delhi, organized by Interdisciplinary Biotechnology Unit, Aligarh Muslim University, Aligarh**,** India, **15-17 January, 2014**

- Presented a poster at "3$^{th}$ Annual meeting of the Indian Academy of Biomedical Sciences & Symposium on Modern Trends in Human Diseases" organized by Department of Biochemistry, JNMC, Aligarh Muslin University, Aligarh, India, **14 -15 December, 2013.**